Modelling human skin: organotypic cultures for applications in toxicology, immunity, and cancer

PhD thesis

to obtain the degree of PhD at the
University of Groningen
on the authority of the
Rector Magnificus Prof. C.Wijmenga
and in accordance with
the decision by the College of Deans

and

to obtain the degree of PhD at the
University of Antioquia
on the authority of the
Rector Prof. J. Arboleda
and in accordance with
the decision by the Corporation of Basic Biomedical Sciences Academic Council

Double PhD degree

by

Catalina Gaviria Agudelo

Supervisors

Prof. dr. L.M. Restrepo Múnera
Prof. dr. ir. F. Foijer

Assessment committee

Prof. dr. P.J. Patiño
Prof. dr. S.M. Robledo
Prof. S. L.A. Correa
Dr. N.Y. Becerra

TABLE OF CONTENTS

LIST OF FIGURES

Chapter 6

LIST OF TABLES

Chapter 1

Chapter 3

Chapter 5

Chapter 6

SUMMARY

Animal models are important tools to better understand different skin processes. These are widely used for chemical hazard identification and to study skin-related pathologies. Despite the complexity they offer, animal skin is not a perfect model of human skin. This and the growing ethical concern about animal experimentation has led to the development of alternative methods that are in line with the 3 rules guidelines (reduction, refinement and replacement of animals in experiments) within the seventh amendment to the EU Cosmetics Directive 76/768/EEC.

One of these alternatives are human skin explant models. Such models contain the main cellular components, a skin barrier function, and a mature stratum corneum, and are therefore highly suitable to replace animal testing. However, they rely on a regular supply of fresh tumor biopsies of proper size, limiting their use in drug testing assays.

Another alternative, *in vitro* bi-dimensional (2D) skin models, have been produced as well, but they are restricted by the lack of similarity to the skin *in vivo* structure, phenotype, and behavior. Therefore, three-dimensional (3D) skin substitutes represent a powerful alternative to animal testing. Over the last years, many elegant studies have developed 3D models composed of human skin cells and extracellular matrix components. Still, most of them are limited to one cellular type, neglecting the contribution of other important elements like the dermis, the immune component, or interaction between different cell types. Therefore, to better understand skin behavior and responses, models that more faithfully mimic the human skin are needed.

In this thesis, we aimed to develop 3D fibrin-based human skin equivalents for applications in the fields of toxicology, immunology, and cancer, containing both the dermal and epidermal compartments.

In recent years, various materials and technologies have been studied to create improved skin substitutes. **Chapter 1** provides an overview of some of the most relevant skin models and summarizes the different methodologies used to assess skin toxicity and produce cancer models. Mice, rabbits, and guinea pigs are typically used for percutaneous absorption studies, tumor development research, and to predict hazardous effects of chemicals and formulations. However, differences between human and animal skin in terms of tissue structure, permeability, immunity, DNA repair mechanisms, and gene expression, have led to the development of human *in vitro* models. Many of them have been able to recreate some of the typical features of both healthy and diseased skin and suggest that complex systems like full-thickness models are highly valuable tools to perform human skin studies. We therefore developed full-thickness fibrin-based 3D skin equivalents adapted for different applications, which are discussed in the following chapters.

In **Chapter 2**, 3D fibrin-based skin models are constructed and the effects of using keratinocytes from different sources are investigated. We examined the morphology, protein expression pattern, and transepithelial electrical resistance of skin substitutes produced with both explant and feeder layer-derived keratinocytes. Although both approaches are suitable for the construction of fibrin-based skin equivalents, we found that feeder layer-derived keratinocytes generate skin models with improved histological features and that early

passage cells produce a tighter epidermal barrier. Our findings highlighted the importance of using highly proliferative and undifferentiated keratinocytes when constructing skin models, characteristics that are lost as the cell passage number increases.

We next validated our model as a platform for chemical hazard identification. In **Chapter 3**, irritation and corrosion tests were carried out with 30 chemical substances following the 431 and 439 OECD test guidelines. Skin substitutes displayed an overall accuracy of 86% for irritation and 94% for corrosion. Our results also indicated that, in response to irritants, the induction of one or more cytokines could be chemical- and model-specific, highlighting the complexity of this process. For comparison, we also tested the already validated model EpiDerm^{TM}, which exhibited a lower performance, most likely due to quality loss during long shipping times. These findings confirmed the suitability of fibrin-based skin equivalents for hazard assessment and underscored the necessity of having a local model for the development and commercialization of chemical products.

In order to develop a platform for the evaluation of skin sensitizers, the construction of a 3D fibrin-based immune skin model is described in **Chapter 4**. Freshly isolated CD14+ cells were incorporated into the epidermal compartment of our skin substitute. Using this approach, we found that the 3D model microenvironment is able to promote CD14+ cells differentiation into dendritic cells, as judged by the immunohistochemical results. Moreover, a preliminary sensitization test revealed that they are able to migrate following chemical exposure, confirming the usefulness of fibrin-based scaffolds to develop immune skin substitutes. We expect that this approach will be used to generate skin equivalents composed of different dendritic cells subtypes that can differently respond to sensitizers and irritants, improving the existing *in vitro* sensitization tests.

Chapter 5 describes a protocol to establish primary basal cell carcinoma (BCC) cultures and to further generate 3D fibrin-based primary BCC models. We used different approaches to culture primary BCC cells and found that a combination of a feeder layer, explants and the addition of rock inhibitor, supported the growth of BCC-derived keratinocytes. We also developed different 3D models with BCC-derived cells and tumor explant fragments. The explant model showed high similarity to human BCC, as it displayed invasive phenotype, high expression of the BCC marker EpCAM, and lateral migration of biopsy-derived keratinocytes. Models composed of a mix of healthy and tumor-derived keratinocytes exhibited impaired morphology and differentiation pattern as the percentage of tumor-derived cells increased, typical features of BCC. Together, these data indicated that fibrin-based skin substitutes have potential to model basal cell carcinoma, recapitulating some of the most relevant characteristics of this type of cancer and could therefore become an important tool to test new therapeutics that target BCC.

To further characterize basal cell carcinoma, in **Chapter 6 (addendum)** we highlight the application of the primary BCC culture system to confirm the presence of the chromosomal instability (CIN) phenotype (common feature in cancer) in a subset of BCC samples. To this end, we cultured, labeled, and time-lapse imaged BCC-derived cells to determine the frequency of mitotic abnormalities. We were able to better characterize BCC and, together with scWGS and RNA-seq, we found that BCC can be classified into distinct karyotypic subclasses associated with specific transcriptome characteristics. This new classification

system is a promising tool to improve current tumor diagnosis and prediction of treatment responses.

Finally, in **Chapter 7**, the results described in this thesis are summarized and discussed.

RESUMEN

Los modelos animales son herramientas importantes para el estudio de la biología de la piel humana y los mecanismos subyacentes. A pesar de la complejidad que ofrecen y de ser ampliamente utilizados para estimar el riesgo potencial de sustancias químicas e investigar diferentes patologías cutáneas, no son modelos perfectos de piel humana. Esto y la creciente preocupación ética por la experimentación animal ha dado lugar al desarrollo de métodos alternativos que estén en línea con el principio de las 3R (reducción, refinamiento y reemplazo de animales de laboratorio) dentro de la séptima enmienda a la Directiva de Cosméticos de la UE 76/768/EEC.

Los explantes de piel humana contienen los principales componentes celulares, conservan la función barrera de la piel y presentan un estrato córneo maduro, por lo que son altamente adecuados como reemplazo de pruebas con animales. Sin embargo, tienen como principal desventaja la necesidad de contar con un suministro constante de biopsias frescas de tamaño adecuado, lo que limita su uso en pruebas de toxicidad.

Asimismo, se han producido varios modelos de piel *in vitro* bidimensionales (2D) que sin embargo, están limitados por la falta de similitud con la estructura, fenotipo y función de la piel nativa. Por otro lado, los modelos de piel tridimensionales (3D) representan una poderosa alternativa contra la experimentación animal. En los últimos años, diferentes estudios se han enfocado en el desarrollo de sustitutos 3D compuestos por células de piel humana y productos de la matriz extracelular. No obstante, la mayoría sólo incluye un tipo celular, pasando por alto la contribución de elementos importantes como la dermis, el componente inmunológico o la interacción entre diferentes tipos de células. Por lo tanto, para un mejor estudio de la piel y sus respuestas, se necesitan modelos que imiten más fielmente la piel humana.

En esta tesis, nos enfocamos en el desarrollo de modelos dermo-epidérmicos 3D de piel humana para aplicaciones en el campo de la toxicología, la inmunología y el cáncer, utilizando como soporte un scaffold de fibrina.

En los últimos años, se han venido estudiando diferentes materiales y técnicas para la construcción de sustitutos de la piel. El **Capítulo 1** ofrece una descripción general de algunos de los modelos cutáneos más relevantes y resume las diferentes metodologías utilizadas para evaluar la toxicidad cutánea y construir modelos de cáncer. Los ratones, conejos y conejillos de indias son típicamente utilizados en estudios de absorción percutánea, crecimiento tumoral y evaluación de efectos tóxicos de productos químicos y formulaciones. Sin embargo, las diferencias entre la piel humana y animal en términos de estructura, permeabilidad, inmunidad, mecanismos de reparación del ADN y expresión génica, han acelerado el desarrollo de modelos de piel *in vitro*. Muchos de ellos han logrado recrear algunas características distintivas de la piel y sugieren que sistemas más complejos, como los modelos dermo-epidérmicos, son herramientas valiosas para investigaciones relacionadas con la piel humana. Por lo tanto, en este estudio se desarrollaron y adaptaron equivalentes dermo-epidérmicos de piel para diferentes aplicaciones, los cuales son descritos en los siguientes capítulos.

En el **Capítulo 2** se construyen modelos 3D de piel y se investiga el efecto del uso de queratinocitos obtenidos por diferentes métodos de cultivo. Para esto, se analizaron la

morfología, la expresión de proteínas y la resistencia eléctrica transepitelial de los sustitutos de piel producidos con queratinocitos cultivados por capa alimentadora y explante. Aunque ambos enfoques resultan ser adecuados para la construcción de equivalentes de piel, encontramos que los queratinocitos obtenidos por capa alimentadora generan modelos con características histológicas superiores y que las células en pases bajos producen una barrera epidérmica con uniones estrechas más fuertes. Nuestros hallazgos destacan la importancia de utilizar queratinocitos indiferenciados y con alta capacidad proliferativa en la construcción de modelos de piel, características que se pierden a medida que aumenta el pase del cultivo.

En el **Capítulo 3** se validó el modelo como plataforma para la identificación del potencial toxicológico de compuestos químicos. Para esto, se realizaron ensayos de irritación y corrosión con 30 sustancias, siguiendo las directrices 431 y 439 de la OECD. Los sustitutos de piel mostraron una precisión del 86% en ensayos de irritación y del 94% en ensayos de corrosión. Nuestros resultados también indicaron que, como respuesta a la exposición a irritantes, la inducción de una o más citoquinas podría depender del tipo de compuesto y del modelo, lo que destaca la complejidad del proceso inflamatorio. Con fines comparativos, se hicieron ensayos en el modelo validado EpiDerm^{TM}, el cual presentó un rendimiento más bajo, probablemente asociado a la pérdida de calidad del producto dados los largos tiempos de envío. Nuestros hallazgos confirmaron la utilidad de los equivalentes de piel para evaluación de sustancias irritantes y corrosivas e hicieron énfasis en la necesidad de contar con un modelo local para el desarrollo y comercialización de productos químicos.

Con el fin de desarrollar un sistema para evaluar sustancias sensibilizantes, en el **Capítulo 4** se describe la construcción de un modelo de piel con componentes inmunes. Para esto, se incorporaron células CD14 + en el compartimento epidérmico de nuestro modelo. Usando esta metodología, encontramos que el microambiente del modelo 3D promueve la diferenciación de células CD14 + en células dendríticas, a juzgar por las tinciones inmunohistoquímicas. Además, los resultados preliminares de un ensayo de sensibilización revelaron que estas células migraron como respuesta a la exposición química, lo que confirma la utilidad de los scaffolds de fibrina en la construcción de sustitutos de piel inmunes. Se espera que este enfoque pueda ser utilizado para desarrollar equivalentes de piel compuestos por diferentes subtipos de células dendríticas con respuestas diferenciales a sensibilizantes e irritantes, contribuyendo así a las pruebas actuales de sensibilización.

El **Capítulo 5** describe un protocolo para establecer cultivos de carcinoma basocelular (BCC) y generar los respectivos modelos 3D. Haciendo uso de diferentes técnicas de cultivo celular, encontramos que la combinación de una capa alimentadora, explantes de piel y la adición de un inhibidor de la via rock, permitió el crecimiento de queratinocitos derivados de muestras de BCC. Esto dio lugar a la posterior construcción de diferentes modelos 3D con células de BCC y fragmentos de explantes de tumores. El modelo de explante presentó una gran similitud con el BCC humano, exhibiendo un fenotipo invasivo, una alta expresión del marcador EpCAM y una migración lateral de células provenientes del explante. Por otro lado, los modelos compuestos por queratinocitos sanos y derivados de tumores, mostraron una alteración en la morfología y diferenciación (características típicas de BCC) a medida que aumentaba el porcentaje de células tumorales. Todo lo anterior, indica que los sustitutos dermo-epidérmicos de fibrina tienen potencial para modelar el carcinoma de células basales, ya que recapitulan algunas de las características más relevantes de este tipo de cáncer y, por

lo tanto, podrían convertirse en una herramienta útil para probar nuevas terapias contra el BCC.

En el **Capítulo 6**, como **apéndice**, se destaca la aplicación del sistema de cultivo de BCC para confirmar la presencia de inestabilidad cromosómica (CIN) (característica común en el cáncer) en un subconjunto de muestras de BCC. Con este fin, cultivamos, marcamos y utilizamos microscopia de células vivas para determinar la frecuencia de anomalías mitóticas en células tumorales. Esto dio lugar a una mejor caracterización del BCC, pues encontramos que se puede subclasificar en distintos tipos cariotípicos asociados con características específicas del transcriptoma. Este nuevo sistema de clasificación es una herramienta prometedora para mejorar el diagnóstico actual del BCC y la predicción de las posibles respuestas al tratamiento.

Finalmente, en el **Capítulo 7**, se resumen y discuten los resultados obtenidos en esta tesis.

CHAPTER 1

General introduction and thesis aim

C. Gaviria [a,b], L.M. Restrepo [a,c]

[a]Tissue Engineering and cell therapy research Group, School of Medicine, University of Antioquia, Colombia
[b]European Research Institute for the Biology of Ageing, University Medical Center Groningen, The Netherlands
[c]Medical Research Institute, School of Medicine, University of Antioquia, Colombia

ABSTRACT

Animal models are commonly used for toxicity screening, cutaneous permeability tests, and to study the biological mechanisms behind skin diseases. However, the differences found between the structure of human and animal skin yield results difficult to extrapolate from animal studies to a human context [1,2]. Moreover, there is an increasing concern about the use of animals for research purposes, which has led to a ban on all animal testing for cosmetics by the European Union [3,4]. This has promoted the development of more reliable, efficient, and cost-effective methods [5].

Skin explants have been used as an alternative, but they require large amounts of fresh skin, which hinders their use [6]. Human skin equivalents (HSEs) represent a potentially powerful alternative to animal testing. Recently, tremendous efforts have been done in the research and development of HSEs, which can also be adapted to study different human skin diseases [7]. Currently, new materials and methodologies are studied in order to improve the quality of human skin equivalents. In this review, we provide an overview of some of the most important existing skin models with a focus on *in vitro* substitutes. To facilitate understanding, an insight into human skin structure and function is also given.

HUMAN SKIN STRUCTURE AND FUNCTION

Human skin provides a barrier that protects the human body against physical and chemical factors to which it is regularly exposed. It also has an essential role in homeostasis, temperature regulation, immunity, self-healing, and the cutaneous sense, and provides a means to transport drugs and reagents into the skin and body [3,8].

The two main layers of the skin are the epidermis and the dermis (see Figure 1). The dermis supports the skin and is made up of 80% water, elastin fibers and, collagen floating in a glycoprotein gel. Fibroblasts (FBs), macrophages, and adipocytes are the three major cell types of this layer [3,8,9]. The epidermis is composed of different types of cells, of which keratinocytes (KCs) represent the majority (90–95%). Other epidermal cells with important roles are melanocytes, Langerhans cells (LCs), and Merkel-Ranvier cells [8,10].

The role of keratinocytes and fibroblasts is discussed below.

Fibroblasts as a key component of the dermis

Fibroblasts are the most prevalent cell type in the dermis (Figure 1), with a spindle-shaped form and an oval flat nucleus. They are the primary source of proteins and polysaccharides that form the extracellular matrix (ECM) [11]. Appropriate combinations of these ECM products give suitable physical and mechanical characteristics to the skin [12].

Fibroblasts can also modify the production of extracellular matrix components according to signals from other cell types. Without these, keratinocyte differentiation is impaired, resulting in only in few layers of well-differentiated epidermal cells [13]. Additionally, cross-talk between fibroblasts and immune cells normally helps to maintain homeostasis in connective tissues [12].

Interestingly, keratinocytes positively affect fibroblasts proliferation. It is believed that the interaction between these cells is due to a double-paracrine mechanism that regulates their growth. According to this hypothesis, keratinocytes secrete IL-1, which stimulates the skin fibroblasts to secret keratinocyte growth factor and granulocyte-monocyte colony-stimulating factor, which in turn positively influence the proliferation of the keratinocytes [13].

The role of keratinocytes in the epidermis

In the epidermis, keratinocytes differentiate to form four layers: the stratum basale, stratum spinosum, stratum granulosum, and stratum corneum (Figure 1), and they are constantly undergoing a process of proliferation, differentiation, keratinization, and exfoliation [3,8,14].

The basal layer represents the germinative compartment in which keratinocytes proliferate. Following cell division, a daughter cell detaches, migrates, and differentiates, forming the stratum spinosum, where cells start producing keratin proteins. Then, in the stratum granulosum, further differentiated keratinocytes become flattened while accumulating keratohyalin granules. Finally, terminally-differentiated keratinocytes generate the stratum corneum, which contains anucleated, non-viable but chemically active cells embedded in

extracellular lipids. This layer provides an epidermal barrier that reduces trans-epidermal water loss and prevents toxins and pathogens from entering the body [3,8].

Additionally, keratinocytes play a key role in skin inflammatory and immunological reactions. In response to physical or chemical stress, keratinocytes produce and release inflammatory mediators such as cytokines and other signaling factors, which rapidly trigger cutaneous inflammation [15,16].

Skin immunity

The skin immune system relies on a rich network of antigen-presenting dendritic cells (DCs) that populate the epidermis and the dermis. Epidermal DCs are known as Langerhans cells (Figure 1) and are located in a supra-basal layer of the epidermis. They account for 3–5% of all cells in the epidermis and are arranged in a network that occupies the interstices between neighboring keratinocytes [17,18].

Through their extended dendrites, LCs form a continuous cellular network that surveys the epidermis for foreign antigens, providing the first immunological barrier to the external environment [18]. Additionally, they express cytokines, growth factors, and other mediators as a response to certain stimuli [19].

Besides the immunological barrier, skin cells have other mechanisms to cope with toxic external agents such as irritants and corrosives.
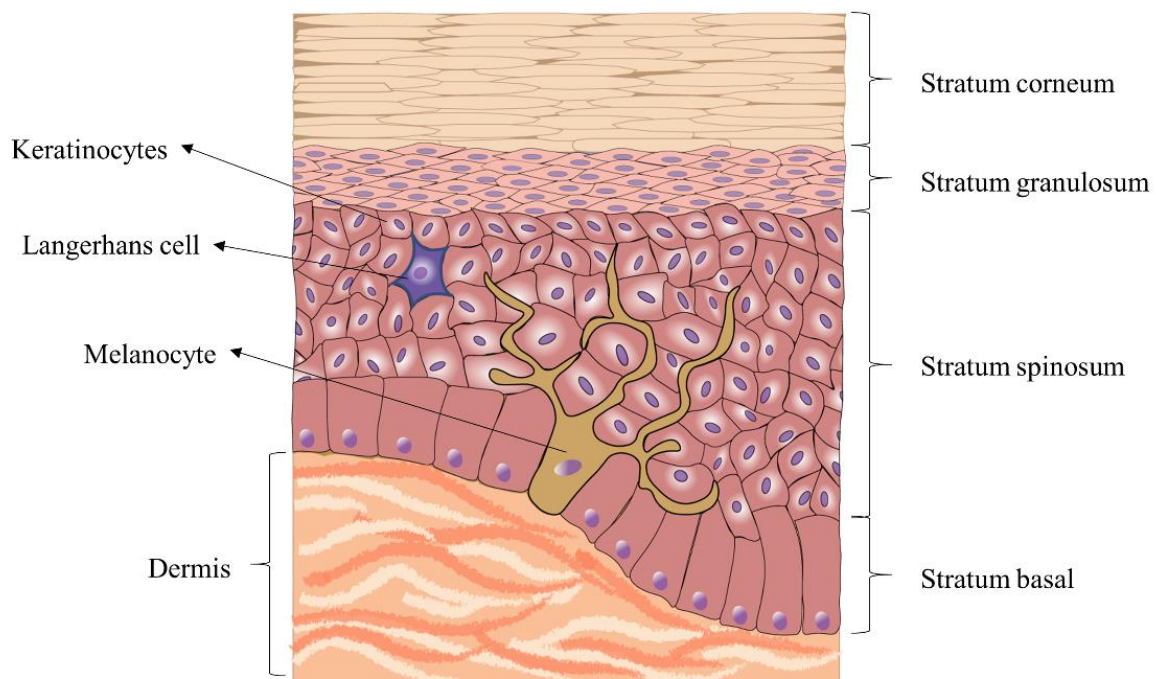

Figure 1. Schematic of human skin

CUTANEOUS TOXICITY

The skin can be damaged by daily exposure to chemicals including pharmaceuticals, cosmetics, cleaning agents, industrial, and agricultural products. Exposure can be accidental

or intentional and, according to the severity and reversibility of possible effects, skin irritation, corrosion, or sensitization will take place [3,20].

Skin irritation

Skin irritation is often the result of reversible damage of the epidermis following exposure to irritants, leading to local inflammation. In response, skin cells release inflammatory mediators (chemokines and cytokines) that increase the diameter and permeability of blood vessels and trigger the migration of immune cells to the site of injury, resulting in clearance and tissue repair. Inflammatory mediators stimulate nerve endings as well, leading to itching and stinging sensations [3,21]. Therefore, the presence of erythema, edema, dryness, fissures, desquamation, itching, and pain are common symptoms of skin irritation and represent the physiological manifestation of a complex chain of biochemical, neural, vascular, and cellular responses following irritation [3].

Mechanisms of action of irritant substances

Many different chemical substances have the potential to cause skin irritation, and various pathways are involved. Chemicals can cause skin irritation by at least two distinct pathways: firstly, via damaging the barrier function of the stratum corneum and secondly, through direct effects on the epidermal cells [3].

Some irritants entering the stratum corneum may cause delipidation and protein denaturation. During delipidation, the balance of lipids is disturbed, producing alterations in lipid composition and organization. Consequently, there is a loss of the barrier function, resulting in increased penetration of irritants to living keratinocytes [3].

The most well-characterized irritation mechanism is the one triggered by surfactants. These substances can disrupt lipids in membranes resulting in the release of the pro-inflammatory cytokine IL-1α [3]. IL-1α represents one of the main components in the inflammatory cascade since it can induce the expression of further cytokines, such as tumor necrosis factor-alpha (TNF-α) or IL-1β, IL-6, IL-7, IL-8, IL-10, IL-12, IL-15, and other signaling factors which rapidly generate cutaneous inflammation [3,22]. The cytokines IL-1β and TNF-α can also activate a number of effector mechanisms to independently trigger an inflammatory response, and thus they are considered primary cytokines [3].

On the other hand, irritants that do not disrupt membrane continuity, probably do not initiate the inflammatory response exclusively by the release of IL-1α. Recently, oxidative stress has been related to irritation. At high levels, reactive oxygen species can oxidize nucleic acids, proteins, and membrane lipids, resulting in altered gene expression or cytotoxicity [22].

Another possible irritation mechanism involves the interaction of agents with receptors or membrane-bound proteins, which may result in altered signal transduction and membrane fluidity, giving rise to irritant responses [22].

Skin corrosion

Corrosive substances irreversibly damage the skin, beyond repair. This results in visible necrosis within the affected area, which can only be regenerated from the healthy skin surrounding the necrotic tissue. Corrosive reactions include ulcers, bleeding, bloody scabs, and, in animal experiments, discoloration due to blanching of the skin, alopecia, and scars [21].

It is thought that the major direct chemical processes leading to chemical corrosion are physicochemical in nature rather than the result of induced inflammatory changes, although inflammation is commonly a consequence of the skin corrosion process [23].

Mechanism of action of corrosive substances

Mechanisms of skin corrosion mainly comprise loss of stratum corneum integrity and barrier function, caused by inorganic acids and bases and strong organic acids with an extreme pH. Contact with acids will alter the skin pH, destroying proteins' secondary and tertiary structure, leading to the loss of their biologic activity, and producing coagulation of proteins and cellular death. In some cases, acids can obstruct cellular metabolism by sequestering calcium and magnesium ions, resulting in necrosis [24]. On the other hand, alkalis react with proteins to form proteinates and with lipids to form soaps, causing tissue necrosis [25].

Corrosive materials mainly affect the epidermis by acid-base reactions of amide and ester hydrolysis. Proteins, which are composed of amide bonds, can be destroyed via amide hydrolysis, while lipids can be decomposed by ester hydrolysis [26]. On the other hand, corrosives like cationic surfactants tend to disrupt cellular membranes, leading to erosion of the tissue and subsequent necrosis [27].

When in contact with water, some chemicals, like titanium chloride, generate an exothermic reaction that releases energy through heat. Given the high water content of the skin, these substances can cause severe skin burns [24].

Skin sensitization

Skin sensitizers are substances able to generate an allergic response following contact with the skin, also known as allergic contact dermatitis (ACD) [21].

Skin sensitization results in skin inflammation and itchiness. It is difficult to distinguish between skin irritation and ACD by eye [22]. In contrast to skin irritation, ACD produces an immunogenic inflammatory reaction, in which the skin becomes increasingly reactive to the substance as a result of subsequent exposures [28].

Mechanism of action of skin sensitization

The induction of skin sensitization requires activation of both the innate and adaptive immune responses, and a variety of cells and molecules have pivotal roles to play in the initiation and orchestration of cutaneous immune responses to chemical allergens [28].

Haptens are small molecules that require the attachment to a large carrier, for instance, a protein, to elicit an immune response. Such compounds are best known as skin sensitizers [28,29]. The induction phase of ACD involves an initial exposure to the hapten on the skin and typically binding the chemical to a protein carrier [30]. LCs capture and internalize the modified protein, resulting in activation and migration [31,32]. Migratory LCs upregulate MHC class II and other costimulatory molecules on their cell surface and downregulate that of E-cadherin, which probably facilitates LC disengagement from keratinocytes. After leaving the epidermis, LCs localize in the T-cell area of the skin-draining lymph nodes [18], where they present the processed antigen to naive T cells. Interactions between the loaded DCs and T-lymphocytes stimulate the proliferation of specific effector and memory T-cell clones. This process is known as sensitization [30].

In the elicitation phase, after subsequent exposure to the same sensitizer, the primed T cells produce an aggressive immune response resulting in a local inflammatory reaction. During this process, re-exposure of the hapten triggers recruitment and activation of T lymphocytes in the dermis, which release cytokines and recruit other inflammatory cells. These events lead to clinically visible tissue inflammation characterized by edema, erythema, scaling, and blistering [30].

Different experimental methods exist to study skin responses to external stimuli. They are widely used to study skin biology and for safety analysis of cosmetics and toxicity screening of various potentially harmful agents, as discussed below.

MODELLING HUMAN SKIN

There are several model systems that recreate different features of human skin and provide a better understanding of skin structure, function, or disease. Here, we present the three major areas in skin modelling: *in vivo*, *ex vivo*, and *in vitro* models.

In vivo models

Animal models are important tools to better understand different skin processes, providing complex systems where several types of cells and tissues are present.

Porcine skin has been extensively used as a model, due to its high similarity to human skin in terms of epidermal thickness, permeability, vascular anatomy, collagen structure, adipose tissue, and cellular composition. However, there are important differences regarding the mechanics of the tissue and the compositions of free fatty acids, ceramides, eccrine glands, and apocrine glands. Moreover, information about porcine skin immunity is still lacking [33–37].

Mice, rats, and guinea pigs are mostly used in percutaneous absorption studies thanks to their availability, low cost, proper size, and easy handling. Yet, several studies have found that rat skin is more permeable than human skin to a wide range of agents [33,34,36].

Although mice are widely used for skin disease studies, mouse skin is significantly thinner, DNA repair mechanisms are different, and oncogene and tumor suppressor gene function seem to differ too. There are also differences in terms of innate and adaptive immunity,

including the balance of leukocyte subsets, defensins, Toll receptors, cytokines and chemokine receptors, Th1/Th2 differentiation, and antigen-presenting function of endothelial cells [34].

Due to the ease of storing, ecological safety, and suitability for experimental animal ethics, snake skin is utilized as a membrane for drug diffusion studies [33]. Nevertheless, various reports describe differential responses to different ethanol concentrations between the snake and human skin, perhaps because of differences in water content and the nature of the intercellular lipids [36,38].

To predict the hazardous effects of substances and formulations, rabbits are the main component of the Draize test [39]. However, rabbit and human skin have different physiological properties and thus, different responses to physical and chemical stimuli. In fact, the Draize irritation test has been criticized for its over or underprediction of human skin irritation. Furthermore, the test is based on a subjective analysis of skin damage, and therefore, different laboratories often report different results [3].

Not many experiments have been performed on humans because of the potential risk of lesions, and intoxication of the subjects. However, mild or non-irritating materials have been tested after ethically approved protocols. The limited available human data on chemical toxicity comes from damage after accidental exposure to severe irritants, or to repeated exposure to moderate irritants. Patch tests have also provided important data from high numbers of volunteers. However, because of possible sensitization reactions, the European Union has strict regulations in this matter [3].

One of the major weaknesses of animal models is that they yield results difficult to extrapolate into a human context, due to the differences between the structure of human and animal skin [1,2]. Additionally, there are ethical issues regarding the use of laboratory animals and the European Union implemented a ban on all animal testing for cosmetics [3,4].

Ex vivo models

Ex vivo human skin models, obtained from cadavers or plastic surgery leftovers, have been successfully used to test substances on real human skin without the risk of harming the test subject. They are relevant and highly suitable models since they contain the main cellular components, a skin barrier function, and a mature stratum corneum [40]. Human explants have been used to study skin processes like barrier repair, wound healing, chemical toxicity, chronic inflammatory diseases, DNA vaccination, and fungal infection [41].

Human explants can conserve the viability and proliferative capacity of human skin for up to 75 days [42], demonstrating their suitability as an alternative method to animal model testing. Xu et al. studied wound healing in a human *ex vivo* skin culture, showing that it retains important elements of *in vivo* skin with several advantages in wound healing studies. Interestingly, epidermal proliferation and differentiation was observed after superficial wounds, as well as collagen deposition in the dermis [43].

The main disadvantage of using *ex vivo* human skin is that it requires a regular supply of fresh biopsies of proper size and skin may not be easy to obtain [1,36,40]. Moreover, cellular

viability and metabolic activity rapidly decrease after tissue removal, then explants need to be promptly used [36].

In vitro models

In vitro skin models are skin substitutes that attempt to mimic the epidermis, the dermis, or both. To date, two kinds of *in vitro* skin models are available: bi- (2D) and three-dimensional (3D) cultures, and include epidermal, dermal, and full-thickness models.

A 2D culture is anchorage-dependent, with cells growing attached to a surface. Despite its simplicity, cells are restricted by their incapacity to mimic the 3D *in vivo* structure and behavior. Cell stratification and differentiation are poor, they may show hyperproliferative growth, and are not the best tool to study cellular responses. In fact, important signaling pathways work only when cells are placed in a 3D structure [7].

In vitro 3D models are bioengineered substitutes composed of human keratinocytes and fibroblasts and components of extracellular matrix like collagen. At the air-liquid interface, the keratinocytes of these systems differentiate and develop a functional barrier [22,44], with proper protein expression, and similar lipid composition [8].

In general, HSEs are applied in two major fields: as clinical skin grafts, and as models for research. Skin grafts rely on dermal substitutes, while pharmacological models use either epidermal or full-thickness models for chemical hazard identification [8]. Skin substitutes are also helpful to study fundamental processes in the skin, such as epidermal development, the interaction between different cell types, stem cells maintenance, wound healing, or infection with different pathogens [13].

One great advantage of *in vitro* models, other than being of human origin, is the possibility of controlling the cellular composition. Researchers can integrate or omit cell components in order to study its importance in the process under investigation [13]. Further, *in vitro* models avoid the need to recruit volunteers, and contribute to the reduction of laboratory animals. Some of these models have been already validated in cutaneous toxicology and pharmacology [45].

To date, three different kinds of HSEs are available: epidermal, dermal, and full skin models.

Epidermal models

Epidermal models are in vitro cultures that consist of different layers of differentiating human keratinocytes. For the production of epidermal substitutes, the epidermis and the dermis of a skin biopsy are separated, and keratinocytes are isolated and cultured on special substrates [8,13].

More recently, some of these models have been validated as a platform for chemical and drug testing and have become commercially available. Table 1 summarizes some available epidermal products.

Table 1. Human epidermal equivalents for toxicity screening.

Product	Company	Description	Reference
EpiDerm™	MatTek	Neonatal human-derived epidermal KCs cultured to form a multi-layered, highly differentiated model of the human epidermis.	[46]
SkinEthic RHE	EpiSkin	Human KCs cultured on an inert polycarbonate filter at the air-liquid interface.	[47]
EpiSkin	SkinEthic	Human KCs cultured on a collagen base leading to a differentiated epidermis with a functional stratum corneum.	[48]
Epidermal Skin Test 1000 (EST1000)	CellSystems	Human KCs cultured on a polycarbonate membrane, leading to a fully differentiated epidermis with a functional stratum corneum.	[49]
Leiden Human Epidermal model	Ponec, Bouwstra, and EI-Ghalbzouri groups	Human KCs cultured on an inert acellular filter and air-exposed to form a differentiated epidermis.	[50]

KCs: Keratinocytes

Epidermal skin substitutes have been further improved by the addition of a dermal layer containing fibroblasts [13] since their presence helps keratinocytes deal with potentially toxic agents [51].

Dermal models

Dermal equivalents are *in vitro* models of the dermal layer of skin, composed of fibroblasts-populated scaffolds, like collagen gels or de-epidermized human dermis. Dermal models are mainly used as grafts for the treatment of full-thickness burns, as the treatment with epidermal grafts alone would result in an inferior performance. In contrast to cultured epidermal sheets, engineered dermal constructs can prevent wounds from contracting and provide greater mechanical stability. Both dermal and epidermal compartments need to be replaced, one after the other, since good dermal vascularization needs to be achieved before the application of the epidermal layer [13].

There is a variety of commercial dermal constructs, both natural as well as synthetic. Some of these substitutes are chemically-treated allografts, in which cells secrete extracellular matrix proteins and different growth factors and cytokines into the wound until they undergo normal apoptosis a few weeks after implantation [13]. Table 2 shows some available dermal substitutes.

Table 2. Human dermal equivalents [8].

Product	Company	Description
Transcyte	Advanced Tissue Sciences	Neonatal human FBs cultured on a polymeric scaffold that is then cryopreserved, making it a non-living wound covering.
Dermagraft	Advanced Biohealing	Human foreskin FBs cultured in a biodegradable polyglactin mesh.

Alloderm	LifeCell Corporation	Intact acellular matrices produced from cadaver skin by removing the epidermis and the antigenic cellular elements in the dermis.	
Integra DRT	Integra Life Sciences Corp	Skin graft composed of an outer layer of a silicon film and an inner layer of crosslinked fibers of bovine collagen and shark chondroitin sulfate.	

FBs: Fibroblasts

Full-thickness skin models

It is known that monolayer cultures of human cells have low relevance due to the lack of 3D structure and interactions between cells and extracellular matrix components. Full-thickness skin substitutes can overcome these problems by culturing human skin-derived cells to form a 3D tissue, composed of both epidermal and dermal layers. The culture of keratinocytes on fibroblasts-populated matrices results in an optimum proliferation and differentiation, generating human epidermis-like histology [8,13].

An advantage of HSEs is the ability to incorporate additional cell types in combination with keratinocytes and fibroblasts. The recent addition of melanocytes and Langerhans cells has broadened the potential applications of these models.

Some full-thickness skin equivalents are listed in Table 3.

Table 3. Full-thickness human skin equivalents for toxicity screening.

Product	Company	Description	Reference
Epiderm[FT]	MatTek	Neonatal human-derived FBs and KCs co-cultured to form a highly differentiated model of the human dermis and epidermis.	[52]
StrataTest	StrataTech	Full-thickness skin model where a human KCs cell line (NIKS) and dermal FBs are utilized.	[53]
RealSkin	SkinEthic/L'Oreal	3D skin model made of KCs and FBs.	[8]
Advanced Skin Test 2000 (AST2000)	CellSystems	Dermal equivalent with embedded FBs and a differentiated epidermal layer of KCs on top.	[54]
TESTSKIN™	Organogenesis	FBs embedded in a bovine collagen matrix and differentiated KCs on top.	[13]
Fibrin-based organotypic cultures	GITTC group	FBs embedded in a fibrin-gel with differentiated KCs on top.	[55]
Pigmented human epidermis with LCs	L'Oreal	Co-culture of KCs, MCs, and CD34+-derived LCs on top of de-epidermized acellular human dermis.	[56,57]
MUTZ-3-derived LCs in HSEs	Gibbs' group and Institute of Pharmacy (Freie Universität Berlin)	Co-culture of KCs and MUTZ-3-derived LCs on top of collagen gels with fibroblasts	[58,59]

KCs: Keratinocytes, FBs: Fibroblasts, MCs: Melanocytes, LCs: Langerhans cells

Chemical compounds can have a significant impact on the skin by triggering specific toxicity-associated responses and the above-discussed models provide a powerful alternative to study such processes. However, there are many other internal and external factors that can also influence skin health, leading to skin diseases like cancer, and that also require suitable systems that allow proper investigation.

SKIN CANCER

Cancer is characterized by the uncontrolled growth of transformed cells. Mutations in the DNA of the transformed cells lead to an imbalance between proliferation and cell death, resulting in tumor formation. When tumor cells enter the circulation, tumors may arise in other organs (metastasis), invading surrounding tissues and taking away nutrients to survive and grow [1,60,61].

Since 1940, there has been a 6-fold increase in the incidence rates of skin cancer worldwide. Each year, between 2 and 3 million new cases are reported, representing around 30% of all newly diagnosed cancers, and making skin cancer by far the most common malignancy [62,63].

Age is a major risk factor in dermatological cancers and can be a result of life-long sun exposure. Additionally, some chemicals, virus infections, and psychological stress are involved in many physiopathological processes and may trigger skin cancer. Also, certain genetic features like freckles, moles, red hair, or blue eyes are associated with increased susceptibility to this pathology [61,64].

There are three main types of skin cancer: melanoma, basal cell carcinoma (BCC), and squamous cell carcinoma (SCC). Melanoma is responsible for most skin cancer-related deaths with survival rates falling to 27% when it metastasizes [65]. BCC and SCC belong to the non-melanoma skin cancer (NMSC) group and represent the vast majority of skin cancers. SCC accounts for most NMSC-related deaths and has a higher rate of metastasis (0.3–3.7%) than BCC (less than 0.1%) [61,66–68]. However, BCC accounts for about 80% of NMSCs and may lead to major deformities and morbidity [67–69], leading to a heavy economic burden on patients and healthcare systems [70].

Pathology of basal cell carcinoma

BCCs arise from abnormal epidermal basal cells and tend to grow slowly. Unlike melanoma and SCCs, it does not present precursor lesions [61].

Genetic mutations can trigger the development of BCC. Particularly, mutation of the tumor suppressor PTCH gene, involved in the Hedgehog (Hh) signaling pathway, has been strongly associated with BCC, along with the constant activation of Gli1 and Gli2 transcription factors. Alterations in genes like CYP, GST, and *p53,* have also been linked to BCC [61,68,69].

Prompt treatment of BCCs is vital because as the tumor grows, it becomes more dangerous and can cause disfiguration. Most BCCs are treated surgically, which is more effective for small early BCC lesions. Radiation therapy is also used, which, however, may require several treatments over a few weeks and some tumor tissue might remain. Therefore, radiotherapy is only applied when tumors cannot be removed surgically. Other common treatments include

cryosurgery, topical medication including SHH inhibitors, and photodynamic therapy, all of which are only effective in superficial BCCs [71,72]. Some SHH signaling pathway blockers have been approved to treat advanced BCCs. However, clinical trials are indicating that not all BCCs respond properly and, in a few cases, death has been reported as a severe side effect [73].

At the cytogenetic level, BCC data is still scarce. Previous studies have found aneuploidy in 80% [74] and 83% [75] of samples. Particularly, gains, losses and/or translocations of chromosomes 1, 4, 5, 7, 9, 14 and X have been reported [76–78]. A variety of chromosomal abnormalities could be associated with intratumoral heterogeneity and histologic features, as shown by Herzberg et al. [74], an therefore, cytogenetic analysis of BCCs can become a potential help in prognosis and treatment.

Representative BCC models are required to have a better understanding of cancer biology and the mechanisms that mediate invasion and metastasis, and enable the development of new therapeutic agents [1,2]. Different model systems are currently used to study distinct aspects of BCC, as discussed below.

MODELLING BASAL CELL CARCINOMA

Given their greater propensity for invasion and metastasis, models of cutaneous melanoma and SCC are the most abundant and diverse [63,79]. Still, some BCC models have been described in the literature, most of which are mouse models or 2D cultures.

In vivo models of BCC

Animal models are a useful tool to increase the understanding of cancer progression and metastasis, events that only occur *in vivo* [1]. Mice are the most commonly used animal. They are typically exposed to UV radiation, chemicals, or viruses with the aim of producing carcinogenesis. Yet, the development of proper BCC mouse models has been difficult, since murine UV-induced BCCs do not mimic the human condition very well [69]. For example, Ptch knockout mice exposed to UV developed BCC-like tumors in 4 months, which, however, did not recreate completely the different types of human BCC tumors [80]. Conversely, promising results have been achieved with epidermal Notch1 knockout mice, which presented increased susceptibility to tumor growth and developed BCC-like tumors after chemical treatment [81].

Genetic BCC mouse models have also been developed by activating components of the Hedgehog signaling pathway. The first animal model of this kind presented BCC-like tumors after 4 days of embryonic skin development [82]. These types of tumors also arose after the overexpression of mutant SMO [83], and the transcription factors Gli1 and Gli2 [84,85].

Another approach is based on tumor xenografts. However, there have only been few reproducible xenograft implantations of human BCCs in animal models [86], since numerous attempts of transplanted human BCC failed to form lesions that closely resembled their human counterpart [86]. In a recent study, 14 BCC tumors were transplanted into 18 SCID-beige mice (T, B, and natural killer cells deficient) of which only 3 yielded anaplastic tumors [87].

When using mice, one should bear in mind that tumor development and progression are influenced by the genetic background of the mice. It is known that some mice strains are tumor-resistant, while others can be highly susceptible to tumors [88]. Moreover, immune responses of transgenic mice affect tumor growth and the ability of the viral vector to infect the cells [86]

The lack of predictive models may delay the development of new therapeutic agents, thereby there is an urgent need for adequate skin disease models that better mimic the human condition.

Ex vivo models of BCC

There are a number of BCC explant models showing a high level of similarity to native tumors. Models based on decellularized human skin provide a proper microenvironment, but inter-donor variability leads to different responses, affecting the reproducibility of these assays [2].

Recently, Hochberg proposed a different way of using BCC biopsies in which skin tumors are sliced and maintained in culture medium. In this system, the sample 3D structure is conserved, keeping the original cell types and extracellular matrix products, positively impacting the results after anti-tumor treatments [86].

Explants models, however, depend on a continuous provision of tumor biopsies of suitable size, which is disadvantageous in drug evaluation studies [1].

In vitro models of BCC

In the last years, advances in the tissue engineering field have provided models to study diseased human skin and early neoplastic progression [7]. These models offer a better understanding of the biological properties of tumor cells, cell proliferation, gene activation, invasive phenotype, and allow the development of efficient therapies [2,63].

In vitro models developed for BCC consist mainly of 2D cultures. For instance, Grando et al. cultured BCC biopsies fragments and obtained different types of cells: normal fibroblasts, keratinocytes, and epithelioid spindle-shaped cells. Trypsin was used to remove contaminating fibroblasts, and normal keratinocytes-like cells were eliminated by cornification after increasing calcium concentration. The remaining cells belonged to nodular BCC, as judged by their biphasic morphology, slow growth, soft agar growing capability, ultrastructural similarities to nodular BCC, and the expression of several BCC-related markers [89].

Likewise, Asada et al. cultured explants from BCC biopsies on mitomycin-treated 3T3 feeder layers. Spindle-shaped cells grew from most of the BCC explants, with differential expression of a number of antibodies when compared to normal keratinocytes. Furthermore, unlike healthy keratinocytes, BCC cells were able to form colonies after being cultured in soft agar [90].

As *in vivo* studies have revealed keratinization impairments in BCC tumor cells, Flaxman and Van Scott studied the keratinization of BCC cells grown *in vitro*. They used biopsy

explants from patients having multiple BCCs, which were incubated in growth medium. Contrary to the *in vivo* situation, biopsy-derived cells presented a highly organized keratinization process, just as exhibited by the healthy counterpart. They concluded that BCC keratinization deficiency may be a reversible defect and that if cells could keratinize *in vivo*, it could lead to the generation of keratin cysts instead of skin tumors [91].

Regarding 3D models, a full-thickness equivalent was developed by Mahmudur to investigate the role of PTCH1 in BCC biology. The dermis component was produced with Matrigel, collagen, and fibroblasts. A keratinocytes cell line (NEB1) with PTCH1 suppression, was grown on top of the Matrigel layer. However, there was no recapitulation of BCC characteristics in the 3D model [61].

Since Lysyl oxidase (LOX) is associated with antitumor activity and is down-regulated in many carcinomas, Bouez et al. investigated its expression in BCC and developed a skin equivalent to study its effect on human keratinocytes behavior. Fibroblasts were seeded on a chitosan-cross-linked collagen-GAG matrix, and keratinocytes and HaCat cell lines (wild-type or LOX silenced) were seeded on top of it. They found an invasive phenotype in the skin equivalent where the protein LOX was specifically absent [92].

Table 4 summarizes the characteristics of different *in vitro* BCC models.

Table 4. In vitro models for BCC.

Model	Strengths	Weaknesses	Reference
Pure cultures of BCC cells obtained by selective elimination of FBs and normal KCs.	Pure culture of BCC cells that showed several similarities to freshly excised nodular BCC.	Bi-dimensional model.	[89]
BCC explants grown on a mitomycin-treated 3T3 feeder layer.	*In vitro* culture of BCC cells that conserve some *in vivo* features.	Bi-dimensional model.	[90]
BCC explants cultured in growth medium.	Allows a deeper understanding of keratinization of BCC cells.	Bi-dimensional model showing distinct keratinization pattern from *in vivo* BCC cells.	[91]
Matrigel, collagen, and a FBs dermal layer and KCs cell lines on top (PTCH1 gene suppression).	Showed that different cell lines lead to different outcomes.	Cell line use; no context of healthy epidermal cells.	[61]
FB within a chitosan-cross-linked collagen-GAG matrix and HaCat (LOX silenced) seeded on top of it.	Invasive tumor phenotype.	Cell lines may not show the same outcome compared to primary cells.	[92]

FBs: fibroblasts, KCs: keratinocytes

CONCLUSIONS

Several models have been developed to study normal and diseased skin. Here, we have presented the three main types of skin models: *in vivo, ex vivo*, and *in vitro*.

In vivo models are useful tools to understand highly complex skin processes, including immune and toxicological responses to external stimuli and tumor progression and spread. Animal skin, however, presents structural and genetic differences to human skin, hampering the correct prediction in the human context.

Ex vivo models are highly suitable to study human skin biology, as they contain all the major cellular and structural components of human skin. Their main disadvantage is the requirement of constant tissue supply and the donor variation they introduce.

In vitro models are a powerful alternative, as they are of human origin, do not require a continuous supply of biopsies, and contribute to the reduction of animal testing. Recent efforts have led to the development of different models of healthy and diseased skin, among which 3D skin equivalents stand out. They have been shown to recapitulate some of the most important characteristics of human skin such as epidermal differentiation, skin barrier formation, and interaction between different cell types, allowing epidermal models to be validated as platforms for chemical hazard identification. The challenge now is validate skin models with an additional dermal layer that can also respond to external stimuli and would more closely mimic the *in vivo* situation.

Currently, efforts are focused on adapting these models to study skin immunology and diseases, most of which are represented by 2D cultures or only involve the use of cell lines. Further improvement is therefore required in order to have systems that more faithfully mimic the real condition. As for immune models, the use of primary dendritic cells is encouraged, as they do not present the genetic or physical modifications of cell lines. In the case of skin cancer, it is necessary to culture cells with malignant potential in the context of a 3D network of healthy cells. To accomplish this goal, engineered human tissues that display the 3D human architecture and cellular composition are essential tools, given their superiority for modelling skin behavior.

THESIS AIM

The aim of the research described in this thesis was to develop full-thickness fibrin-based skin equivalents for applications in the toxicology, immunology, and cancer fields. To this end, we first determined the suitability of keratinocytes obtained by two culture systems (explants and feeder layers) to produce fibrin-based organotypic cultures. We next validated our model for toxicological purposes by evaluating the irritant and corrosive potential of different substances, according to the OECD guidelines. To further broaden the possible applications of the model, we increased its complexity by modulating the epidermal composition in 2 ways: 1) by adding immune cells precursors (CD14+ cells) and 2) by incorporating basal cell carcinoma-derived cells. The resulting skin equivalents were evaluated morphologically and functionally.

ACKNOWLEDGMENTS

REFERENCES

1. Bergers LIJC, Reijnders CMA, van den Broek LJ, Spiekstra SW, de Gruijl TD, Weijers EM, et al. Immune-competent human skin disease models. Drug Discov Today. 2016;21(9):1479–88.

2. Hill DS, Robinson NDP, Caley MP, Chen M, Toole EAO, Jane L. A novel fully-humanised 3D skin equivalent to model early melanoma invasion. Mol Cancer Ther. 2016;14(11):2665–73.

3. Costin G-E, Raabe H, Curren R. in Vitro Safety Testing Strategy for Skin Irritation Using the 3D Reconstructed Human Epidermis. Rom J Biochem. 2009;46(2):165–86.

4. Saito K, Nukada Y, Takenouchi O, Miyazawa M, Sakaguchi H, Nishiyama N. Development of a new in vitro skin sensitization assay (Epidermal Sensitization Assay; EpiSensA) using reconstructed human epidermis. Toxicol Vitr. 2013;27(8):2213–24.

5. Vinardell, MP1; Mitjans M. Alternative methods for eye and skin irritation tests: an overview. J Pharm Sci. 2008;1(97):46–59.

6. Ouwehand K, Spiekstra SW, Waaijman T, Scheper RJ, de Gruijl TD, Gibbs S. Technical advance: Langerhans cells derived from a human cell line in a full-thickness skin equivalent undergo allergen-induced maturation and migration. J Leukoc Biol. 2011 Nov;90(5):1027–33.

7. Garlick J a. Engineering skin to study human disease--tissue models for cancer biology and wound repair. Adv Biochem Eng Biotechnol. 2007;103(January):207–39.

8. Zhang Z, Michniak-Kohn BB. Tissue engineered human skin equivalents. Pharmaceutics. 2012;4(1):26–41.

9. L'OREAL - SKIN-SCIENCE. The dermis [Internet]. [cited 2016 Aug 5]. Available from: http://skin-science.com/_int/_en/topic/topic_sousrub.aspx?tc=SKIN_SCIENCE_ROOT%5EAN_ORGAN_REVEALED%5ETHE_DERMIS

10. Di Meglio P, Perera GK, Nestle FO. The Multitasking Organ: Recent Insights into Skin Immune Function. Immunity. 2011;35(6):857–69.

11. Ramin S, Shariati P, Shokrgozar MA, Vossoughi M, Eslamifar A. In vitro Co-Culture of Human Skin Keratinocytes and Fibroblasts on a Biocompatible and Biodegradable Scaffold. Vol. 13, Iranian Biomedical Journal. 2009.

12. Williams IR. Fibroblasts. In: Encyclopedia of Immunology [Internet]. Elsevier; 1998 [cited 2019 Dec 13]. p. 905–9. Available from: https://linkinghub.elsevier.com/retrieve/pii/B0122267656002486

13. Groeber F, Holeiter M, Hampel M, Hinderer S, Schenke-Layland K. Skin tissue engineering — In vivo and in vitro applications. Adv Drug Deliv Rev. 2011;63(4–5):352–66.

14. HeadandNeckCancerGuide.org. Skin Cancer Anatomy [Internet]. [cited 2016 Aug 6]. Available from: http://www.headandneckcancerguide.org/adults/introduction-to-head-and-neck-cancer/skin-cancer/anatomy/

15. Keratinocytes Structure and Function, Role in Immunity, and Differentiation [Internet]. [cited 2016 Aug 6]. Available from: http://www.keratinocyte-transfection.com/

16. Coquette A, Berna N, Vandenbosch A, Rosdy M, De Wever B, Poumay Y. Analysis of interleukin-1a (IL-1a) and interleukin-8 (IL-8) expression and release in in vitro reconstructed human epidermis for the prediction of in vivo skin irritation and/or sensitization. Toxicol Vitr. 2003;17(3):311–21.

17. Seité S, Zucchi H, Moyal D, Tison S, Compan D, Christiaens F, et al. Alterations in human epidermal Langerhans cells by ultraviolet radiation: quantitative and morphological study. Br J Dermatol. 2003;148(2):291–9.

18. Merad M, Ginhoux F, Collin M. Origin, homeostasis and function of Langerhans cells and other langerin-expressing dendritic cells. Nat Rev Immunol. 2008;8(12):935–47.

19. Aiba S, Terunuma A, Manome H, Tagami H. Dendritic cells differently respond to haptens and irritants by their production of cytokines and expression of co-stimulatory molecules. Eur J Immunol. 1997;27(11):3031–8.

20. European Union Reference Laboratory for alternatives to animal testing (EURL-ECVAM). Skin Irritation [Internet]. 2012 [cited 2016 Jul 14]. Available from: https://eurl-ecvam.jrc.ec.europa.eu/validation-regulatory-acceptance/topical-toxicity/skin-irritation

21. European Union Reference Laboratory for alternatives to animal testing (EURL-ECVAM). Skin Irritation [Internet]. [cited 2016 Aug 23]. Available from: https://eurl-ecvam.jrc.ec.europa.eu/validation-regulatory-acceptance/topical-toxicity/skin-irritation

22. Welss T, Basketter DA, Schröder KR. In vitro skin irritation: Facts and future. State of the art review of mechanisms and models. Toxicol Vitr. 2004;18(3):231–43.

23. Robinson MK, Cohen C, de Fraissinette A d. B, Ponec M, Whittle E, Fentem JH. Non-animal testing strategies for assessment of the skin corrosion and skin irritation potential of ingredients and finished products. Food Chem Toxicol. 2002 May;40(5):573–92.

24. Iribarren B. O, González G. C. Quemaduras por agentes químicos. Cuad Cirugía. 2001 Dec;15(1):61–9.

25. Saracco S. Recomendaciones para la atención de intoxicaciones por cáusticos [Internet]. [cited 2016 Sep 8]. Available from: http://www.msal.gob.ar/images/stories/ministerio/intoxicaciones/guias/recomendaciones.pdf

26. A Corrosive Substance [Internet]. [cited 2016 Jul 8]. Available from: https://www.scribd.com/document/246881187/A-Corrosive-Substance

27. Worth A, Barroso J, Bremer S, Burton J, Casati S, Coecke S, et al. Alternative methods for regulatory toxicology – a state-of-the-art review. Science and Policy Report by the Joint Research Centre. 2014. 1–30 p.

28. Medical dictionary. Skin sensitization [Internet]. [cited 2016 Aug 8]. Available from: http://medical-dictionary.thefreedictionary.com/skin+sensitization

29. Basketter D, Darlenski R, Fluhr JW. Skin irritation and sensitization: mechanisms and new approaches for risk assessment. Skin Pharmacol Physiol. 2008;21(4):191–202.

30. Skin Sensitisation Assessment [Internet]. [cited 2016 Aug 11]. Available from: http://www.cyprotex.com/topicalandcosmetics/skinsensitisation

31. Facy V, Flouret V, Régnier M, Schmidt R. Reactivity of Langerhans cells in human reconstructed epidermis to known allergens and UV radiation. Toxicol Vitr. 2005;19(6):787–95.

32. Tuschl H, Kovac R. Langerhans cells and immature dendritic cells as model systems for screening of skin sensitizers. Toxicol In Vitro. 2001;15(4–5):327–31.

33. Kerimoğlu O, Şahbaz S. Animal Skin Models for Percutaneous Absorption Studies. J Biopharm Ther Challenges. 2018;2(1):1.

34. Avci P, Sadasivam M, Gupta A, De Melo WC, Huang YY, Yin R, et al. Animal models of skin disease for drug discovery. Vol. 8, Expert Opinion on Drug Discovery. 2013. p. 331–55.

35. Summerfield A, Meurens F, Ricklin ME. The immunology of the porcine skin and its value as a model for human skin. Vol. 66, Molecular Immunology. Elsevier Ltd; 2015. p. 14–21.

36. Abd E, Yousef SA, Pastore MN, Telaprolu K, Mohammed YH, Namjoshi S, et al. Skin models for the testing of transdermal drugs. Vol. 8, Clinical Pharmacology: Advances and Applications. Dove Medical Press Ltd; 2016. p. 163–76.

37. Ranamukhaarachchi SA, Schneider T, Lehnert S, Sprenger L, Campbell JR, Mansoor I, et al. Development and Validation of an Artificial Mechanical Skin Model for the Study of Interactions between Skin and Microneedles. Macromol Mater Eng. 2016 Mar;301(3):306–14.

38. Megrab NA, Williams AC, Barry BW. Oestradiol permeation through human skin and silastic membrane: effects of propylene glycol and supersaturation. J Control Release. 1995;36(3):277–94.

39. Lotz C, Kiesewetter L, Schmid FF, Hansmann J, Walles H, Groeber-Becker F. Replacing the Draize eye test: Impedance spectroscopy as a 3R method to discriminate between all GHS categories for eye irritation. Sci Rep. 2018 Dec 1;8(1):1–13.

40. Genoskin. Ready-to-use ex vivo human skin models for cosmetic testing [Internet]. 2018 [cited 2019 Dec 12]. Available from: https://www.genoskin.com/skin-models-cosmetic-testing/

41. Corzo-León DE, Munro CA, MacCallum DM. An ex vivo Human Skin Model to Study Superficial Fungal Infections. Front Microbiol. 2019 Jun 5;10.

42. Andrade TA, Aguiar AF, Guedes FA, Leite MN, Caetano GF, Coelho EB, et al. Ex vivo model of human skin (hOSEC) as alternative to animal use for cosmetic tests. In: Procedia Engineering. Elsevier Ltd; 2015. p. 67–73.

43. Xu W, Jong Hong S, Jia S, Zhao Y, Galiano RD, Mustoe TA. Application of a partial-thickness human ex vivo skin culture model in cutaneous wound healing study. Lab Investig. 2012 Apr;92(4):584–99.

44. Augustin C, Collombel C, Damour O. Use of Dermal Equivalent and Skin Equivalent

Models for in Vitro Cutaneous Irritation Testing of Cosmetic Products: Comparison with in Vivo Human Data. J Toxicol Cutan Ocul Toxicol. 1998 Jan 27;17(1):5–17.

45. Poumay Y, Coquette A. Modelling the human epidermis in vitro: Tools for basic and applied research. Arch Dermatol Res. 2007;298(8):361–9.

46. EpiDerm^TM - Overview - MatTek Corporation [Internet]. Available from: https://www.mattek.com/products/epiderm/

47. EpiSkin. SkinEthic RHE Reconstructed Human Epidermis [Internet]. [cited 2021 Aug 1]. Available from: https://www.episkin.com/SkinEthic-RHE

48. EpiSkin. EpiSkin epidermal model [Internet]. [cited 2021 Aug 1]. Available from: https://www.episkin.com/Episkin

49. Hoffmann J, Heisler E, Karpinski S, Losse J, Thomas D, Siefken W, et al. Epidermal-skin-test 1000 (EST-1000) - A new reconstructed epidermis for in vitro skin corrosivity testing. Toxicol Vitr. 2005 Oct;19(7):925–9.

50. Biomimiq. Leiden epidermal skin model (LEM) [Internet]. [cited 2016 Sep 20]. Available from: http://www.biomimiq.com/products/Healthy Skin Models/Epidermal Skin Model (LEM)

51. MacNeil S. Progress and opportunities for tissue-engineered skin. Nature. 2007 Feb 22;445(7130):874–80.

52. MatTek. EpiDermFT in vitro 3D Tissue | MatTek Life Sciences [Internet]. [cited 2021 Aug 1]. Available from: https://www.mattek.com/products/epidermft/

53. Rasmussen C, Gratz K, Liebel F, Southall M, Garay M, Bhattacharyya S, et al. The StrataTest® human skin model, a consistent in vitro alternative for toxicological testing. Toxicol In Vitro. 2010 Oct;24(7):2021–9.

54. CellSystems. Specification Sheet AST2000 (Advanced Skin Test 2000) Human Full Thickness Skin Model [Internet]. [cited 2021 Aug 1]. Available from: www.cellsystems.biz

55. Morales M, Pérez D, Correa L, Restrepo L. Evaluation of fibrin-based dermal-epidermal organotypic cultures for in vitro skin corrosion and irritation testing of chemicals according to OECD TG 431 and 439. Toxicol Vitr. 2016;36:89–96.

56. Régnier M, Staquet M-J, Schmitt D, Schimdt R. Integration of Langerhans Cells into a Pigmented Reconstructed Human Epidermis. J Invest Dermatol. 1997 Oct;109(4):510–2.

57. Régnier M, Patwardhan a, Scheynius a, Schmidt R. Reconstructed human epidermis composed of keratinocytes, melanocytes and Langerhans cells. Med Biol Eng Comput. 1998;36(November):821–4.

58. Kosten IJ, Spiekstra SW, de Gruijl TD, Gibbs S. MUTZ-3 derived Langerhans cells in human skin equivalents show differential migration and phenotypic plasticity after allergen or irritant exposure. Toxicol Appl Pharmacol. 2015;287(1):35–42.

59. Bock S, Said A, Müller G, Schäfer-korting M, Zoschke C, Weindl G. Characterization of reconstructed human skin containing Langerhans cells to monitor molecular events in skin sensitization. Toxicol Vitr. 2018;46:77–85.

60. Skin Cancer: Melanoma, Basal Cell and Squamous Cell Carcinoma [Internet]. [cited 2018 Apr 7]. Available from: https://www.webmd.com/melanoma-skin-cancer/guide/skin-cancer#1-1

61. Mahmudur M. Characterisation of a novel in vitro model of Basal cell carcinoma (BCC) through stable PTCH1 suppression in immortalised human keratinocytes. Queen Mary Unoversity of London; 2013.

62. World Health Organization. Radiation: Ultraviolet (UV) radiation and skin cancer [Internet]. 2017 [cited 2021 Aug 7]. Available from: https://www.who.int/news-room/q-a-detail/radiation-ultraviolet-(uv)-radiation-and-skin-cancer

63. Odashiro AN, Pereira PR, Marshall JC, Godeiro K, Burnier MN. Skin cancer models. Drug Discov Today Dis Model. 2005;2(1):71–5.

64. Spandidos D, Carutu C, Constantin C, Boda D, Zurac S, Spandidos DA, et al. Chemically induced skin carcinogenesis: Updates in experimental models (Review). Oncol Rep. 1994;35(5):2516–28.

65. Skin Cancer Foundation. Skin Cancer Facts & Statistics [Internet]. [cited 2021 Jul 30]. Available from: https://www.skincancer.org/skin-cancer-information/skin-cancer-facts/

66. Caulin C, Nguyen T, Lang GA, Goepfert TM, Brinkley BR, Cai W-W, et al. An inducible mouse model for skin cancer reveals distinct roles for gain- and loss-of-function p53 mutations. J Clin Invest. 2007 Jul;117(7):1893–901.

67. Canadian Cancer Society. What is non-melanoma skin cancer? [Internet]. [cited 2018 Apr 7]. Available from: http://www.cancer.ca/en/cancer-information/cancer-type/skin-non-melanoma/non-melanoma-skin-cancer/?region=on

68. Samarasinghe V, Madan V. Nonmelanoma skin cancer. J Cutan Aesthet Surg. 2012;5(1):3–10.

69. Gober MD, Bashir HM, Seykora JT. Reconstructing skin cancers using animal models. Cancer Metastasis Rev. 2013;32(1–2):123–8.

70. Wu X, Elkin EE, Marghoob AA. Burden of basal cell carcinoma in USA. Futur Oncol. 2015;11(22):2967–74.

71. Tyagi N, Bhardwaj A, Srivastava SK, Arora S, Marimuthu S, Deshmukh SK, et al. Development and Characterization of a Novel in vitro Progression Model for UVB-Induced Skin Carcinogenesis. Sci Rep. 2015;5(13894):1–11.

72. The Skin Cancer Foundation. Basal Cell Carcinoma Treatment [Internet]. [cited 2019 Dec 12]. Available from: https://www.skincancer.org/skin-cancer-information/basal-cell-carcinoma/bcc-treatment-options/#curettage

73. Sekulic A, Migden MR, Oro AE, Dirix L, Lewis KD, Hainsworth JD, et al. Efficacy and Safety of Vismodegib in Advanced Basal-Cell Carcinoma. N Engl J Med. 2012 Jun 7;366(23):2171–9.

74. Herzberg A, Garcia J, Kerns B, Jordan P, Pence J, Rotter S, et al. DNA ploidy of basal cell carcinoma determined by image cytometry of fresh smears. J Cutan Pathol. 1993;20(3):216–22.

75. Böcking A, Schunck K, Auffermann W. Exfoliative-cytologic diagnosis of basal-cell

carcinoma, with the use of DNA image cytometry as a diagnostic aid. Acta Cytol. 1987;31(2):143–9.

76. Kawasaki RS, Caldeira LF, André FS, Gasques JAL, Castilho WH, Bozola AR, et al. Translocation (4;14) and concomitant inv(14) in a basal cell carcinoma. Cancer Genet Cytogenet. 1991 Oct 15;56(2):177–80.

77. Kawasaki R, Caldeira L, André F, Gasques J, Castilho W, Bozola A, et al. Multiple cytogenetic clones in a basal cell carcinoma. Cancer Genet Cytogenet. 1991;54(1):33–8.

78. Koyama N, Nishihira J, Nakabayashi H, Nishi S, Hoshi N, Fujimoto S, et al. Aneuploidy of sex chromosomes in basal cell carcinoma: Its clonality and involvement in the development of carcinogenesis. Int J Oncol. 2000;16:15–23.

79. Semlin L, Schäfer-Korting M, Borelli C, Korting HC. In vitro models for human skin disease. Drug Discov Today. 2011;16(3–4):132–9.

80. Aszterbaum M, Epstein J, Oro A, Douglas V, LeBoit PE, Scott MP, et al. Ultraviolet and ionizing radiation enhance the growth of BCCs and trichoblastomas in patched heterozygous knockout mice. Nat Med. 1999;5(11):1285–91.

81. Nicolas M, Wolfer A, Raj K, Kummer JA, Mill P, van Noort M, et al. Notch1 functions as a tumor suppressor in mouse skin. Nat Genet. 2003;33(3):416–21.

82. Oro AE, Higgins KM, Hu Z, Bonifas JM, Epstein EH, Scott MP. Basal cell carcinomas in mice overexpressing sonic hedgehog. Science. 1997;276(5313):817–21.

83. Xie J, Murone M, Luoh S-M, Ryan A, Gu Q, Zhang C, et al. Activating Smoothened mutations in sporadic basal-cell carcinoma. Nature. 1998;391(6662):90–2.

84. Nilsson M, Unden AB, Krause D, Malmqwist U, Raza K, Zaphiropoulos PG, et al. Induction of basal cell carcinomas and trichoepitheliomas in mice overexpressing GLI-1. Proc Natl Acad Sci. 2000;97(7):3438–43.

85. Grachtchouk M, Mo R, Yu S, Zhang X, Sasaki H, Hui C, et al. Basal cell carcinomas in mice overexpressing Gli2 in skin. Nat Genet. 2000;24(3):216–7.

86. Hochberg M. Experimental Models for BCC. J Dermatology Clin Res. 2013;1(1).

87. Carlson JA, Combates NJ, Stenn KS, Prouty SM. Anaplastic neoplasms arising from basal cellcarcinoma xenotransplants into SCID-beige mice. J Cutan Pathol. 2002;29(5):268–78.

88. Huang P, Balmain a. Modeling Cutaneous Squamous Carcinoma Development in the Mouse. Cold Spring Harb Perspect Med. 2014;1–24.

89. Grando SA, Schofield OM, Skubitz AP, Kist DA, Zelickson BD, Zachary CB. Nodular basal cell carcinoma in vivo vs in vitro. Establishment of pure cell cultures, cytomorphologic characteristics, ultrastructure, immunophenotype, biosynthetic activities, and generation of antisera. Arch Dermatol. 1996;132(10):1185–93.

90. Asada M, Schaart F-M, Detmar M, Mischke D, de Almeida HL, Gollnick H, et al. Growth Characteristics and Differentiation of Basal Cell Carcinoma In Vitro–Immunohistochemical, Gel Electrophoretic, and Ultrastructural Analysis. J Invest Dermatol. 1992;99(4):474–81.

91. Flaxman BA, Van Scott EJ. Keratinizationin vitro of Cells From a Basal Cell Carcinoma. JNCI J Natl Cancer Inst. 1968;40(2):411–22.

92. Bouez C, Reynaud C, Noblesse E, Liethe¤ Pot A, Gleyzal C, Kanitakis J, et al. The Lysyl Oxidase LOX Is Absent in Basal and Squamous Cell Carcinomas and Its Knockdown Induces an Invading Phenotype in a Skin Equivalent Model. Hum Cancer Biol. 2006;12(5):1463–9.

CHAPTER 2

Explant culture and feeder as a source keratınocytes for the constructıon of human skın equıvalents: a pılot study

C. Gaviria [a,b], N.Y. Becerra [a], L.A. Correa [a,c,d], S. Estrada [a], L.M. Restrepo [a,e]

[a]Tissue Engineering and cell therapy research Group, School of Medicine, University of Antioquia, Colombia
[b]European Research Institute for the Biology of Ageing, University Medical Center Groningen, The Netherlands
[c]Dermatology Department, School of Medicine, University of Antioquia, Colombia
[d]Laboratorio Clínico VID, Congregación Mariana, Colombia
[e]Medical Research Institute, School of Medicine, University of Antioquia, Colombia

ABSTRACT

Human skin equivalents (HSEs) are *in vitro* models constructed from primary human cells isolated from skin biopsies. The function and morphology of primary cells are particularly dependent on the donor and the cell isolation and culture method, which are crucial factors for achieving reliable skin tissues.

In this study, two approaches were used to obtain keratinocytes: explant culture and a feeder layer of mouse fibroblasts. Skin samples were taken from three patients and each sample was processed by both methods. For the construction of HSEs, explant culture and feeder layer-derived keratinocytes, in both low and high passages, were seeded on a fibrin gel containing fibroblasts. The morphology and expression of epidermal markers were evaluated by hematoxylin-eosin staining and immunohistochemistry. The integrity of the epidermal barrier was studied by measuring the transepithelial electrical resistance.

Both methods produced fibrin-based HSEs showing similar morphological characteristics to those of native skin and expressing epidermal differentiation markers. Keratinocytes were able to differentiate and the integrity of thigh junctions was confirmed. The use of a feeder layer allowed a faster growth of keratinocytes, which generated a healthier, thicker, and more organized epidermis, improving the outcome obtained with explant culture.

INTRODUCTION

Human skin equivalents (HSEs) are bioengineered skin substitutes composed of primary cells (keratinocytes, fibroblasts, and/or stem cells) and/or components of the extracellular matrix. In the last decades, tremendous efforts have been made in the research and development of HSEs, leading to skin models for the evaluation of pharmaceutical and cosmetic products. Those accepted by international bodies like the European Centre for the Validation of Alternative Methods (ECVAM) are composed of human keratinocytes seeded on a support and cultured in such a way as to form a differentiated epidermis, mimicking the architecture of human skin, and allowing the direct application of various chemicals [1,2].

An essential step for producing HSEs is cell isolation and culture. Today, the most common methods for isolating keratinocytes from skin biopsies are based on the use of explant fragments and feeder layers. In the former, cells are obtained by cutting the skin into small pieces which are placed on a cell culture dish and air-dried until proper attachment is achieved. Basal keratinocytes migrate from the skin fragment occupying the culture surface, and fibroblasts only grow until some days later. However, one of the main limitations of the explant method is that fibroblasts may outgrow the keratinocytes [3]. Therefore, they must be harvested before they can take over the culture. Additionally, calcium and serum-containing media can lead to the rapid differentiation of basal keratinocytes, decreasing their proliferative capacity and applicability in subsequent applications.

The second approach, the gold standard method, is based on Green and Rheinwald's studies [4]. Keratinocytes are disaggregated by proteolytic enzymes and cell suspensions are seeded on lethally irradiated mouse fibroblasts that promote human keratinocytes growth [5,6]. Among its many advantages, Green and Rheinwald's protocol has led to high expansion rates [4,7,8], preservation of keratinocyte stemness, and regenerative capacity. There has been no evidence of adverse effects on cell growth and development due to the use of mouse cells [7,9].

Previous work in our group showed the feasibility of obtaining fibrin-based skin substitutes with explant culture as a source of keratinocytes [10]. The question remains as to whether such models can benefit from the advantages associated with Green and Rheinwald's method. We, therefore, investigated whether keratinocytes obtained by using a fibroblasts feeder layer are as suitable as explants to produce fibrin-based skin models.

MATERIALS AND METHODS

Skin cells isolation and culture

After informed consent, skin samples were obtained from blepharoplasties leftovers performed at the IPS Universitaria of the University of Antioquia, Colombia. The samples were taken from 3 patients, 2 men and 1 woman, aged from 46 to 53 years.

Each sample was divided into 2 equal pieces and explant culture and fibroblasts feeder layer were used as culture methods. For the former, the protocol described by Morales et al. [10] was followed. Briefly, skin biopsies were mechanically fragmented and placed on T25

culture flasks (Falcon™) with no media to allow attachment. Then, DMEM supplemented with 10% (v/v) fetal bovine serum (FBS) and 1% (v/v) penicillin-streptomycin (all from Lonza) was added. Both keratinocytes and fibroblasts were obtained. To keep fibroblasts from taking over the entire culture, fragments of epidermis were carefully cut and placed on the flask surface.

For the second approach, described by Rheinwald and Green [4], we used mitomycin C-treated murine fibroblasts (3T3/J2) as a feeder layer for keratinocytes. Skin samples were mechanically fragmented and incubated (37°C, 5% CO_2) in 0.25% Trypsin/EDTA (Sigma-Aldrich) under stirring. Then, a cell strainer (70 μm) was used, and disaggregated cells were cultured in T25 flasks containing mitomycin C-treated 3T3/J2 cells and QN medium. QN consisted of DMEM:HAM F12 (3:1) (Lonza/Sigma) supplemented with 10% (v/v) FBS, 1% penicillin/streptomycin (Lonza), 1% L-glutamine (Lonza), 8 ng/mL cholera toxin (Life Technologies), 24 μg/mL adenine, 5 μg/mL insulin, 0.4 μg/ mL hydrocortisone and 1.3 ng/mL triiodothyronine (all from Sigma).The medium was changed every 2–3 days. 10 ng/mL Epidermal Growth Factor (Austral Biologicals) was added to QN medium, now called QC, on the 3rd day.

Fibroblasts were also obtained by seeding cell suspensions in T25 flasks containing DMEM supplemented with 10% (v/v) fetal bovine serum (FBS) and 1% (v/v) penicillin-streptomycin.

To investigate the effect of cell passage number, propagation of cells obtained by both methods was performed on mitomycin C-treated 3T3 fibroblasts. Therefore, for each sample, 4 culture conditions were used: 1) Low passage (P1) cells obtained by explant culture, 2) High passage (P>1) cells obtained by explant culture, 3) P1 cells obtained by feeder layer, and 4) P>1 cells obtained by feeder layer.

Human skin equivalents construction

For the construction of the dermal equivalent, Morales' protocol was followed [10]. Briefly, a mix of human plasma, 0.9% NaCl (Corpaul), Tranexamic Acid (Ropsohn), and a fibroblast solution (0.7×10^4 cells/mL) was prepared. To promote fibrin polymerization, 1% $CaCl_2$ (Sigma) was added and the solution was gently mixed, poured into a 12-well plate Corning 3460 Transwell, and incubated (37 °C, 5% CO_2) for 15 min.

Once the dermal gel was formed, 3×10^4 keratinocytes were seeded on top, and the HSE was kept in QN medium for 3 days and then QC was added. After 7 days, the culture was exposed to the air-liquid interface for 14 days more to stimulate keratinocytes differentiation.

For every culture condition, at least 3 HSEs were produced.

Histology and immunohistochemistry

On the 21st day, HSEs were fixed in 10% paraformaldehyde. After fixation, tissues were dehydrated and embedded in paraffin. Five micrometers sections were cut and stained with hematoxylin-eosin (H&E). The slides were examined under the microscope.

For immunostaining, 4 µm sections were washed and rehydrated with ethanol/xylene. Primary antibody was incubated for 1 h at room temperature and, after 2 washes with TBST, horseradish peroxidase was used for the subsequent color-based reaction. The antibodies used for epidermal characterization were: mouse monoclonal anti-Cytokeratin 14, mouse monoclonal anti-Loricrin, and mouse monoclonal anti-Integrin (all from Abcam).

Transepithelial electrical resistance (TEER) measurement

TEER measurement was used to evaluate the integrity of tight junctions as an indicator of the tightness of the epidermal barrier [11]. On the 21st day, culture media was removed and 800 µL of PBS was added into both apical and basolateral sides. For measurements, a Millicell-ERS2 volt-ohm meter (Millipore, Bedford, MA, USA) was used. A pair of electrodes were immersed into the insert and the outer well.

To assess the impedance, a squared wave current was applied. Results from at least three different measurements for each tissue replicate were recorded. The mean values are expressed in ohms per unit of surface area.

RESULTS

Co-culture with 3T3 cells yields higher amounts of keratinocytes

After an average of 14 days following biopsy processing, cells from all samples were harvested by trypsinization. The average keratinocytes density of the three biopsies is reported in Figure 1. The feeder layer approach yielded significantly higher amounts of keratinocytes when compared with the explant culture method.
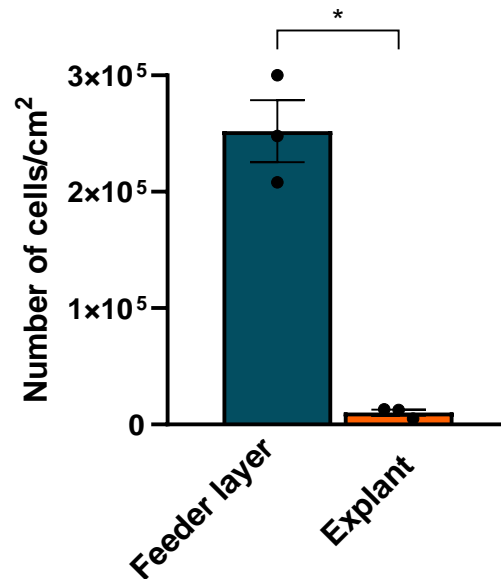

*Figure 1. Cell density obtained after the first harvest. Data represent the mean ± SEM of 3 samples. For statistical analysis, a two-tailed t-test was applied. *p≤0.05*

Feeder layer-derived HSEs show higher histological resemblance to native skin

After 21 days of culture, histological and immunohistochemical characteristics of the HSEs were evaluated.

H&E staining of tissues composed of cells of 3 different samples, processed by 2 different methods, and in both low and high passages are presented in Figure 2. A separation between dermis and epidermis can be seen in all cases. Feeder layer-derived HSEs (Figure 2a and b) displayed a healthy, thick epidermis with columnar basal cells. The formation of the 4 different epidermal layers can be appreciated as well: basal layer (black head arrow), spinous layer (blue head arrow), granular layer (red head arrow), and horny layer (green head arrow). Moreover, necrosis is low and a healthy fibroblasts populated dermis is present.

Even though explant-derived HSEs showed a thick epidermis, keratinocytes seem to be unorganized and the four layers are not easily distinguishable (Figures 2d-f). Sample 3 derived-HSEs showed impairment in the differentiation process, regardless of the cell culture method (Figure 2c, f).

On the other hand, high passage keratinocytes (P>1) formed a tissue where the epidermis is not as continuous and thick as expected, and the formation of the four epidermal differentiation stages is not always present (Figures 2g-l). In some cases, there is no evidence of stratum corneum formation (Figures 2g, h, j, k), and basal cells were already flattened or irregular (Figures 2i-l). A certain degree of parakeratosis is present in sample 3 HSEs (yellow head arrows).

Together, these results indicate that cells grown on a murine 3T3 feeder layer are able to produce skin models with more morphological similarities to native skin, especially in early passages.
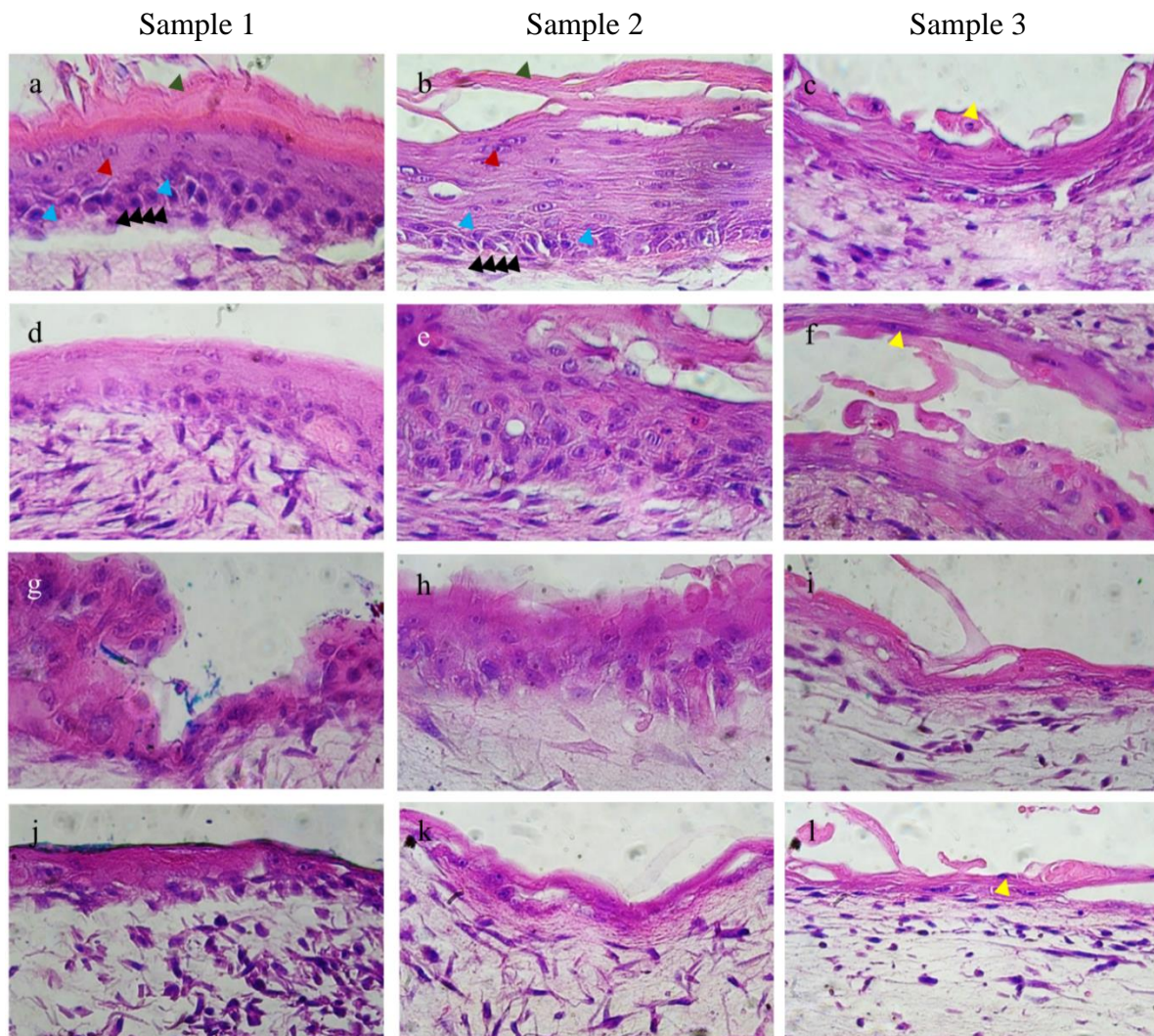

Figure 2. Histological characteristics of HSEs determined by H&E staining. a), b) and c) Low passage feeder layer-derived HSEs of samples 1, 2, and 3; d), e) and f) Low passage explant culture-derived HSEs of samples 1, 2, and 3; g), h) and i) High passage feeder layer-derived HSEs of samples 1, 2 and 3; j), k) and l) High passage explant culture-derived HSEs of patients 1, 2 and 3. 80X.

Feeder layer-derived keratinocytes produce HSEs with more epidermal cell layers

Next, we evaluated epidermal thickness by assessing the number of cell layers in the models (Figure 3). To this end, the number of cell layers in the epidermis of different H&E images sections were counted. Significant differences were found between HSEs with low and high

passages keratinocytes, regardless of the cell culture method, as well as between different methods. Low passage keratinocytes of both explant culture and feeder layer, gave rise to tissues with a higher number of cell layers, doubling the high passage counterpart. Explant culture cells, of both low and high passages, provided significantly fewer layers when compared to feeder layer-derived cells.

Feeder layer HSEs showed to be the approach that generated the overall greatest epidermal thickness and, importantly, the passage number significantly compromised the number of epidermal layers.
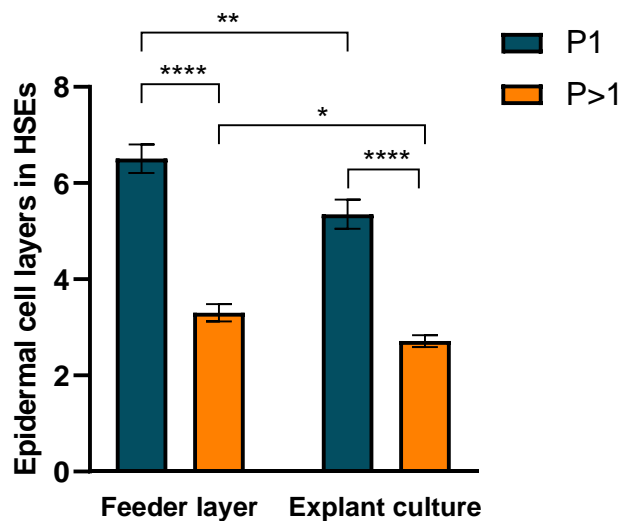

Figure 3. Number of epidermal cell layers in HSEs composed of cells obtained by explant culture or feeder layer. Data represent the mean ± SEM of at least 7 image sections per culture condition. For statistical analysis, a two-tailed t-test was applied. *p≤0.05, **p≤0.01, ****p≤0.0001

Expression of epidermal markers is no affected by keratinocytes source

Figure 4 shows the immunohistochemistry staining of three epidermal markers expressed by HSEs.

Cytokeratin 14 (K14) is one of the major structural proteins of stratifying epithelia and is synthesized by the basal proliferative layer [12]. The HSEs showed a strong K14 expression (Figure 4a, d, g, and j), comparable to that of human skin (Figure 4m).

Integrin plays an important role as one of the components of hemidesmosomes and serves as an anchoring site between dermis and epidermis [13]. Although to a lesser extent than native skin (Figure 4n), integrin staining was stronger in the basal layer of the HSEs (Figure 4b, e, h, and k).

In order to evaluate the formation of the stratum corneum, loricrin expression was examined. Loricrin is a terminally differentiating structural protein comprising more than 70% of the cornified envelope. Even though its presence is faint, it was found, predominantly, in the horny layer of both feeder layer and explant culture HSEs (Figure 4c, f, i, and l). Its presence in HSEs in which incomplete differentiation was found, as judged by histology results (Figure 2), is indicative of premature differentiation (Figure 4f and l).

These results indicate that the expression pattern of cytokeratin 14, integrin, and loricrin is not affected by keratinocytes culture method nor passage.

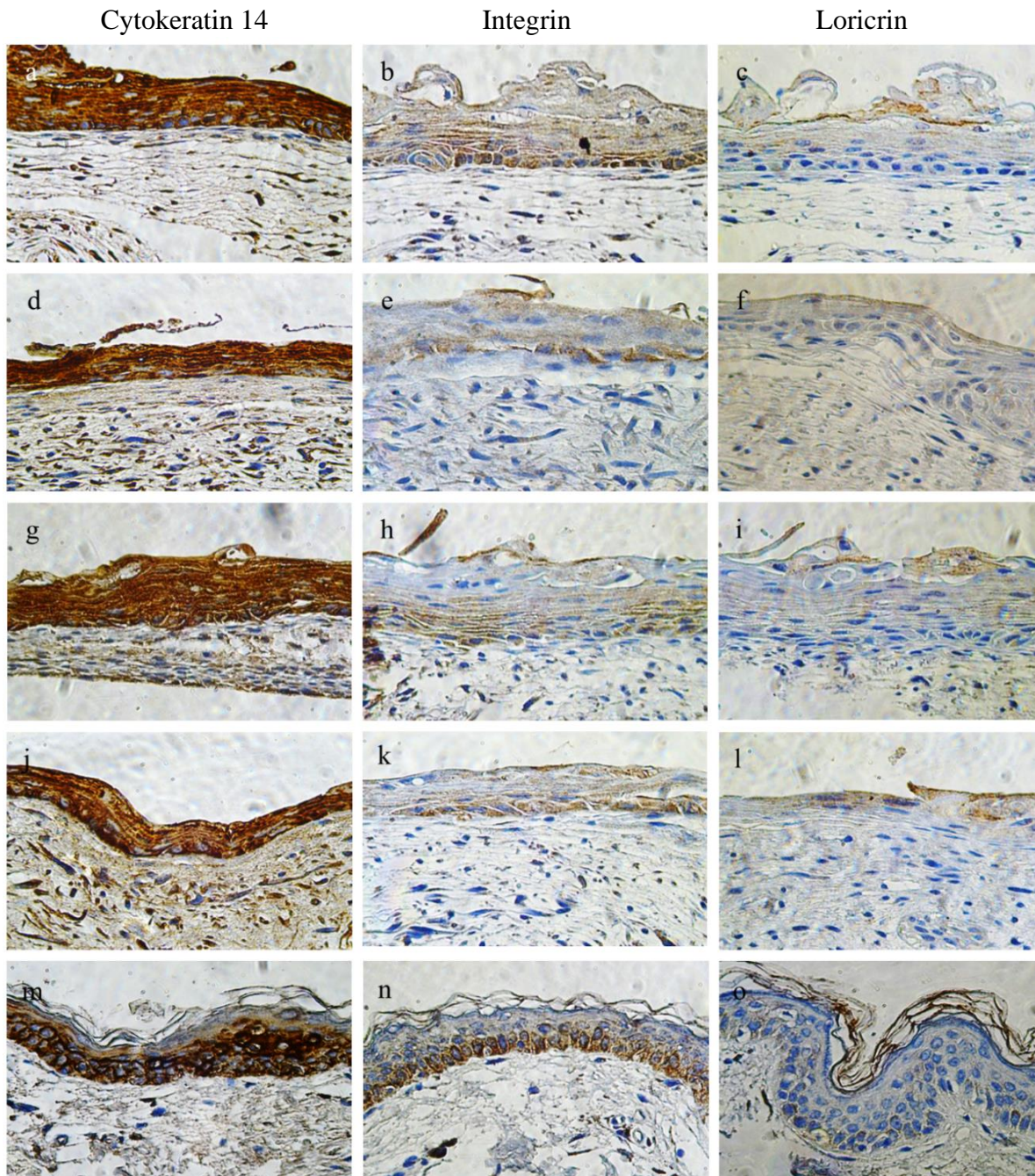| Cytokeratin 14	Integrin	Loricrin

Figure 4. Expression pattern of epidermal markers HSEs. Cytokeratin 14 expression of a) Low passage feeder layer HSEs, d) High passage feeder layer HSEs, g) Low passage explant culture HSEs, j) High passage explant culture HSEs, and m) native skin. Integrin expression of b) Low passage feeder layer HSEs, e) High passage feeder layer HSEs, h) Low passage explant culture HSEs, k) High passage explant culture HSEs, and n) native skin. Loricrin expression of c) Low passage feeder layer HSEs, f) High passage feeder layer HSEs, i) Low passage explant culture HSEs, l) High passage explant culture HSEs, and o) native skin. Images are representative of all the samples. 80X.

Transepithelial Electrical Resistance is affected by cell passage

As transepithelial electrical resistance (TEER) values are indicative of tight junction strength, the integrity of the barrier function of HSEs was evaluated by measuring the TEER in all tissues after 21 days of culture (Figure 5). There were no differences in TEER between cell culture approaches, but significant differences were found between HSEs composed of P1 and P>1 keratinocytes. Low passage keratinocytes of both explant culture and feeder layer, gave rise to tissues with tighter epidermal barriers when compared to the high passage counterpart. These data suggest that high passage keratinocytes may show synthesis and/or functional defects of tight junction proteins when producing HSEs.
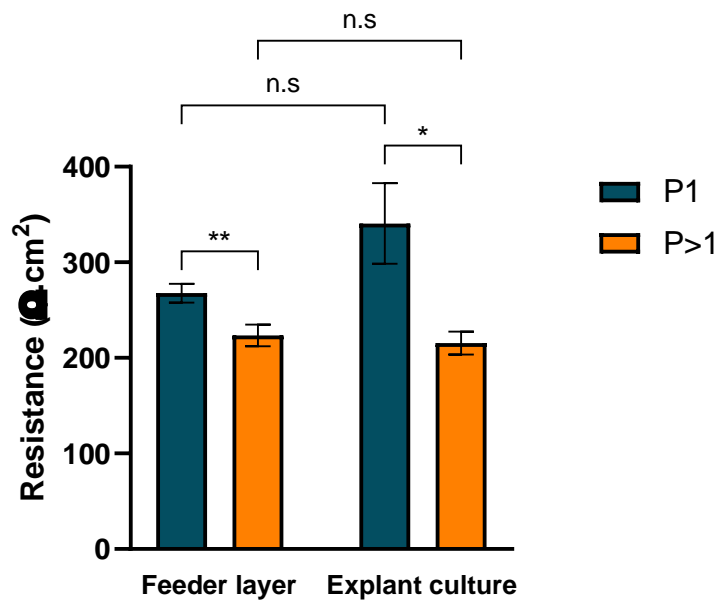

Figure 5. TEER of HSEs composed of cells obtained by explant culture or feeder layer. Data represent the mean ± SEM of at least 3 tissues per culture condition. For statistical analysis, a two-tailed t-test was applied. n.s: non-significant; *p≤0.05; ** p≤0.01.

DISCUSSION

In this study, we investigated the feasibility of feeder layer-derived keratinocytes to generate fibrin-based skin models, using explant culture cells for comparison. We found that feeder layer-derived cells produced HSEs with similar morphological and immunohistochemical characteristics to native skin. Moreover, they displayed improved histological features when compared to explant culture-derived models.

Our results showed that keratinocytes yield after co-culture with murine fibroblasts was significantly higher than that of the explant method. It is known that feeder layers release extracellular matrix proteins and growth factors that promote keratinocytes growth [5,6]. Moreover, they can detoxify the culture medium, act as a substrate for the attachment of cells, contribute to the suppression of keratinocyte differentiation, and extend keratinocytes' life span [7,9]. Therefore, the 3T3 feeder layer allows keratinocytes to conserve the proliferative and undifferentiated state, increasing the final yield.

For explants, the final yield depends on 1) the number and dimension of the skin fragments, 2) the presence of a proliferative promoting agent, and 3) the presence of calcium in culture media. Thus, the number of cells is dictated by the size of the biopsy and the media that indirectly promotes the rapid differentiation of cells. A number of studies have highlighted the importance of using low calcium concentration during the first days of culture since this ion reduces the proliferation rate and promotes sequential differentiation [15–18]. In this work, low calcium concentration was not used, which likely contributed to the lower number of keratinocytes obtained by this method.

Orazizadeh et al. [3] compared the enzymatic and explant methods for monolayer cultures of keratinocytes. In contrast to our results, they found no attachment of skin cells to either feeder layer or type I collagen scaffold. Perhaps, seeding cell density was not high enough or trypsin treatment was harsh. However, the authors found that explant keratinocytes could grow for multiple passages and expressed pan-cytokeratin when plated on a collagen scaffold surface, which confirms the importance of having extracellular matrix support for the long-term growth of keratinocytes.

Concerning 3D models, histology results showed that P1 feeder layer-derived keratinocytes were able to generate tissues that more closely resembled human skin structure. In native skin, each layer of the epidermis is characterized by a unique morphology and function of cells that lose their columnar shape as they differentiate. Such transition was more evident in P1 feeder layer-derived HSEs, which, accordingly, presented columnar-shaped cells in the basal layer, and anucleated cells in the corneum stratum, in addition to greater epidermal thickness. In opposition, HSEs composed of explant culture cells presented a less organized differentiation process.

As keratinocytes express specific proteins and cytokeratins along their differentiation path, we examined the presence of cytokeratin 14, integrin, and loricrin in HSEs. There were no considerable differences in the expression of differentiation markers between HSEs, irrespective of the culture method and passage number. All HSEs were positive to cytokeratin 14, integrin, and loricrin, indicative of a stratification process. The slighter strong staining of

integrin in P1 feeder layer-derived skin models can be explained by the higher amount of columnar-shaped basal cells, which results in a more developed basement membrane. Importantly, P>1 HSEs expressed loricrin despite presenting incomplete stratification, suggesting disturbances in the differentiation process. In effect, models lacking stratum corneum presented flattened basal cells in the first layers of the epidermis.

HSEs composed of P1 cells showed significantly higher levels of TEER when compared to high passage models, indicating that the integrity of the barrier function was improved and suggesting that cells health plays an important role in HSEs development. In fact, the lowest resistance values correspond to HSEs with the thinner and unstratified epidermis, as judged by H&E results. Considering that culture time and calcium presence contribute to keratinocytes differentiation [15–18], it is expected that early passage cultures contain a greater number of cells with high proliferative capacity that can lead to the formation of stronger tight junctions, more cell layers, and a continuous basal layer.

Our finding that low passage feeder layer-derived cells are associated with improved fibrin-based skin models, indicates the importance of cell fitness when HSEs are constructed. Keratinocytes seeded on a dermal support should initially proliferate and cover the surface, thanks to the cells in a basal and undifferentiated state. Differentiation is later induced by exposure to the air-liquid interface and by the confluence itself. Consequently, seeding differentiated and low proliferative keratinocytes (i.e high passage cells) will hinder the epithelialization of the dermal surface, leading to impairments in the stratification process. As we did not study the effect of low calcium, we cannot discount the possibility that healthy cells in higher passages can be obtained with other nutritionally optimized media.

In summary, this work shows that feeder layer-derived keratinocytes are suitable to generate fibrin-based HSEs. When compared to explant culture HSEs, histological features were improved. Of note, a tighter epidermal barrier was achieved when early passage keratinocytes were used. These results highlight the necessity of using undifferentiated and highly proliferative epidermal cells when skin models are constructed.

ACKNOWLEDGMENTS

REFERENCES

1.   Zhang Z, Michniak-Kohn BB. Tissue engineered human skin equivalents. Pharmaceutics. 2012;4(1):26–41.

2.   Vinardell, MP1; Mitjans M. Alternative methods for eye and skin irritation tests: an overview. J Pharm Sci. 2008;1(97):46–59.

3.   Orazizadeh M, Hashemitabar M, Bahramzadeh S, Dehbashi FN, Saremy S. Comparison of the enzymatic and explant methods for the culture of keratinocytes isolated from human foreskin. 2015;1–5.

4.   Rheinwald JG, Green H. Serial cultivation of strains of human epidermal keratinocytes: the formation of keratinizing colonies from single cells. Cell. 1975;6(3):331–43.

5.   Gragnani A, Sobral C, Ferreira L. Thermolysin in human cultured keratinocyte isolation. Brazilian J Biol. 2007;67(1):105–9.

6.   Dragunova J, Kabat P, Koller J. Skin explant cultures as a source of keratinocytes for cultivation. Cell Tissue Bank. 2013 Jun;14(2):317–24.

7.   Green H. The birth of therapy with cultured cells. BioEssays. 2008;30(9):897–903.

8.   Llames SG, Del Rio M, Larcher F, García E, García M, José Escamez M, et al. Human plasma as a dermal scaffold for the generation of a completely autologous bioengineered skin. Transplantation. 2004;77(3):350–5.

9.   Gray TE, Thomassen DG, Mass MJ, Barrett JC. Quantitation of cell proliferation, colony formation, and carcinogen induced cytotoxicity of rat tracheal epithelial cells grown in culture on 3T3 feeder layers. In Vitro. 1983;19(7):559–70.

10. Morales M, Pérez D, Correa L, Restrepo L. Evaluation of fibrin-based dermal-epidermal organotypic cultures for in vitro skin corrosion and irritation testing of chemicals according to OECD TG 431 and 439. Toxicol Vitr. 2016;36:89–96.

11. Srinivasan B, Kolli AR, Esch MB, Abaci HE, Shuler ML, Hickman JJ. TEER measurement techniques for in vitro barrier model systems. J Lab Autom. 2015;20(2):107–26.

12. Rugg EL, Irwin McLean W, Birgitte Lane E, Pitera R, McMillan JR, Dopping-Hepenstal PJ, et al. A functional "knockout" of human keratin 14. Genes Dev. 1994;8(21):2563–73.

13. Geuijen CAW, Sonnenberg A. Dynamics of the alpha6beta4 integrin in keratinocytes. Mol Biol Cell. 2002;13(11):3845–58.

14. Guo A, Jahoda CAB. An improved method of human keratinocyte culture from skin explants: cell expansion is linked to markers of activated progenitor cells. Exp Dermatol. 2009 Aug;18(8):720–6.

15. Pillai S, Bikle DD, Mancianti M-L, Cline P, Hincenbergs M. Calcium regulation of growth and differentiation of normal human keratinocytes: Modulation of differentiation competence by stages of growth and extracellular calcium. J Cell Physiol. 1990;143(2):294–302.

16. Bikle DD, Xie Z, Tu C-L. Calcium regulation of keratinocyte differentiation. Expert Rev

Endocrinol Metab. 2012;7(4):461–72.

17.   Borowiec A-S, Delcourt P, Dewailly E, Bidaux G. Optimal Differentiation of In Vitro
        Keratinocytes Requires Multifactorial External Control. Mantovani R, editor. PLoS
        One. 2013 Oct;8(10):e77507.

18.   Elsholz F, Harteneck C, Muller W, Friedland K. Calcium - a central regulator of
        keratinocyte differentiation in health and disease. Eur J Dermatology. 2014;24(6):650–
        61.

CHAPTER 3

Dermo-epidermal organotypic cultures for the *in vitro* evaluation of skin irritation and corrosion

C. Gaviria [a,b], N.Y. Becerra [a], J.D. Vergara [a], L.A. Correa [a,c,d], S. Estrada [a], L.M. Restrepo [a,e]

[a]*Tissue Engineering and cell therapy research Group, School of Medicine, University of Antioquia, Colombia*
[b]*European Research Institute for the Biology of Ageing, University Medical Center Groningen, The Netherlands*
[c]*Dermatology Department, School of Medicine, University of Antioquia, Colombia*
[d]*Laboratorio Clínico VID, Congregación Mariana, Colombia*
[e]*Medical Research Institute, School of Medicine, University of Antioquia, Colombia*

ABSTRACT

In recent years different *in vitro* skin models for chemical hazard identification have been developed. Most of them consist only of human keratinocytes, neglecting the contribution of other skin constituents. Cultures containing the dermal and epidermal components provide an attractive system to investigate, in a more realistic model, toxicological responses, which represents a distinct advantage over keratinocytes-based models that do not faithfully mimic the *in vivo* environment.

This study aimed to validate dermo-epidermal organotypic cultures (ORGs) as a platform to perform irritation and corrosion tests. Skin models were constructed by seeding keratinocytes on fibroblast-containing fibrin gels. Following the 431 and 439 OECD tests guidelines, the irritant and corrosive potential of 30 substances were determined by means of viability measurements (MTT assay). Cytokine release was used as a second endpoint for the evaluation of irritants. For comparison, the commercially available EpiDerm^{TM} model was also tested.

Skin models displayed similar histological characteristics to native skin and were able to classify different substances with high accuracy, showing their applicability to skin irritation and corrosion tests. Cytokines release showed to be a complex process, as judged by the distinct upregulation between chemicals and models. Further studies are required to confirm how cytokine release is linked to irritation potential.

INTRODUCTION

The skin can be damaged after topical exposure to several chemicals, leading to irritation and corrosion. Irritation is characterized by reversible damage of the tissue, resulting in a local inflammatory reaction that is manifested through the release of cytokines, erythema, and edema. Corrosion irreversibly damages the epidermis and the dermis, beyond repair, causing ulcers and bleeding. Consequently, the assessment of potential human health risks posed by chemical substances is required by many regulatory bodies such as the OECD (Organization for Economic Co-operation and Development) before commercialization [1,2].

Nowadays, studies for chemical hazard identification are mainly based on animal experiments. One of the most popular methods is the Draize test, which attempts to predict the possible irritation or corrosion by applying chemicals on the skin and connective tissue of rabbits [3,4]. Nevertheless, ethical issues raised by animal research have led to the development of *in vivo* systems to evaluate skin toxicological responses. Most of them consist of human keratinocytes deposited on special supports and cultured in such a way as to form a stratified epidermis, mimicking the architecture of human skin, and allowing the direct application of various chemicals [2,5].

Among commercially available human skin models, EpiDerm, EpiSkin, and SkinEthic RHE [3,5]. However, they are only composed of keratinocytes, ignoring the effect of other skin constituents that can respond to toxic stimuli and express secondary inflammatory biomarkers. Cultures containing the dermal and epidermal components could provide an attractive *in vivo* system to investigate, in a more realistic model, toxicological skin responses. This represents a distinct advantage over keratinocytes-based models, which do not mimic faithfully the *in vivo* environment [6]. To date, there are not commercially available, validated dermo-epidermal models used for evaluating the effects of chemical substances.

By developing a fibrin-based dermal-epidermal organotypic culture (ORG), preliminary results from previous work in our group showed a system with the potential to classify chemical substances [7]. The aim of this study was to validate the performance of our in-house model as a system for chemical hazard identification, by performing irritation and corrosion tests with 30 different chemical substances (19 of which are contained in the most recent OECD test guidelines –TG-), along with cytokine release quantification. For comparison, the validated commercial model EpiDerm[TM] was tested as well.

MATERIALS AND METHODS

EpiDerm[TM] model

Given that the full-thickness model EpiDerm[FT] is not yet validated by OECD for irritation and corrosion tests, here, we use the widely known and validated epidermal model EpiDerm[TM], which is a highly differentiated tissue consisting of normal, human-derived epidermal keratinocytes cultured on specially prepared tissue culture inserts.

EpiDerm[TM] tissues (EPI-200-SIT and EPI-200-SCT) were obtained from MatTek Corporation. DMEM based media for maintaining cultures was supplied by the manufacturer (EPI-100-NMM and EPI-100-ASY). The tissues were maintained according to the supplier's

instructions: upon reception, models were inspected and transferred to 6-well plates prefilled with medium and pre-incubated, for 1h, at 37°C, 5% CO_2, and 95% RH. At the end of the pre-incubation period, inserts were transferred to new wells and EPI-200-SIT tissues were incubated again overnight. EPI-200-SCT tissues were used immediately.

Skin cells isolation and culture

After informed consent, human skin samples were obtained from blepharoplasties and circumcisions' leftovers.

Based on Morales' protocol [7], skin samples were taken and mechanically fragmented. Fragments were either placed on T25 culture flasks (Falcon™) or incubated (37°C, 5% CO_2) in 0.25% Trypsin/EDTA (Sigma-Aldrich) under stirring. Skin fragments and half of the cells obtained after Trypsin treatment, were cultured in DMEM supplemented with 10% (v/v) fetal bovine serum (FBS) and 1% (v/v) penicillin-streptomycin (all from Lonza).

To grow keratinocytes, suspension cells were cultured in a mitomycin C-treated 3T3 feeder layer and QN medium. QN consisted of DMEM:HAM F12 (3:1) (Lonza/Sigma) supplemented with 10% (v/v) FBS, 1% penicillin/ streptomycin (Lonza), 1% L-glutamine (Lonza), 8 ng/mL cholera toxin (Life Technologies), 24 µg/mL adenine, 5 µg/mL insulin, 0.4 µg/ mL hydrocortisone and 1.3 ng/mL triiodothyronine (all from Sigma). The medium was changed every 2-3 days. 10 ng/mL Epidermal Growth Factor (Austral Biologicals) was added to QN medium, now called QC, at day 3-4.

ORGs construction

For the construction of the dermal equivalent, Morales' protocol was used [7]. Briefly, a mix of human plasma, 0.9% NaCl (Corpaul), tranexamic acid (Ropsohn), and a fibroblast solution ($7x10^3$ cells/mL) was prepared. To promote fibrin polymerization, 1% $CaCl_2$ (Sigma) was added, and the solution was gently mixed, poured into a 12-well plate Corning 3460 Transwell, and incubated (37°C, 5% CO_2) for 15 minutes.

Once the dermal gel was formed, $27x10^3/cm^2$ keratinocytes were placed on top and the ORGs were kept in QN medium for 3 days. On day 4, QC was added. After 7 days, the culture was exposed to the air-liquid interface for 14 days to stimulate keratinocytes differentiation.

Histological studies

On the 21st day, ORGs were collected and fixed in 10% paraformaldehyde at room temperature. After fixation, tissues were dehydrated and embedded in paraffin. Five micrometers sections of the samples were stained with hematoxylin-eosin (H&E). The stained slides were examined under the microscope.

Skin corrosion test

The test was carried out on the 21st day of culture. Sixteen chemicals, 7 non-corrosives, and 9 corrosives were evaluated (see Table 1) following 431 OECD test guidelines [8]. The ORGs and EPI-200-SCT tissues were topically treated with the test substances for 3 min and 60 min. 8N KOH and H_2O were used as positive and negative controls, respectively. After

exposure, tissues were washed and the MTT assay was performed immediately. Two tissue replicates were used for each chemical substance, control, and exposure time.

Skin irritation test

The test was carried out on the 21st day of culture. Fourteen chemicals, 6 non-irritants, and 8 irritants were evaluated (see Table 1) following 439 OECD test guidelines [9]. The ORGs and EPI-200-SIT tissues were topically treated with the test substances for 60 min (25 min at room temperature and 35 min at standard conditions). 5% SDS and 0.9% NaCl were used as positive and negative controls, respectively. Following exposure, tissues were washed and incubated again for 42h. After 24h, supernatants were harvested and stored at -20°C for cytokine release analysis. At the end of incubation time, the MTT assay was performed. Three tissue replicates were used for each chemical substance and control.

Acceptability criteria

Based on 431 and 439 OECD test Guidelines, a tissue batch was considered as conforming if:

- For Epiderm™, the mean OD values of the negative control are between 0.8 and 2.8 for every exposure time.
- For the ORGs, the mean OD values of the negative control are between 0.6 and 2.8 for every exposure time, as it is the range that includes all OECD validated models.
- The mean viability of the tissue replicates exposed for 1 hour to the positive control is < 15%.
- For irritation, the standard deviation (SD) is ≤ 18.
- For corrosion, in the range 20 - 100% viability, the Coefficient of Variation (CV) between tissue replicates is ≤ 30%.

The run was only valid if tissue replicates and controls meet their respective acceptance criteria.

To evaluate the barrier function of the tissues an acceptability range for the IC50 was established based on EpiSkin™ and LabCyte EPI-MODEL24 SIT values. A range between 1 and 4 mg/mL was accepted.

Table 1. Characteristics of tested substances.

Test substance	# CAS	Chemical class	MSDS classification
Water	7732-18-5	Neutral inorganic	Non-irritant
Isopropanol	67-63-0	Alcohol	Non-irritant
Tween 20 10% (w/v)	9005-64-5	Non-ionic surfactant	Non-irritant
Methyl stearate	112-61-8	Ester	Non-irritant
Heptyl butyrate	5870-93-9	Ester	Non-irritant
Hexyl salicylate	6259-76-3	Ester	Non-irritant
Naphthaleneacetic acid	86-87-3	Aromatic compound	Irritant
1-methyl-3-phenyl-1-piperazine	5271-27-2	Organic base	Irritant
1-Bromohexane	111-25-1	Halocarbon	Irritant
Potassium hydroxide 5% (w/v)	1310-58-3	Inorganic base	Irritant

Triton X-100 1% (w/v)	9002-93-1	Non-ionic surfactant	Irritant
Cyclamen aldehyde	103-95-7	Aldehyde	Irritant
Cinnamaldehyde	104-55-2	Electrophile	Irritant
Sodium dodecyl sulfate 1% (w/v)	151-21-3	Anionic surfactant	Irritant
Eugenol	97-53-0	Neutral organic	Non-corrosive
Calcium carbonate	471-34-1	carbonic salt	Non-corrosive
Phenethyl bromide	103-63-9	Electrophile	Non-corrosive
Sodium carbonate	497-19-8	Inorganic base	Non-corrosive
4-Amino-1,2,4-triazole	584-13-4	Organic base	Non-corrosive
4-(Methylthio)benzldehyde	3446-89-7	Electrophile	Non-corrosive
Lauric acid	143-07-7	Organic acid	Non-corrosive
Sodium dodecyl sulfate 20% (w/v)	151-21-3	Anionic surfactant	Corrosive
Potassium hydroxide 10% (w/v)	1310-58-3	Inorganic base	Corrosive
Bromoacetic acid	79-08-3	Organic acid	Corrosive
Glyoxylic acid monohydrate	563-96-2	Organic acid	Corrosive
Ethanolamine	141-43-5	Organic base	Corrosive
Hydrochloric acid 14.4% (v/v)	7647-01-0	Inorganic acid	Corrosive
Boron trifluoride dihydrate	13319-75-0	Inorganic acid	Corrosive
Dichloroacetyl chloride	79-36-7	Electrophile	Corrosive
Trizol*30)	-	Monophasic solution	Corrosive

*431 OECD Test guideline covers the use of phenol as a test substance. In this work, Trizol was used instead, which contains more than 50% content of phenol, along with Guanidinium thiocyanate, both classified as corrosives.

Viability assay

At the end of chemical treatment, tissue viability was evaluated by the MTT assay. Tissue samples were washed with 0.9% NaCl and the medium of each well was replaced by 600 μL of MTT (Alfa Aesar) solution (1 mg/mL in PBS -Sigma-) at the basolateral side. Tissues were incubated at standard conditions for 3 hours. The MTT was removed, and the tissues were washed with 0.9% NaCl. The culture inserts were then immersed in 2 ml/well of isopropanol for the extraction of formazan crystals, and culture plates were covered with parafilm, protected from light, and left at room temperature overnight. After extraction, samples of the formazan solution of each well were mixed and transferred in three aliquots of 200 μL each into 96-well plates. The optical density (OD) of the samples was read at 570 nm and corrected against blanks. Viability was expressed as a percentage relative to negative controls:

$$\% \, Viability = \frac{OD \, sample}{OD \, negative \, control} x100$$

To identify the substances that may reduce MTT into formazan, a pre-check was performed by mixing the test substance with MTT solution and incubating it for 60 min at standard conditions. If the MTT mixture containing the test chemical turned blue/purple, the test chemical was presumed to reduce the MTT and freeze-killed controls were used. These control tissues then underwent the whole skin corrosion or irritation test. The true tissue viability was then calculated as follows:

$$\% \, Viability = \frac{OD \; living \; tissue - OD \; freeze \; killed \; tissue}{OD \; negative \; control} x100$$

Barrier function (IC50 assay)

After 21 days of culture, the IC50 assay was carried out. Eight concentrations of SDS (from 0 to 5 mg/mL) were tested and cell viability was assessed at 18 h. A curve fitting was performed and the IC50 value was estimated by the SDS concentration required to reduce cell viability by 50%. Three tissue replicates were used for each concentration.

Proinflammatory cytokines release assay

Proinflammatory cytokines were detected in the media harvested from tissues 24 h after the irritation test. To this end, a Cytometric Bead Array human inflammatory cytokines kit (Becton Dickinson) was used. Each bead in the kit provides a capture surface for Interleukin 1β (IL-1β), Interleukin 6 (IL-6), Interleukin-8 (IL-8), Interleukin10 (IL-10), and Tumor Necrosis Factor α (TNF-α). The assay was performed according to supplier instructions.

Prediction model

The prediction models to assess chemical hazard were based on 431 and 439 OECD test guidelines, which use viability thresholds to classify a substance as irritant, corrosive, or none (Table 2).

Table 2. Prediction models based on viability endpoint.

Prediction model	Viability	Classification
Irritation	≤ 50% after 60 min exposure	Irritant
	> 50% after 60 min exposure	Non-irritant
Corrosion	< 50% after 3 min exposure	Corrosive
	≥ 50% after 3 min exposure and < 15% after 60 min exposure	Corrosive
	≥ 50% after 3 min exposure and ≥ 15% after 60 min exposure	Non-corrosive

Statistical analysis

Data are presented as mean ± standard deviation (SD). Quantitative differences between samples and the viability threshold were assessed by the one-way student's t-test and a p-value < 0.05 was considered statistically significant.

Contingency table statistics were used for evaluating the predictive ability of the models. Specificity corresponds to the percentage of non-irritant chemicals (according to the MSDS classification) identified as non-irritants in our test. Sensitivity represents the percentage of irritant chemicals (according to the MSDS classification) identified as irritants in our test. Accuracy corresponds to the overall percentage of correct classification.

RESULTS

Histological characteristics of the skin models

After 21 days of culture, histological characteristics of the ORGs were evaluated.

H&E staining of the skin model is presented in Figure 1. For comparison, an image of the validated commercial model EpiDerm^{TM} is also shown. A separation between dermis and epidermis can be seen (dashed line) in both native skin and the ORGs. In both models (Figure 1a and b) a healthy and thick epidermis and intercellular spaces (blue arrow) are observed. Our model presents an epidermal thickness similar to that of native skin, while the one of EpiDerm^{TM} is thicker. It is possible to see the four different epidermal layers: basal layer (black head arrow), spinous layer (blue head arrow), granular layer (red head arrow), and horny layer (green head arrow). Moreover, necrosis is low and a healthy dermis is present.

Columnar-like basal cells are present in EpiDerm^{TM} (Figure 1b) and native skin (Figure 1c). In our model, basal cells were not that easily distinguishable.

Figure 1. Histological characteristics of the skin models determined by H&E staining. a) ORGs, b) EpiDerm^{TM}, and c) native human skin. A separation between dermis and epidermis (dashed line), intercellular spaces (blue arrow), basal layer (black head arrow), spinous layer (orange head arrow), granular layer (red head arrow), and horny layer (green head arrow) are shown. 80X.

Barrier function (IC50 assay)

To evaluate the ability of the stratum corneum of the ORGs to resist the rapid penetration of SDS, the IC50 of ORGs value was determined. Upon application of various SDS concentrations (from 0 to 5 mg/mL) and subsequent viability measurement, the value required to reduce tissue viability by 50% was determined to be 2.009 mg/mL (Figure 2).
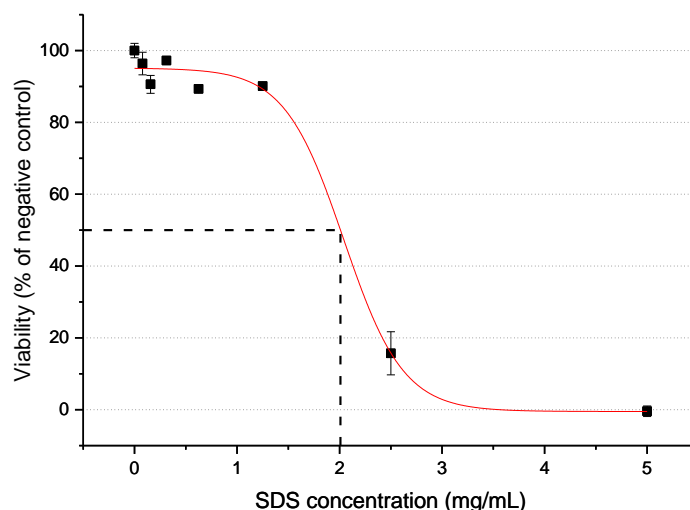
Figure 2. IC50 curve for a representative batch of the ORGs. Dashed lines show the IC50 value, which was determined by curve fitting (red).

Skin corrosion test

For the in-house model, 16 substances were evaluated. The OD values of the negative control of different batches varied between 0.6 and 1.7, meeting the acceptance criteria of $0.6 \leq$ OD ≤ 2.8. The mean viability of the positive control (relative to negative control) varied between 3.2% and 11.7%, meeting the acceptance criteria of < 15%. In the range 20 - 100% viability, the CV was $\leq$ 30% for all substances except for Phenithyl bromide at 60min.

According to viability results (Figure 3) and MSDS classification (Table 1), all substances, but Phenithyl bromide, were correctly classified (Table 6). For the calculations, invalid tests were considered misclassified.

In the case of EpiDerm^{TM}, 7 chemicals were tested. The acceptance criteria for negative control OD was not met for Lauric acid, 4-(Methylthio) benzaldehyde, and boron trifluoride dehydrate (3.3 ± 0.5), but was correct for all the other substances (1.5 ± 0.01). The mean viability of the positive control (relative to negative control) varied between 1.3% and 11.9%, meeting the acceptance criteria of < 15%. In the range 20 - 100% viability, the CV was $\leq$ 30%, for all substances except for KOH 10% at 60min.

EpiDerm^{TM} correctly classified 3 out of 7 substances (Figure 4 and Table 6). For the calculations, invalid tests were considered misclassified.
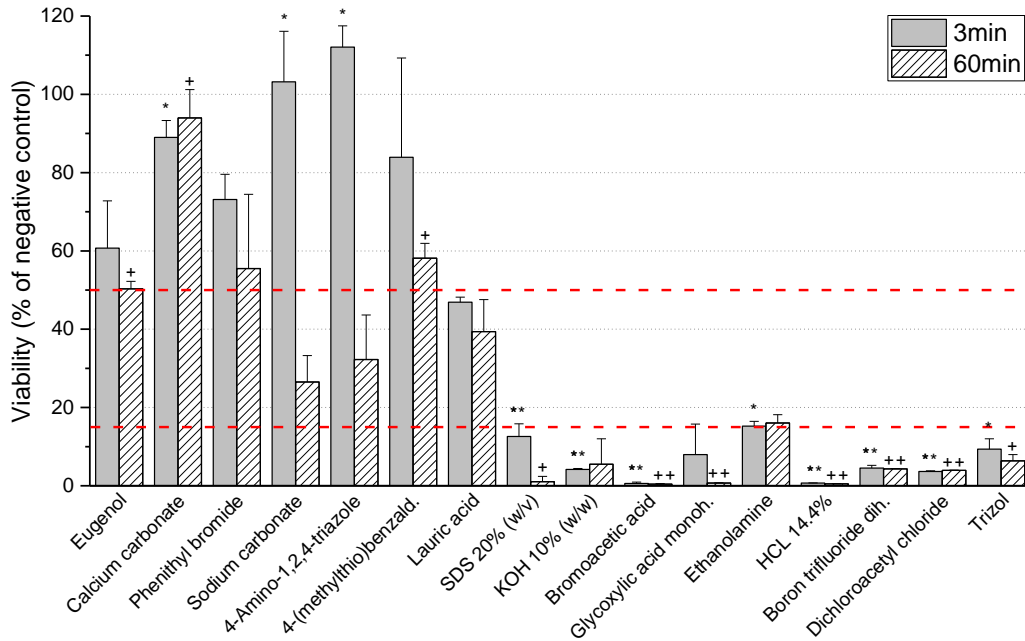
*Figure 3. ORGs viability after exposure to corrosive substances, according to 431 OECD TG. Dashed lines indicate 15% and 50% viability thresholds. Data shown represent the mean ± SD for n=2. *p < 0.05, **p < 0.01, and ***p < 0.001 compared to 50% viability threshold. +p < 0.05, ++p < 0.01 compared to 15% viability threshold.*
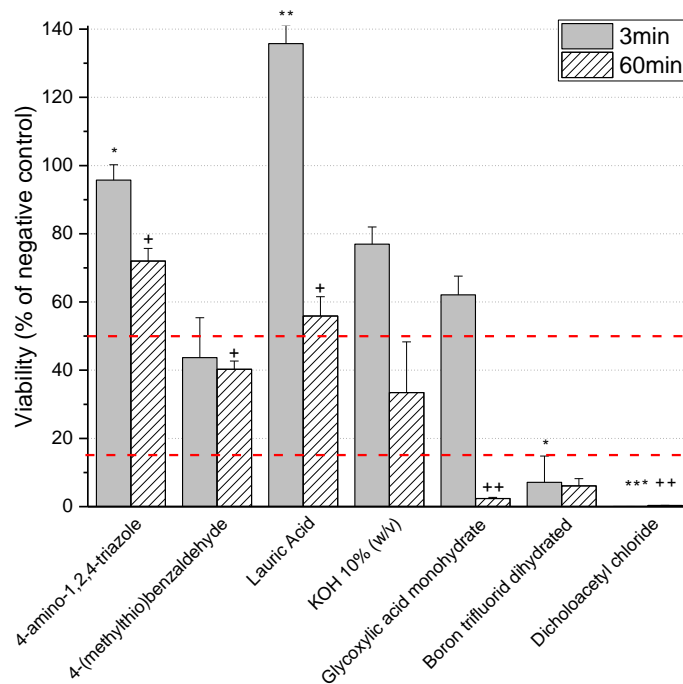

*Figure 4. EpiDerm^{TM} viability after exposure to corrosive substances, according to 431 OECD TG. Dashed lines indicate 15% and 50% viability thresholds. Data shown represent the mean ± SD for n = 2. *p < 0.05, **p < 0.01, and ***p < 0.001 compared to 50% viability threshold. +p < 0.05, ++p < 0.01 compared to 15% viability threshold.*

Skin irritation test

For the in-house model, 14 substances were evaluated. The OD values of the negative control of different batches varied between 0.6 and 1.7, meeting the acceptance criteria of $0.6 \leq OD \leq 2.8$. The mean viability of the positive control (relative to negative control) varied between 3.2% and 11.7%, meeting the acceptance criteria of $< 15\%$, and the SD was always $\leq 18\%$.

According to viability results (Figure 5) and MSDS classification (Table 1), all substances but Tween 20 (10%) and Methyl stearate were correctly classified (Table 6).

In the case of EpiDerm^{TM}, 12 chemicals were tested. The negative control OD varied between 1.8 and 1.9, meeting the acceptability criteria. The mean viability of the positive control (relative to negative control) varied between 4.2% and 5.5%, meeting the acceptance criteria of $< 15\%$, and the SD was always $\leq 18\%$.

EpiDerm^{TM} correctly classified 9 out of 12 substances. Isopropanol, 1-Bromohexane, and KOH 5% were misclassified (Figure 6 and Table 6).
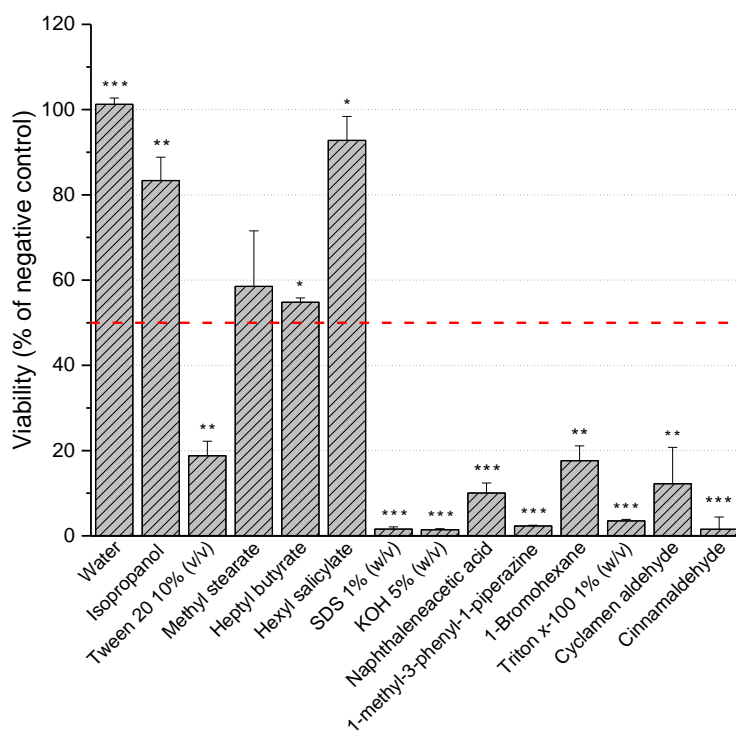

*Figure 5. ORGs viability after exposure to irritant substances, according to 439 OECD TG. Dashed line indicates 50% viability threshold. Data shown represent the mean $\pm$ SD for $n = 3$. *$p < 0.05$, **$p < 0.01$, and ***$p < 0.001$ compared to 50% viability threshold.*
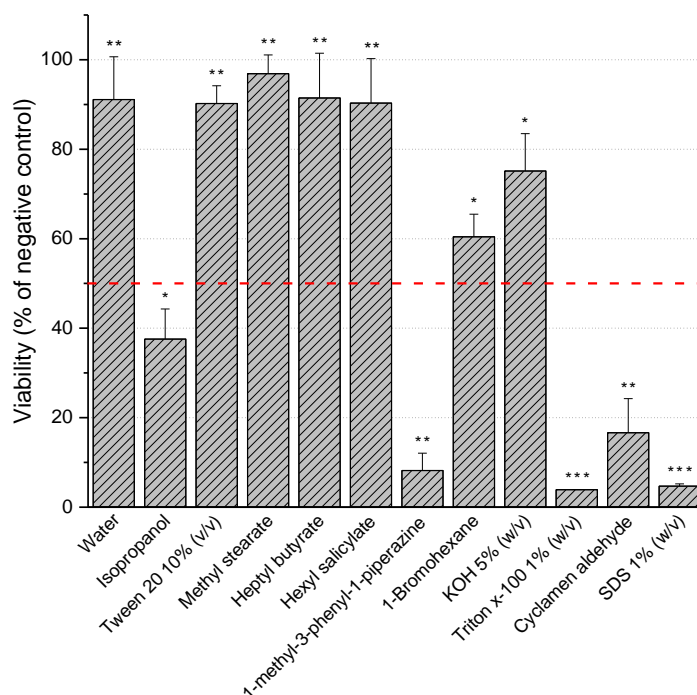
Figure 6. EpiDerm^TM viability after exposure to irritant substances, according to 439 OECD TG. Dashed line indicates 50% viability threshold. Data shown represent the mean ± SD for n = 3. *p < 0.05, **p < 0.01, and ***p < 0.001 compared to 50% viability threshold.

Proinflammatory cytokines release assay

In response to chemically-induced tissue trauma, skin cells release inflammatory chemokines and cytokines [10]. To determine whether cytokines release could be used as an irritation predictor, 5 different cytokines were measured (IL-1β, IL-6, IL-8, IL-10, and TNF-α).

Our model did not show considerable cytokine increase following irritant exposure. Instead, a tendency for cytokine reduction was observed after the challenge (Table 3). Interestingly, ORGs secreted outstanding amounts of IL-6 and IL-8 even in basal conditions, while with both irritant and non-irritant compounds, IL 10 and TNF were released in small quantities, below the detection limit, which may explain their high variability.

Compared to our model, EpiDerm^TM released lower quantities of IL-1β, IL-6, and IL-8 for all tested substances (Table 4), although IL-6 and IL-8 presented the highest values as well. TNF-α levels were higher than those found in our model, but there was no considerable change during the tests. IL-10 was not detected at all. Interestingly, all irritants, but SDS, induced IL-8 release after exposure (more than 80% over negative control).

Table 3. Cytokine release in ORGs following irritation tests

Test substance	IL-1β		IL-6		IL-8		IL-10		TNF-α	
	pg/mL	IL/NC	pg/mL	IL/NC	pg/mL	IL/NC	pg/mL	IL/NC	pg/mL	IL/NC
Water	11.0 ± 5.4	0.3	4489.0 ± 1648.7	1.2	4624.4 ± 2676.6	0.4	0.2 ± 0.2	1.0	6.6 ± 5.7	1.2
Isopropanol	12.3 ± 4.5	0.3	3700.2 ± 2151.5	1.0	2727.3 ± 3253.4	0.2	0.1 ± 0.1	0.7	5.5 ± 4.7	1.0
Tween 20 10% (w/v)	93.1 ± 93.2	5.9	4874.9 ± 2192.4	0.8	7633.0 ± 3807.6	1.0	0.3 ± 0.3	1.4	4.8 ± 4.2	0.8
Methyl stearate	30.3 ± 14.5	0.8	3660.7 ± 2541.7	3.7	2002.5 ± 586.9	1.3	0.5 ± 0.5	0.1	5.6 ± 5.0	0.9
Heptyl butyrate	39.1 ± 36.5	3.1	2203.4 ± 1922.9	0.7	7443.5 ± 4842.2	1.3	0.3 ± 0.3	2.3	5.5 ± 4.8	1.0
Hexyl salicylate	23.1 ± 18.9	1.9	2327.4 ± 3356.1	0.7	5821.7 ± 4382.8	1.0	0.2 ± 0.2	1.5	5.7 ± 5.0	1.1
Naphthaleneacetic acid	10.4 ± 5.8	1.0	32.7 ± 7.9	0.0	228.8 ± 135.0	0.2	0.1 ± 0.1	0.4	4.8 ± 4.2	0.9
1-methyl-3-phenyl piperazine	9.9 ± 5.8	0.3	616.3 ± 366.8	0.2	5782.0 ± 1574.3	0.5	0.1 ± 0.2	0.7	5.4 ± 4.7	1.0
1-Bromohexane	10.0 ± 5.9	0.9	234.7 ± 302.6	0.3	1181.8 ± 1024.4	1.3	0.2 ± 0.2	1.2	5.5 ± 4.8	1.1
KOH 5% (w/v)	10.1 ± 6.0	0.2	113.0 ± 89.4	0.0	4126.2 ± 1598.1	0.3	0.3 ± 0.3	1.5	7.0 ± 6.1	1.2
Triton X-100 1% (w/v)	16.6 ± 1.5	0.4	860.6 ± 340.9	0.2	6587.3 ± 2418.2	0.6	0.2 ± 0.2	0.8	5.6 ± 5.0	1.0
Cyclamen aldehyde	70.2 ± 103.7	5.6	1038.1 ± 1612.7	0.3	2702.6 ± 3991.1	0.5	0.3 ± 0.3	2.0	6.2 ± 5.8	1.1
Cinnamaldehyde	10.7 ± 5.4	0.3	785.9 ± 356.8	0.2	2686.0 ± 480.4	0.2	0.3 ± 0.3	1.5	5.6 ± 5.9	1.3
SDS 1% (w/v)	11.7 ± 6.5	0.3	441.5 ± 315.4	0.1	6182.4 ± 1424.6	0.5	0.2 ± 0.2	0.8	5.6 ± 4.2	0.9

Each value represents the cytokine concentration in supernatants and is expressed as mean ± S.D of three tissue samples.

IL/NC: ratio of cytokine concentration in treated tissues (mean) to negative control (mean).

Table 4. Cytokine release in EpiDerm^{TM} following irritation tests

Test substance	IL-1β		IL-6		IL-8		TNF-α	
	pg/mL	IL/NC	pg/mL	IL/NC	pg/mL	IL/NC	pg/mL	IL/NC
Water	5.1 ± 0.3	1.12	6.3 ± 3.6	0.81	162.6 ± 57.1	1.03	19.1 ± 0.1	1.01
Isopropanol	5.3 ± 0.7	1.18	13.6 ± 2.8	1.75	570.6 ± 45.7	3.61	19.3 ± 0.6	1.02
Tween 20 10% (w/v)	6.2 ± 0.1	1.37	5.4 ± 1.2	0.69	195.9 ± 38.7	1.24	18.9 ± 0.1	1.00
Methyl stearate	5.7 ± 0.4	1.05	7.6 ± 1.4	1.15	300.7 ± 47.6	1.40	19.0 ± 0.2	1.00
Heptyl butyrate	6.3 ± 0.8	1.05	7.3 ± 0.9	1.11	347.6 ± 138.6	1.62	19.0 ± 0.2	1.00
Hexyl salicylate	4.8 ± 0.2	1.18	4.8 ± 0.8	0.62	134.6 ± 30.9	0.85	19.1 ± 0.1	1.01
1-methyl-3-phenyl piperazine	5.3 ± 0.9	1.69	38.0 ± 30.2	5.80	1676.1 ± 1215.5	7.83	19.1 ± 0.3	1.01
1-Bromohexane	11.3 ± 2.2	1.38	8.6 ± 1.2	1.31	989.8 ± 219.0	4.62	19.2 ± 0.1	1.01
KOH 5% (w/v)	6.2 ± 0.6	2.09	13.7 ± 1.8	2.09	394.7 ± 23.2	1.84	18.9 ± 0.7	0.99
Triton X-100 1% (w/v)	7.7 ± 0.1	0.98	5.2 ± 1.0	0.67	607.3 ± 71.6	3.85	19.3 ± 0.1	1.02
Cyclamen aldehyde	6.3 ± 1.1	1.14	8.3 ± 1.7	1.07	862.8 ± 144.5	5.46	19.1 ± 0.3	1.01
SDS 1% (w/v)	5.0 ± 0.2	0.93	3.2 ± 0.1	0.49	97.9 ± 21.1	0.46	19.1 ± 0.1	1.00

Each value represents the cytokine concentration in supernatants and is expressed as mean ± S.D of three tissue samples.
IL/NC: ratio of cytokine concentration in treated tissues (mean) to negative control (mean)

Prediction capacity

While ORGs did not show an obvious trend, for EpiDerm™ a tendency was observed for irritants to increase IL-8 release (relative to negative control). Therefore, to improve the capacity of classifying the chemicals as irritant or non-irritant, we proposed a possible additional prediction model based on viability and cytokines endpoints (Table 5): a chemical was classified as non-irritant when cell viability was above 50% and the ratio between IL-8 mean release and negative control mean release was < 1.8. A chemical was classified as an irritant in all the other cases.

Table 5. Proposed prediction models based on viability and cytokine release.

Skin model	Viability endpoint	Cytokines endpoint	Classification
ORGs	≤ 50% after 60 min exposure	No impact on classification	Irritant
	> 50% after 60 min exposure	No impact on classification	Non-irritant
EpiDerm™	≤ 50% after 60 min exposure	No impact on classification	Irritant
	> 50% after 60 min exposure	IL-8/NC < 1.8	Non-irritant

IL/NC: ratio of cytokine concentration in treated tissues (mean) to negative control (mean)

The classification capacity of the prediction models is presented in Table 6.

Table 6. Prediction capacity of models.

Test substance	ORGs	EpiDerm™		MSDS
	v	v	v + c	classification
Water	NI	NI	NI	NI
Isopropanol	NI	I	I	NI
Tween 20 10% (w/v)	I	NI	NI	NI
Methyl stearate	I	NI	NI	NI
Heptyl butyrate	NI	NI	NI	NI
Hexyl salicylate	NI	NI	NI	NI
Naphthaleneacetic acid	I	-	-	I
1-methyl-3-phenyl-1-piperazine	I	I	I	I
1-Bromohexane	I	NI	I	I
Potassium hydroxide 5% (w/v)	I	NI	I	I
Triton X-100 1% (w/v)	I	I	I	I
Cyclamen aldehyde	I	I	I	I
Cinnamaldehyde	I	-	-	I
Sodium dodecyl sulfate 1% (w/v)	I	I	I	I
Eugenol	NC	NC	NC	NC
Calcium carbonate	NC	NC	-	NC
Phenethyl bromide	C*	NC	-	NC
Sodium carbonate	NC	NC	-	NC
4-Amino-1,2,4-triazole	NC	NC	-	NC
4-(Methylthio)benzldehyde	NC	C*	-	NC
Lauric acid	NC	C*	-	NC
Sodium dodecyl sulfate 20% (w/v)	C	C	-	C
Potassium hydroxide 10% (w/v)	C	NC*	-	C
Bromoacetic acid	C	C	-	C

Glyoxylic acid monohydrate	C	C	-	C
Ethanolamine	C	C	-	C
Hydrochloric acid 14.4% (v/v)	C	C	-	C
Boron trifluoride dihydrate	C	NC*	-	C
Dichloroacetyl chloride	C	C	-	C
Trizol	C	C	-	C

v: viability endpoint, c: cytokine endpoint, NI: non-irritant, I: irritant, NC: non-corrosive, C: corrosive, *: acceptability criteria was not met and the substance was considered misclassified.

The specificity, sensitivity, and accuracy were assessed based on the viability endpoint alone and on the combination of viability and cytokine release. The results are shown in Table 7. The number of substances included for the sensitivity, specificity, and accuracy calculations is presented in parenthesis.

Table 7. Irritation and corrosion tests performance on ORGs and EpiDerm^{TM}.

| Prediction model | ORGs | | EpiDerm^{TM} | | |
	Irritation v	Corrosion	Irritation v	Irritation v + c	Corrosion
Sensibility	100% (8/8)	100% (9/9)	67% (4/6)	100% (6/6)	50% (2/4)
Specificity	67% (4/6)	86% (6/7)	83% (5/6)	83% (5/6)	33% (1/3)
Accuracy	86% (12/14)	94% (15/16)	75% (9/12)	92% (11/12)	43% (3/7)

v: viability endpoint, c: cytokine endpoint

DISCUSSION

In this study, the performance of fibrin-based dermo-epidermal organotypic cultures was validated by using the irritation and corrosion protocols established by the OECD, along with a measurement of released cytokines as a complement for the irritation test. Preliminary irritation and corrosion tests indicated that ORGs were a good candidate model to discriminate irritant and corrosive substances [7]. Our results reveal that ORGs are able to classify irritants and corrosives, with an overall accuracy of 86% and 94%, respectively.

Before the use of any of the OECD validated methods, it is recommended to verify the morphology and barrier function of the tissues. Histological characterization of fibrin-based models showed that keratinocytes proliferated and differentiated forming different epidermal layers. The tissues further present a healthy and thick dermis with well-distributed fibroblasts. Additionally, the acceptance criteria for barrier function were met, as assessed by IC50. These results indicate that our model shows proper morphology and that the stratum corneum is strong enough to resist the rapid penetration of SDS, confirming the suitability for toxicology tests.

To evaluate the performance of the skin models, 30 proficiency substances were tested in the ORGs, 14 for irritation and 16 for corrosion (1 misclassified: Phenithyl bromide). Phenithyl bromide is water-insoluble, and as such it easily passes through the lipid layer of the stratum corneum, rapidly reaching the underlying components and causing damage. Therefore, any difference in stratum corneum characteristics of replicates may have led to increased variability. Validated models such as EpiDerm[TM] display a thicker corneum stratum, which will likely keep Phenethyl Bromide from passing into the deeper layers.

Chemical weight can play an important role as well. Methyl Stearate was incorrectly classified and, along with Phenithyl bromide, it presents a high molecular weight (298.5 g/mol and 185.1 g/mol, respectively), a reason why they are likely to associate with skin tissues for longer periods [11], resulting in their retention and subsequent invalidation and/or misclassification. These findings suggest that ORGs are more sensitive to high molecular weight compounds. Shorter exposure times or stratum corneum strengthening could be of help to better classify these types of compounds.

Surfactants as Tween 20 and SDS caused problems during the irritation tests in the ORGs. SDS partially destroyed the fibrin matrix and Tween 20 (10%) was misclassified, suggesting that surfactants have a deleterious effect on our system. It would be convenient to test other non-irritant surfactants to confirm our hypothesis.

As for EpiDerm[TM], 19 substances were tested, 12 for irritation and 7 for corrosion (4 invalidated: Lauric acid, 4-(Methylthio) benzaldehyde, boron trifluoride dehydrate, and KOH 10%,). EpiDerm[TM] misclassified isopropanol, 1-Bromohexane, and KOH 5%. This model displayed 75% accuracy for irritation and 43% for corrosion. Since EpiDerm[TM] has been already validated for the tested chemicals, the annulled tests and misclassifications are likely due to quality decreased. Indeed, according to the EpiDerm[TM] supplier, EPI-200-SIT and EPI-200-SCT have a shelf life of 96 h at 2-8°C and extended periods of time are not

recommended. In our case, shipping times were slightly above the limit of 96 h, which probably affected the results.

These findings indicate that ORGs can discriminate in a competitive way the irritation and corrosion potential of different chemicals and highlight the necessity of having a local model to avoid quality loss during international models shipping.

As several inflammatory biomarkers are produced during skin irritation, we next measured the release of different inflammatory cytokines and evaluated its suitability as a second endpoint to assess irritation potential.

Of all the cytokines produced by keratinocytes, IL-1α, IL-1β, and TNF-α act as primary alarm signals and are able to independently trigger cutaneous inflammation [12,13], whilst IL-10 limits the inflammatory effects [12]. ORGs and EpiDerm[TM] release of IL-1β, TNF-α, and IL-10 was quite discrete, and EpiDerm[TM] showed no release of the latter. A possible explanation is that their maximum release is not reached in the first 24 h due to their low secretion rate. Cells may also uptake these cytokines as part of their normal metabolism, reducing their levels in the medium. There was not an obvious trend when comparing the release of IL-1β, TNF-α, and IL 10 before and after exposure. Interestingly, misclassified substances such as Tween 20 10%, 1-Bromohexane, and KOH 5%, substantially increased IL-1β levels over negative control.

Both skin models released outstanding levels of IL-8. Of note, under basal conditions, ORGs IL-8 secretion was about 45 higher than EpiDerm[TM]. In agreement with this, Bernhofer et al. [14] reported that full-thickness models secrete 100–150-fold higher amounts of IL-8 than epidermal equivalents alone. Studies on keratinocytes secretion of cytokines indicate that, upon stimulation, keratinocytes release IL-1α, inducing other keratinocytes and fibroblasts to upregulate IL-8 production [12,13,15], which can explain the high concentrations reached by our dermo-epidermal model. However, there is no obvious trend in ORGs IL-8 release after irritant exposure, while EpiDerm[TM] did show an IL-8 pattern: almost all irritant substances rose IL-8 levels more than 80% over the negative control. This finding allowed us to go further and propose a prediction model combining both viability and cytokine release endpoints, which indeed increased EpiDerm[TM] prediction capacity.

ORGs secreted noteworthy IL-6 levels. IL-6 is produced by both keratinocytes and fibroblasts after stimulation with IL-1α and TNF [11] and plays an important role in perpetuating skin inflammation and promoting keratinocytes proliferation [12]. We observed that 24 h after treatment, irritant substances reduced IL 6 release to less than 70% of negative control, indicative of detrimental effects on the tissues after the treatment. Indeed, IL-6 diminution was accompanied by viability decrease, suggesting that irritants induced significant cytotoxicity and that shorter exposure times and/or lower chemical concentrations could be of help to better classify irritants.

It is worth mentioning that ORGs released high amounts of IL-6 and IL-8 under basal conditions. Fibrin provides a provisional matrix at sites of injury and inflammation, stimulating keratinocytes and fibroblasts to behave as they usually do in an inflammatory context, that is, releasing proinflammatory cytokines. Therefore it is possible that

keratinocytes-derived IL-1 has stimulated the release of IL-6 and IL-8 in both keratinocytes and fibroblasts [13,16,17].

These results show that different substances seem to differently alter the release of cytokines and this changes from one model to another. The different cytokines and cells involved in irritation response highlight the complexity of this process, and perhaps the induction of one or more cytokines could be concentration-, chemical-, and model-specific. Further studies are needed to determine whether cytokine release will increase accuracy when testing several types of irritant compounds. In any case, IL-6 and IL-8 might be a good indicator of irritation, since they are general mediators in tissue injury [12] and could be of help to better classify chemicals.

Irritation and corrosion tests performed in the ORGs were based on the protocol proposed for EpiDerm^{TM} in the OECD test guidelines. However, all models have differences regarding structure, morphology, and composition and each one must establish the exposure times and the amount of chemical to be applied that generate the most reliable results. Cell viability and cytokine release measurements at different time points along with chemical concentration curves could be a useful tool to establish our own protocol, improve the outcome, and determine the advantages of using cytokines as a second endpoint.

Our demonstration that OECD irritation and corrosion tests can be applied to ORGs indicate that they are able to identify chemicals hazard. This is important at the local level since several research groups and pharmaceutical companies in Colombia carry out irritation and corrosion tests to evaluate their products. As the importation of internationally validated skin equivalents is hampered by quality loss and difficult administrative and legal norms, our in-house model represents an advantage for the development and commercialization of chemical products in our country.

In summary, our results indicated that fibrin-based organotypic cultures fulfill the morphology and barrier function requirements for the application of OECD protocols and confirmed that they are a useful tool for chemical hazard identification. Further studies are now needed to gain insight into the cytokines secretion pattern in response to irritation. If there is indeed an association between cytokine production in ORGs and irritation potential, this could allow a sub-categorization of irritants, improving the prediction capacity of the model.

ACKNOWLEDGMENTS

REFERENCES

1. European Union Reference Laboratory for alternatives to animal testing (EURL-ECVAM). Skin Irritation [Internet]. [cited 2016 Aug 23]. Available from: https://eurl-ecvam.jrc.ec.europa.eu/validation-regulatory-acceptance/topical-toxicity/skin-irritation

2. Vinardell, MP1; Mitjans M. Alternative methods for eye and skin irritation tests: an overview. J Pharm Sci. 2008;1(97):46–59.

3. Wilkinson JB, Moore RJ. Irritación y sensibilización de la piel. In: Díaz de Santos SA, editor. Cosmetología de Harry. Madrid; 1990. p. 29–41.

4. Vega Montalvo R, Álvarez Fong M. Irritación ocular: Modelos alternativos. Rev Cuba Farm. 2001;35(3):211–8.

5. Zhang Z, Michniak-Kohn BB. Tissue engineered human skin equivalents. Pharmaceutics. 2012;4(1):26–41.

6. Rheins LA, Edwards SM, Miao O, Donnelly TA. Skin2TM: An in vitro model to assess cutaneous immunotoxicity. Toxicol Vitr. 1994;8(5):1007–14.

7. Morales M, Pérez D, Correa L, Restrepo L. Evaluation of fibrin-based dermal-epidermal organotypic cultures for in vitro skin corrosion and irritation testing of chemicals according to OECD TG 431 and 439. Toxicol Vitr. 2016;36:89–96.

8. OECD. 431 OECD Guideline for the testing of chemicals. In Vitro skin corrosion: reconstructed human epidermis (RHE) test method. [Internet]. 2016. Available from: https://read.oecd-ilibrary.org/environment/test-no-431-in-vitro-skin-corrosion-reconstructed-human-epidermis-rhe-test-method_9789264264618-en#page1

9. OECD. 439 OECD Guideline for the testing of chemicals. In Vitro Skin Irritation: Reconstructed Human Epidermis Test Method. [Internet]. OECD; 2015 [cited 2016 Nov 12]. Available from: https://read.oecd-ilibrary.org/environment/test-no-439-in-vitro-skin-irritation-reconstructed-human-epidermis-test-method_9789264242845-en#page1

10. European Union Reference Laboratory for alternatives to animal testing (EURL-ECVAM). Skin Irritation [Internet]. 2012 [cited 2016 Jul 14]. Available from: https://eurl-ecvam.jrc.ec.europa.eu/validation-regulatory-acceptance/topical-toxicity/skin-irritation

11. Mallampati R, Patlolla RR, Agarwal S, Babu RJ, Hayden P, Klausner M, et al. Evaluation of EpiDerm full thickness-300 (EFT-300) as an in vitro model for skin irritation: Studies on aliphatic hydrocarbons. Toxicol Vitr. 2010;24(2):669–76.

12. Lee HY, Stieger M, Yawalkar N, Kakeda M. Cytokines and chemokines in irritant contact dermatitis. Mediators Inflamm. 2013;2013:1–7.

13. Corsini E, Galli CL. Cytokines and irritant contact dermatitis. Toxicol Lett. 1998;102–103:277–82.

14. Bernhofer L., Seiberg M, Martin K. The Influence of the Response of Skin Equivalent Systems to Topically Applied Consumer Products by Epithelial--Mesenchymal Interactions. Toxicol Vitr. 1999;13(2):219–29.

15. Newby CS, Barr RM, Greaves MW, Mallet AI. Cytokine release and cytotoxicity in human keratinocytes and fibroblasts induced by phenols and sodium dodecyl sulfate. J

Invest Dermatol. 2000;115(2):292–8.

16. Werner S, Krieg T, Smola H. Keratinocyte–Fibroblast Interactions in Wound Healing. J Invest Dermatol. 2007;127:998–1008.

17. Laurens N, Koolwojk P, De Maat P. Fibrin structure and wound healing. J Thromb Haemost. 2006;4:932–9.

CHAPTER 4

Incorporating dendritic cells into dermo-epidermal organotypic cultures

C. Gaviria [a,b], F. Foijer [b], L.M. Restrepo [a,c]

[a]Tissue Engineering and cell therapy research Group, School of Medicine, University of Antioquia, Colombia
[b]European Research institute for the Biology of Ageing, University Medical Center Groningen, The Netherlands
[c]Medical Research Institute, School of Medicine, University of Antioquia, Colombia

ABSTRACT

In the last years, different *in vitro* skin models have been created for studying skin biology and as platforms for chemical hazard identification. However, most of them are mainly composed of keratinocytes and/or fibroblasts and largely lack the immune component. Immunocompetent skin equivalents provide an attractive system for determining the skin sensitization potential of chemicals and to investigate, in a more relevant model, immunological processes.

There are a few reports on the development of immune skin models and the vast majority uses Langerhans cells as an immune component. Here, we describe the construction of a skin model composed of freshly isolated CD14+ cells co-cultured with keratinocytes and fibroblasts. To this end, keratinocytes and CD14+ cells were seeded on a fibrin gel populated by fibroblasts. The morphology and expression of dendritic cell markers were evaluated by hematoxylin-eosin and immunohistochemistry staining, respectively. We further performed a preliminary sensitization test to assess the capability to respond to skin allergens.

Skin models displayed similar histological characteristics to native skin and induced the differentiation of CD14+ cells into dendritic cells. The fibrin-based dermal compartment supported the migration of dendritic cells. Given the heterogeneous nature of CD14+ precursors, this system highlighted the possibility of engineering skin equivalents with different dendritic cells populations.

INTRODUCTION

Dendritic cells (DCs) are responsible for initiating immune responses by processing antigens and presenting them to T lymphocytes [1]. Skin sensitizers penetrate through the epidermis and are captured by epidermal residing DCs, referred to as Langerhans cells (LCs). During the sensitization phase, LCs process antigens and migrate to lymphoid nodes to present them to T cells [2,3]. During this phase, DCs undergo a maturation process and acquire an immunostimulatory phenotype [1,2]. In the elicitation phase, repeated exposure to the same sensitizer causes the activation of memory T cells leading to allergic inflammation [4].

Currently, the identification and evaluation of chemicals are based on animal experimentation [5,6]. The development of *in vitro* tests for evaluating sensitization potential of chemicals has been driven by 1) ethical issues raised by animal research, 2) the European Union ban on animal testing for cosmetics [7], and 3) the very clear differences found between human and animal skin immunology [8].

Fresh human skin explants are relevant *in vitro* models to study LCs biology and responses. However, they introduce high donor variation and rely on the constant supply of biopsies of proper size [8–11]. Other *in vitro* alternatives are based on chemical reactivity or responses of primary and immortalized cell lines in monocultures. Nevertheless, bi-dimensional cultures lack the architecture, morphology, phenotype, and behavior found *in vivo* [5], yielding limited information.

Three-dimensional constructs are a suitable alternative, as they more faithfully mimic the *in vivo* environment. Current commercially available models are mainly composed of keratinocytes and/or fibroblasts, but largely lack the immune component [12]. To date, only a few immune 3D constructs have been described. L'Oreal developed a reconstructed epidermis with CD34+-derived LCs, using a collagen matrix [4] and a de-epidermized acellular matrix [13] as a dermal compartment. This model, however, requires a fresh cord blood supply, which may not always be accessible, and lacks a fibroblasts-populated dermal component, which plays an essential role during LCs migration [14]. Kosten's [8] and Bock's [12] studies showed the feasibility of co-seeding keratinocytes and MUTZ-3-derived LCs in a full-thickness skin equivalent containing collagen gels with fibroblasts. The model provided a promising tool for chemical hazard identification and LCs biology, even though cell lines may not fully mimic *in vivo* cellular processes. In another approach, monocyte-derived LCs [8,12,15] and monocyte-derived dermal DCs [15] were successfully cultured onto collagen gels populated by fibroblasts, showing specific responses to allergens or UV light.

There is no gold standard method for the construction of an immune *in vitro* model of the skin. Knowing that keratinocytes can release IL4 and GM-CSF into the culture medium [15–17] and that they are able to induce differentiation of hematopoietic progenitors into LCs [18], we investigate whether freshly isolated CD14+ cells could be used to develop a 3D immune skin model that promotes their differentiation into dendritic cells. To our knowledge, no protocol has been established for the use of freshly isolated monocytes in skin equivalents. We further tested its capability to respond to skin sensitizers.

MATERIALS AND METHODS

3T3 maintenance and feeder layer preparation

NIH 3T3 cells were maintained in culture in DMEM supplemented with 10% (v/v) fetal bovine serum (FBS,) and 1% (v/v) penicillin-streptomycin (all from Gibco). Cells were passaged when a 70-80% confluence was reached. To establish the feeder layer, 3T3 cells were seeded at a density of $12x10^3$ cells/cm^2 and the next day were gamma-irradiated with a dose of 60 Gy (i3T3).

Human skin cells isolation and culture

Keratinocytes and fibroblasts

After informed consent, human skin samples were obtained from blepharoplasties and mammary reductions leftovers, performed at the Department of Plastic Surgery at the UMCG, Groningen, The Netherlands

Samples were washed in phosphate-buffered saline (PBS, Gibco), immersed in 70% ethanol for 1 min, and mechanically fragmented. Fragments were placed on 10 mm culture dishes (Greiner Bio-One) and air-dried for 15-20min. Then, QN medium (described in Chapter 2) supplemented with 10 uM Rock Inhibitor (Y-27632, STEMCELL Technologies) was added. The medium was changed every 2-3 days. 10 ng/mL Epidermal Growth Factor (EGF, Preprotech) was added to QN medium at day 3-4. Both keratinocytes and fibroblasts were obtained. For subsequent passages fibroblasts were cultures in DMEM supplemented with 10% (v/v) fetal bovine serum (FBS) and 1% (v/v) penicillin-streptomycin (all from Gibco).

Keratinocytes were also obtained by dissociation with 0.25% Trypsin and subsequent seeding on a gamma-irradiated NIH 3T3 feeder layer. Culture medium was used as described above.

Preparation if keratinocytes conditioned medium

When confluence was higher than 60%, keratinocytes supernatant was collected, centrifuged for 5 min at 200xg and sterile filtrated through 0.2 µm. It was stored at 4°C if promptly used or -20°C for longer periods.

Monocytes and monocytes-derived DCs (mo-DCs)

Peripheral blood mononuclear cells (PBMC) were obtained from buffy coats following density gradient centrifugation using Lymphoprep (STEMCELL). After 3 washes with PBS, monocytes were isolated by magnetic separation using MojoSort™ Human CD14 Nanobeads (Biolegend), according to the manufacturer's instructions.

Monocytes were cultured at a concentration of $1x10^6$ cells/mL in either keratinocytes conditioned medium or RPMI 1640 medium (Gibco). For the latter, 10% heat-inactivated FBS (hiFBS), 1% L-Glutamine, and 1% (v/v) penicillin-streptomycin were used. Differentiation into dendritic cells was induced by stimulation with 20 ng/ml recombinant human IL-4 and 100 ng/ml recombinant human GM-CSF (all from Preprotech) and incubated

at 37 °C and 5% CO_2. Every 2 days, re-stimulation with IL-4 and GM-CSF was performed. Cells were harvested on day 7.

Phenotypic analysis

Before incorporation into the skin model, cell cytometry was used to analyze the expression of phenotypic markers in both fresh isolated CD14 and mo-DCs. Briefly, $0.5-5 \times 10^5$ cells were incubated on ice for 30 min at RT with the following monoclonal antibodies: APC-conjugated anti-human CD14 (Invitrogen) and PE-conjugated anti-human CD209 (DC-SIGN, BioLegend). Cells were then washed in PBS plus 0.2% BSA (Gibco) and flow cytometry was performed with the BD FACSCanto™ System. Histograms were analyzed using the FlowJo vX software.

Three-dimensional model construction

Skin equivalents with and without immune cells were constructed. To this end, freshly isolated monocytes were used.

For the generation of the dermal equivalent, a mix of human plasma, 0.9% NaCl (Sigma-Aldrich), tranexamic acid (Sigma-Aldrich), and a fibroblast solution (7×10^4 cells/mL) was prepared. To promote fibrin polymerization, 1% $CaCl_2$ (Fisher Chemical) was added, and the solution was gently mixed, poured into 12-well cell culture inserts (0.4 μm pore size, Greiner bio-one), and incubated (37°C, 5% CO_2) for 30 minutes. Subsequently, each gel was covered with DMEM containing 10% FBS, 1% L-glutamine, and 1% penicillin/streptomycin, and incubated overnight at 37 °C.

The next day, the medium was removed, and the gels were equilibrated with QN medium for 2h at 37 °C. For the epidermal compartment, 1×10^5 keratinocytes alone or a mix of 1×10^5 keratinocytes and 1×10^5 CD14+ cells were seeded onto the fibrin gels. The constructs were incubated for 1.5 h at 37 °C to allow cells to adhere to the dermal compartment and then kept in QN medium supplemented with 10 uM ROCK inhibitor for 3 days. Then, 10 ng/ml EGF were added and, at day 7, constructs were raised to the air-liquid interface and ROCK inhibitor was removed. The medium was changed every other day for the next 14 days.

Chemical treatment

The test was carried out after 21 days of culture. Three chemicals, 1 irritant and 2 strong sensitizers, were evaluated to test the predictive performance of our model. The tissues were treated with the substances for 24h at a non-toxic concentration, as assessed by MTT assay. PBS (control), sodium dodecyl sulfate (SDS, irritant; Sigma-Aldrich), Formaldehyde (sensitizer, Sigma-Aldrich), and Manganese (II) Chloride Tetrahydrate ($MnCl_2·4H_2O$, sensitizer; Fisher Chemical), dissolved in PBS, were applied to the apical side of the constructs (30 uL/cm^2).

SDS was applied at a concentration of 1 mg/mL, as it has been reported before that 0.5-5 mg/mL SDS causes a minor decrease in different skin equivalents viability [6,8,12], and our model previously displayed a reduction of more than 90% viability when treated with 10 mg/mL SDS (Chapter 3). Formaldehyde was used at 2 mg/mL based on Gibbs et al. studies showing insignificant cytotoxic effects in the epiCS® model. Previous studies have reported

a MnCl$_2$ lethal concentration of 1 mM for dendritic cells [19,20], and a significant viability decrease experienced by keratinocytes at 386 uM [21]. To ensure a non-toxic concentration, a 100-fold dilution of MnCl$_2$ lethal dose was used. Following exposure, tissues were washed and fixed in paraformaldehyde 4%.

Histology and immunohistochemistry

On the 21st day, tissues were collected and fixed in 4% paraformaldehyde at room temperature. After fixation, tissues were dehydrated and embedded in paraffin. Five micrometers sections of the samples were stained with hematoxylin-eosin (H&E).

For immunostaining, 5 μm sections of paraffin-embedded tissues were washed with xylene and rehydrated with ethanol. The primary antibody was incubated overnight at 4°C. After 3 washes with PBST, the secondary antibody was applied for 30min. Finally, horseradish peroxidase was used for the 3,3′-Diaminobenzidine (DAB)-based color reaction.

The antibodies used for epidermal characterization were mouse anti-CD1a and rabbit anti-Langerin (all from Abcam).

RESULTS

Phenotypic characterization of monocytes and mo-DCs

We first evaluated the phenotypic characteristics of freshly isolated monocytes and *in vitro* differentiated monocytes. Cells were analyzed by flow cytometry for the surface expression of CD14 and CD209 (monocyte-derived dendritic cell marker). As expected, magnetic isolation of CD14 cells from PBMC, led to an enrichment of CD14 (Figure 1a).

We then studied the ability of keratinocytes conditioned medium to induce differentiation of CD14+ cells over a period of 7 days and compared it to the commonly used medium RPMI plus hiFBS, GM-CSF, and IL-4.

After 7 days of culture in both RPMI with GM-CSF and IL-4 or keratinocytes conditioned medium, differentiation was induced and cells displayed typical dendritic morphology (Figures 1f and g) and started increasing CD209 expression at similar levels (Figure 1c) as well as granularity (Figure 1d) while decreasing CD14 levels (Figure 1b).

These results indicate that keratinocytes conditioned medium is able to induce differentiation of CD14+ cells in a similar manner to supplemented RPMI.
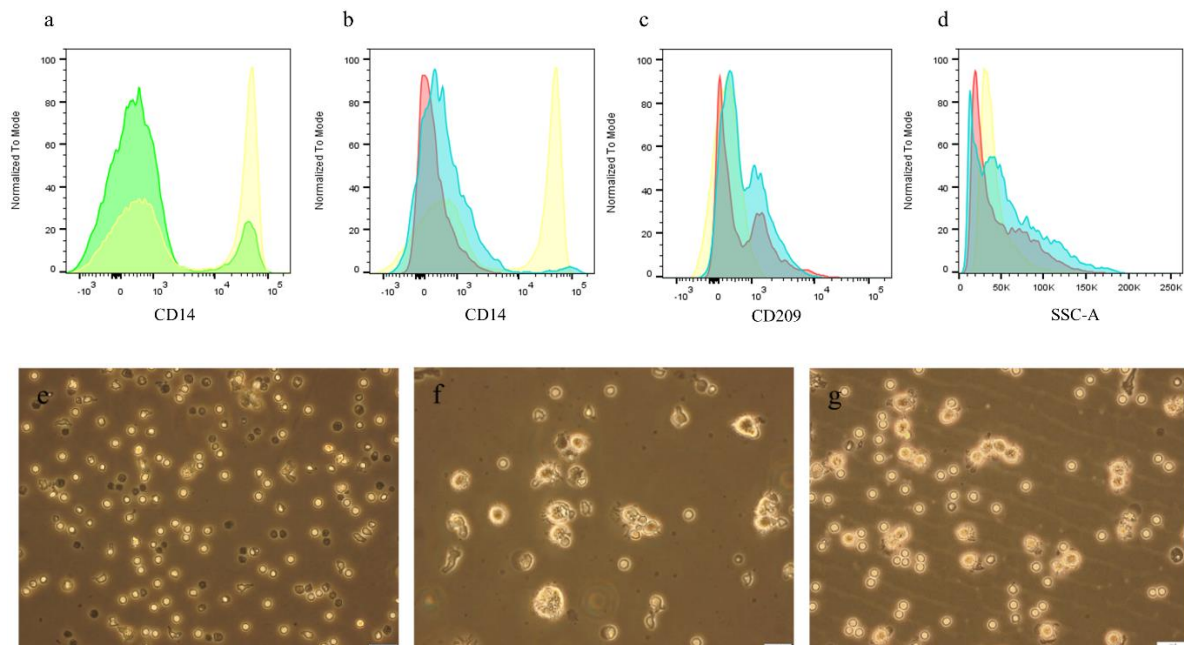

Figure 1. Phenotypic characteristics of monocytes and mo-DC. a) CD14 cells enrichment (yellow-shadowed) after isolation by magnetic beads from PBMCs (green-shadowed). The CD14+ enriched population was cultured in RPMI with hiFBS, GM-CSF, and IL-4 (red-shadowed) or in keratinocytes conditioned medium (blue-shadowed) for 7 days. The expression of b) CD14, c) CD209, and d) granularity was analyzed by flow cytometry. Morphological changes of CD14+ cells from e) day 0, to day 7 in f) RPMI or g) keratinocytes conditioned medium.

Development of a skin model with an immune component

Knowing that keratinocytes conditioned medium can promote CD14+ differentiation (Figure 1), we developed a 3D fibrin-based skin model consisting of keratinocytes and fibroblasts, with or without CD14+ cells.

An illustration of the process is shown in Figure 2a. We examined the morphology and dendritic cells markers expression (CD1a and Langerin) of the resulting models. Histological and immunohistochemical characteristics are presented in Figure 2b-j. For comparison, images of native skin are shown (Figure 2d, g, and j).

The tissues were able to form a continuous epidermis over the dermal layer (Figure 2b and c), showing a stratification process with different epidermal layers. There was a clear separation between dermis and epidermis with keratinocytes attached to the basal membrane. Importantly, the incorporation of CD14 cells did not alter the morphology of the equivalents (Figure 2c).

Immunohistochemical staining for langerin, a Langerhans cells marker, revealed positive expression in models containing CD14+ cells (Figure 2f). Unlike native skin (Figure 2g), langerin-positive cells were mainly found in the dermis. CD1a was dimmer, showing a wide-spread pattern in the epidermis (Figure 2i), with positive cells in both dermis and epidermis.
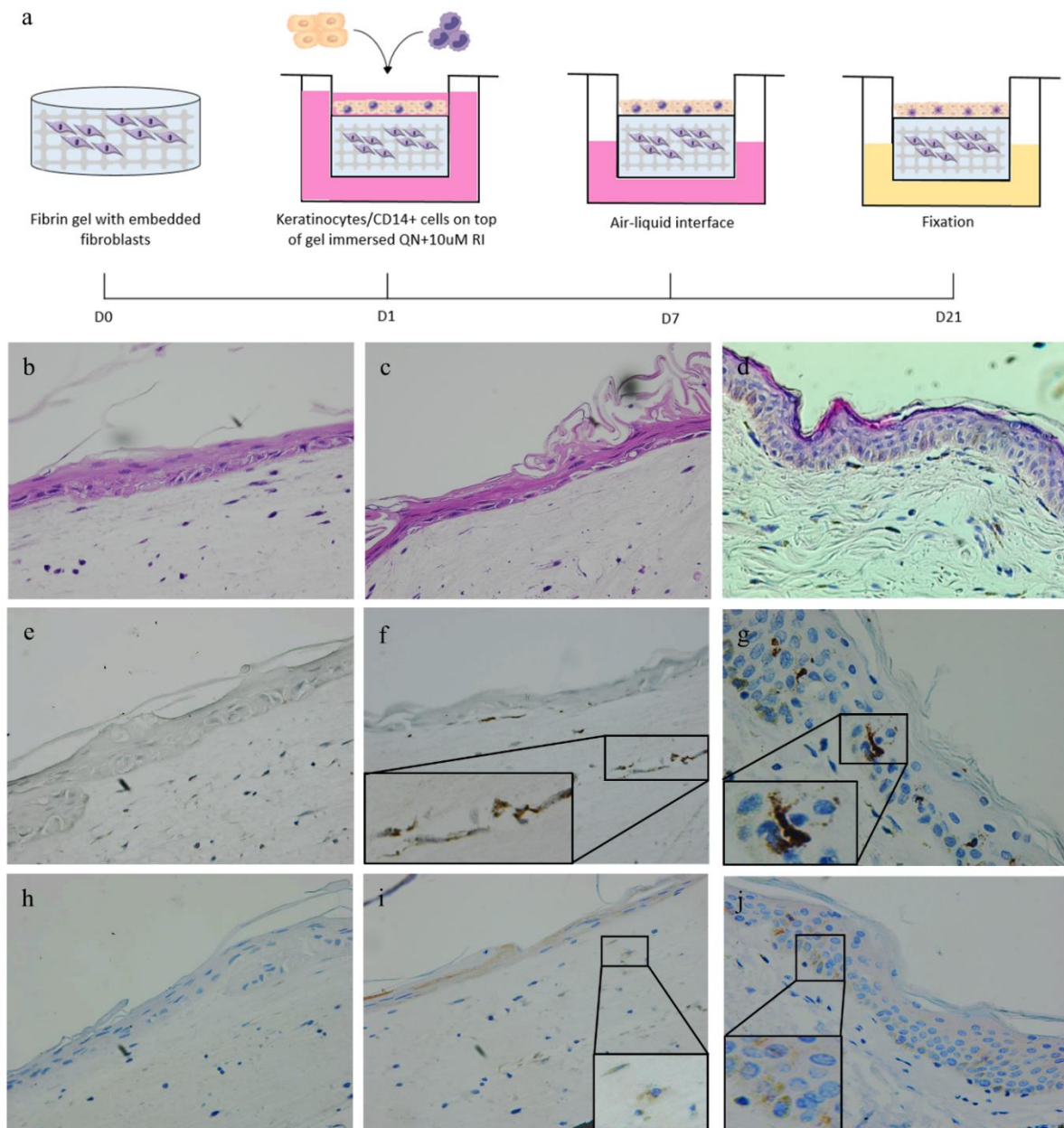
Figure 2. Characterization of HSEs containing mo-DCs. a) schematic illustration of the protocol for the construction of skin equivalents from day 0 to day 21. Histological characteristics of HSEs constructed with b) keratinocytes, c) keratinocytes and freshly isolated CD14+ cells, and d) native skin. Expression of langerin in HSEs constructed with e) keratinocytes, f) keratinocytes and freshly isolated CD14+ cells, and g) native skin. Expression of CD1a in HSEs constructed with h) keratinocytes, i) keratinocytes and freshly isolated CD14+ cells, and j) native skin.

Sensitization test

To provide an insight into the feasibility of the model to identify sensitizers, we performed a sensitization test with three substances: 1 irritant and 2 strong sensitizers. MTT assay confirmed that chemical concentration did not cause major viability issues (not shown).

Histological changes

There were no considerable alterations in morphology after application of the two sensitizers, except for a slight thinning of the epidermis following formaldehyde treatment (compare Figure 3e with Figure 2c), while the irritant agent (SDS) partially damaged the epidermis (compare Figures 3a and d with Figures 2b and c), which started detaching during washing steps.
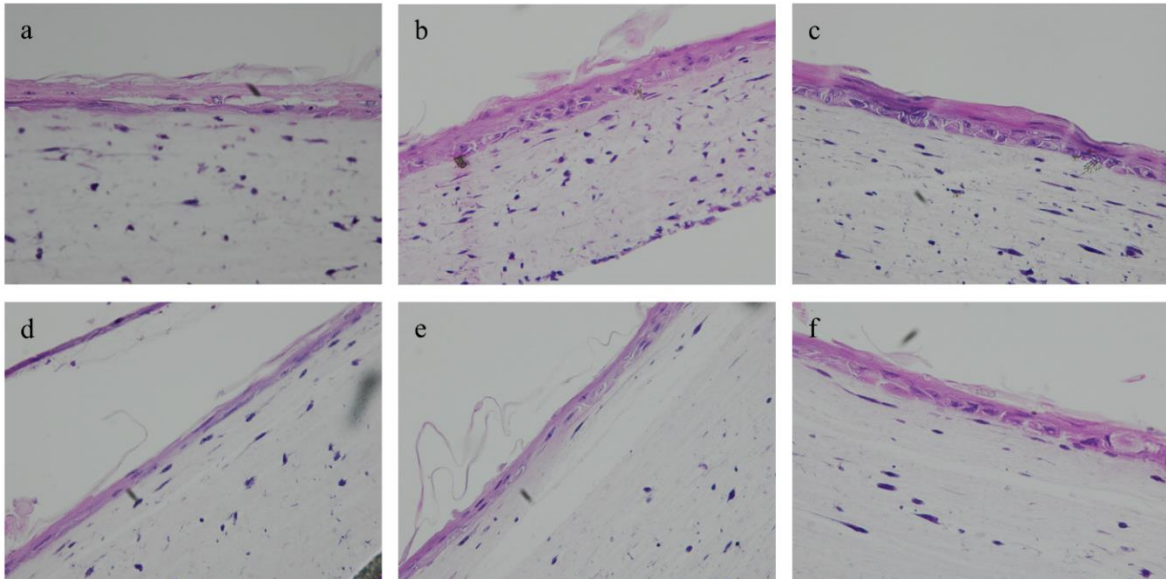

Figure 3. Histological characteristics of HSEs after the sensitization assay. Models constructed with keratinocytes after the exposure to a) 1 mg/ml SDS, b) 2 mg/ml formaldehyde, and c) 10 uM MnCl$_2$. Models constructed with keratinocytes and CD14+ cells after the exposure to d) 1 mg/ml SDS, e) 2 mg/ml formaldehyde, and f) 10 uM MnCl$_2$.

Presence and distribution of langerin-positive cells

We next investigated whether the number and distribution of langerin positive cells were affected after the challenge with the test substances. Following stimulation, cells were counted in at least 6 random fields of vision and the percentage of langerin positive cells was calculated. For comparison, models containing only keratinocytes are presented (Figure 4a-c). Langerin positive staining could be found in all conditions (Figures 4d-f) with frequencies ranging from 3 to 11% of total cells (Figure 4g). Interestingly, after irritant exposure, all stained cells were present in the dermis, while sensitizers led to an accumulation of positive cells in the upper dermis. Epidermal langerin+ percentage did not change after formaldehyde treatment, whereas stained cells were no longer located in the epidermis following MnCl$_2$ exposure (Figure 4h).
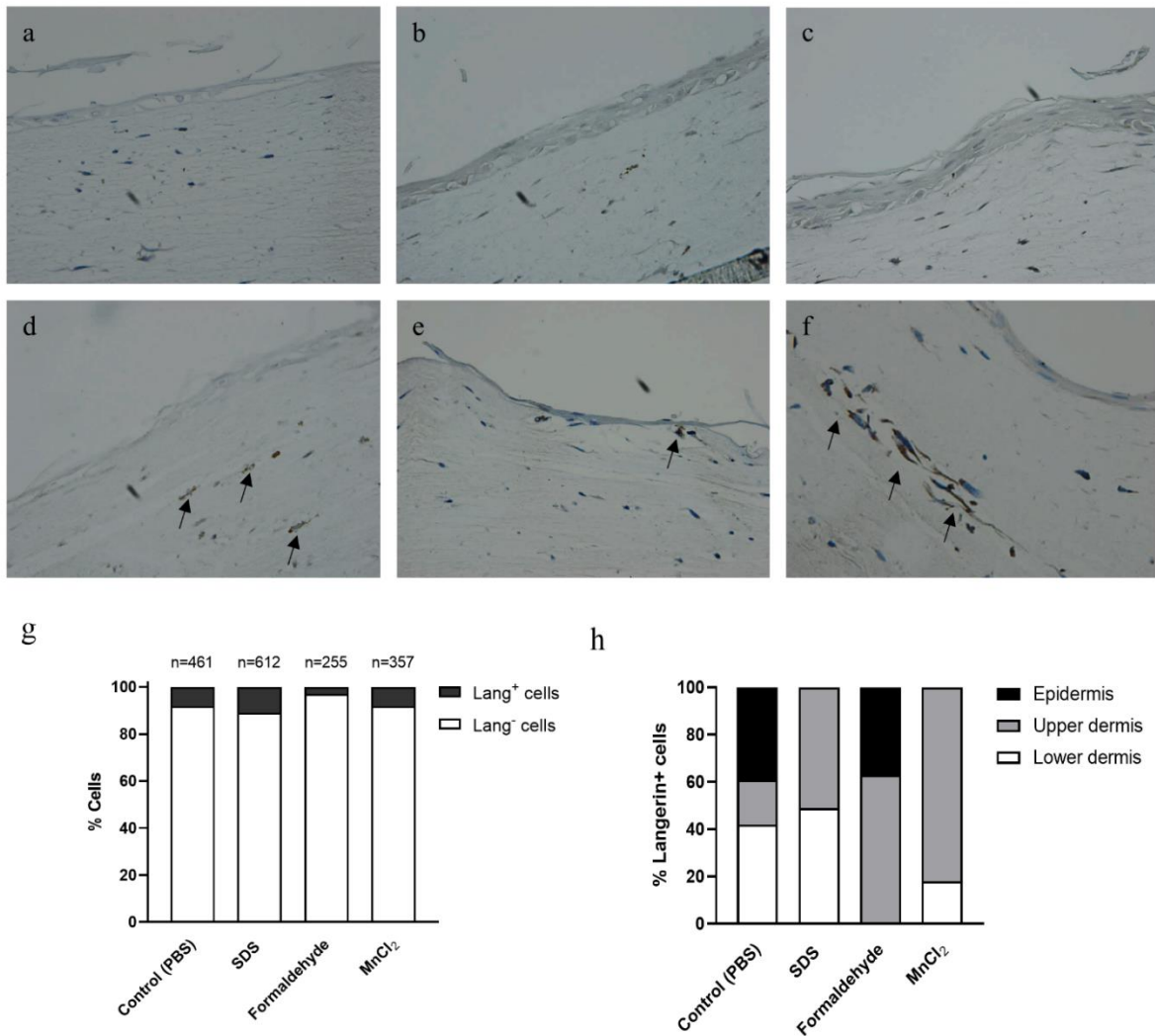
Figure 4. Langerin expression of HSEs after the sensitization assay. Models constructed with keratinocytes after the exposure to a) 1 mg/ml SDS, b) 2 mg/ml formaldehyde, and c) 10 uM MnCl₂. Models constructed with keratinocytes and CD14+ cells after the exposure to d) 1 mg/ml SDS, e) 2 mg/ml formaldehyde, and f) 10 uM MnCl₂. g) Langerin positive and negative frequencies of indicated cell number (n) in models exposed to test substances. h) Distribution of langerin positive cells in models exposed to test substances.

DISCUSSION

In this study, we investigated whether freshly isolated CD14 cells could differentiate into dendritic cells when incorporated into a 3D skin model. We describe the development and initial characterization of fibrin-based models composed of keratinocytes, fibroblasts, and CD14+ cells. Our results show that freshly isolated CD14+ cells are able to differentiate into dendritic cells in a 3D setting, as judged by the expression of langerin and CD1a. Moreover, they displayed migration capacity through the fibrin network.

Our finding that CD14+ cells can differentiate into dendritic cells in an *in vitro* skin environment is supported firstly by our monolayer cultures. After seven days in keratinocytes conditioned medium, cells acquired a dendritic morphology, started expressing a specific monocytes-derived dendritic cells marker (CD209), and became granular, while downregulating CD14 levels. This was achieved in a similar way to RPMI medium supplemented with IL4 and GM-CSF, the standard method to obtain monocytes-derived dendritic cells. In agreement, previous studies have shown that keratinocytes can release IL4 and GM-CSF [15–17], essential factors to stimulate differentiation of monocytes.

Freshly isolated CD14 cells were then incorporated into a fibrin-based skin model. Histochemical analysis revealed a stratified epithelium that was not altered after the addition of CD14+ cells. Confirming the previous result, both langerin and CD1a positive cells were detected, indicating that co-culture with keratinocytes and fibroblasts in a 3D structure promotes the differentiation into Langerhans cells and, likely, other types of CD1a+ dendritic cells. Consistent with our findings, Régnier et al. previously showed that CD34+ progenitors give rise to LCs when incorporated in a reconstructed epidermis [18]. Evidence of an association between skin equivalent microenvironment and dendritic cell generation also comes from Bechetoille et al. work. These authors found that a skin model containing keratinocytes and fibroblasts secreted important factors for the maintenance of dendritic cells (GM-SCF, TGF-b1, IL-4, IL-13, and IL-15) [15]. Our results indicate that our culture system is a reservoir of growth factors and cytokines that promotes the generation of dendritic cells from CD14+ precursors.

Given the complex network of cytokines produced by keratinocytes and fibroblasts, we did not expect the CD14+ cells to differentiate into a unique population, but rather, into different subtypes of dendritic cells. In fact, it has been shown that there is a heterogeneous population of monocytes [22] and that *in vitro* differentiation of these cells gives rise to different populations of DCs [23]. Indeed, in this study isolated CD14+ cells included both CD209+ and CD209- subsets (not shown), which may have differentiated into distinct populations. The cytokine network inside our model led to the generation of epidermal DCs, as shown by positive langerin staining, and possibly of dermal DCs. Despite its weak and diffuse staining, CD1a levels indicated the presence of dendritic cells in both epidermal and dermal compartments. The possibility that all CD1a+ dendritic cells are Langerhans cells is unlikely, given the complexity of the system. Angel et al. demonstrated that CD14+, CD1a+, and migratory Langerhans cells co-exist in the healthy human dermis as different subsets [24], which may be present in our system. Definitive proof of the presence of different dermal DCs subsets in our model will require further studies with more DCs markers.

Although some langerin-stained cells could be observed in the epidermis, LCs were mainly located in the dermal compartment, suggesting that they were activated, had a migratory phenotype, and/or matured spontaneously under basal conditions. We previously showed that our fibrin-based model releases IL-1β, IL-6, IL-8, and, to a lesser extent, TNF-α (Chapter 3), and probably other inflammatory cytokines that might induce DCs maturation. In fact, commonly used maturations cocktails include TNF-α, IL-1α, IL-1β, IFN-γ, and others, in different combinations [23,25]. In addition, a recent study found that IL-6 is required for chemotaxis of mature DCs [26], which may have contributed to DCs migration through the fibrin-based dermal model. Further research is needed to address which culture conditions (different media supplementation) and cell composition are essential for dendritic cells localization and maturation.

To gain insight into the capability of our skin equivalent to identify sensitizers, we report preliminary results of a small sensitization test. Exposure to two strong sensitizers (formaldehyde and $MnCl_2$) did not substantially affect the morphology or viability of the tissues, while the irritant (SDS) provoked partial detachment of the epidermis. Unexpectedly, after SDS treatment all langerin+ cells were in the dermis, unlike control tissue which displayed around 40% of LCs in the epidermis. Because the percentage of LCs within the tissues did not vary significantly, these results suggest that irritant exposure induced epidermal LCs migration. It has been shown before that application of a skin irritant can cause a transient DCs migration [27,28] as a result of a rapid maturation, in contrast to the long-lasting migration induced by mechanical injury [28]. Another possible contributing aspect is the fact that irritation induces apoptosis of skin cells [29], which can contribute to DCs maturation and migration, as reported by Bertho et al. [30]. On the other hand, a strong sensitizer like $MnCl_2$ effectively triggered the migration of epidermal LCs towards the dermis, particularly the upper region, without changing the proportion of these cells in the tissue. Formaldehyde application, however, did not change LCs localization, except for an accumulation in the upper dermis and a slight reduction in the percentage of DCs. It is unclear whether this is caused by a subset of dead or rapid migratory DCs. These data suggest that LCs inside our 3D skin model can respond differently to chemical treatment with specific migration patterns for irritants and sensitizers. Additional experiments including more chemicals, a wider range of concentrations, and other markers will be required to resolve this matter.

Our results showed that a 3D skin equivalent composed of keratinocytes and fibroblasts effectively promotes the differentiation of CD14+ cells into dendritic cells. Importantly, it highlighted the possibility of obtaining a skin model composed of different subsets of DCs from a single population of CD14+ precursors, which would provide an improved system to model skin immunity. This approach, to the best of our knowledge, has not been attempted before. A major advantage of this type of model is that different DCs subsets could differently respond to sensitizers and irritants, improving the current *in vitro* sensitization assays. Further, they can offer deeper insight into DCs behavior and interaction with the surrounding tissue and other skin cells.

In summary, we have constructed an immune 3D skin model by co-seeding CD14+ cells with keratinocytes and fibroblasts, which promoted the differentiation of CD14 cells into dendritic cells. Our results revealed the presence of both CD1a+ cells and Langerhans cells, which

displayed migratory capacities through the fibrin-based dermal compartment. Considering the heterogeneity of CD14+ cells and the complex skin model microenvironment, this approach provides the means of obtaining improved models with different DCs subsets.

ACKNOWLEDGMENTS

REFERENCES

1.	Toebak MJ, Gibbs S, Bruynzeel DP, Scheper RJ, Rustemeyer T. Dendritic cells: Biology of the skin. Contact Dermatitis. 2009;60(1):2–20.

2.	Ryan CA, Kimber I, Basketter DA, Pallardy M, Gildea LA, Gerberick GF. Dendritic cells and skin sensitization : Biological roles and uses in hazard identification. 2007;221:384–94.

3.	Masterson AJ, Sombroek CC, Gruijl TD De, Graus YMF, Vliet HJJ Van Der, Lougheed M, et al. MUTZ-3 , a human cell line model for the cytokine-induced differentiation of dendritic cells from CD34+ precursors. 2019;100(2):701–4.

4.	Facy V, Flouret V, Régnier M, Schmidt R. Reactivity of Langerhans cells in human reconstructed epidermis to known allergens and UV radiation. Toxicol Vitr. 2005;19(6):787–95.

5.	Basketter D, Darlenski R, Fluhr JW. Skin irritation and sensitization: mechanisms and new approaches for risk assessment. Skin Pharmacol Physiol. 2008;21(4):191–202.

6.	Gibbs S, Corsini E, Spiekstra SW, Galbiati V, Fuchs HW, DeGeorge G, et al. An epidermal equivalent assay for identification and ranking potency of contact sensitizers. Toxicol Appl Pharmacol. 2013;272(2):529–41.

7.	Saito K, Nukada Y, Takenouchi O, Miyazawa M, Sakaguchi H, Nishiyama N. Development of a new in vitro skin sensitization assay (Epidermal Sensitization Assay; EpiSensA) using reconstructed human epidermis. Toxicol Vitr. 2013;27(8):2213–24.

8.	Kosten IJ, Spiekstra SW, de Gruijl TD, Gibbs S. MUTZ-3 derived Langerhans cells in human skin equivalents show differential migration and phenotypic plasticity after allergen or irritant exposure. Toxicol Appl Pharmacol. 2015;287(1):35–42.

9.	Bergers LIJC, Reijnders CMA, van den Broek LJ, Spiekstra SW, de Gruijl TD, Weijers EM, et al. Immune-competent human skin disease models. Drug Discov Today. 2016;21(9):1479–88.

10.	Genoskin. Ready-to-use ex vivo human skin models for cosmetic testing [Internet]. 2018 [cited 2019 Dec 12]. Available from: https://www.genoskin.com/skin-models-cosmetic-testing/

11.	Abd E, Yousef SA, Pastore MN, Telaprolu K, Mohammed YH, Namjoshi S, et al. Skin models for the testing of transdermal drugs. Vol. 8, Clinical Pharmacology: Advances and Applications. Dove Medical Press Ltd; 2016. p. 163–76.

12.	Bock S, Said A, Müller G, Schäfer-korting M, Zoschke C, Weindl G. Characterization of reconstructed human skin containing Langerhans cells to monitor molecular events in skin sensitization. Toxicol Vitr. 2018;46:77–85.

13.	Régnier M, Staquet M-J, Schmitt D, Schimdt R. Integration of Langerhans Cells into a Pigmented Reconstructed Human Epidermis. J Invest Dermatol. 1997 Oct;109(4):510–2.

14.   Lee HY, Stieger M, Yawalkar N, Kakeda M. Cytokines and chemokines in irritant contact dermatitis. Mediators Inflamm. 2013;2013:1–7.

15.   Bechetoille N, Dezutter-Dambuyant C, Damour O, André V, Orly I, Perrier E. Effects of solar ultraviolet radiation on engineered human skin equivalent containing both langerhans cells and dermal dendritic cells. Tissue Eng. 2007;13(11):2667–79.

16.   Pastore S, Cavani A, Girolomoni G. Epidermal cytokine and neuronal peptide modulation of contact hypersensitivity reactions. Immunopharmacology. 1996;31(2–3):117–30.

17.   Mann A, Breuhahn K, Schirmacher P, Blessing M. Keratinocyte-derived granulocyte-macrophage colony stimulating factor accelerates wound healing: Stimulation of keratinocyte proliferation, granulation tissue formation, and vascularization. J Invest Dermatol. 2001;117(6):1382–90.

18.   Régnier M, Patwardhan a, Scheynius a, Schmidt R. Reconstructed human epidermis composed of keratinocytes, melanocytes and Langerhans cells. Med Biol Eng Comput. 1998;36(November):821–4.

19.   Aiba S, Terunuma A, Manome H, Tagami H. Dendritic cells differently respond to haptens and irritants by their production of cytokines and expression of co-stimulatory molecules. Eur J Immunol. 1997;27(11):3031–8.

20.   Mizuashi M, Ohtani T, Nakagawa S, Aiba S. Redox imbalance induced by contact sensitizers triggers the maturation of dendritic cells. J Invest Dermatol. 2005 Mar 1;124(3):579–86.

21.   Shallcross L, Ritchie S, Harberts E, Tammaro A, Gaitens J, Gaspari AA. Manganese oxidation state as a cause of irritant patch test reactions. Dermatitis. 2014 Mar;25(2):66–71.

22.   Kapellos T, Bonaguro L, Gemünd I, Reusch N, Saglam A, Hinkley E, et al. Human Monocyte Subsets and Phenotypes in Major Chronic Inflammatory Diseases. Front Immunol. 2019;10(2035).

23.   Wołkow P, Gębska A, Korbut R. In vitro maturation of monocyte-derived dendritic cells results in two populations of cells with different surface marker expression, independently of applied concentration of interleukin-4. Int Immunopharmacol. 2018 Apr 1;57:165–71.

24.   Catherine E A, Aisha L, Chun-Jen C, Stephen G E, Lena L O, P Rod D. CD14+ antigen-presenting cells in human dermis are less mature than their CD1a+ counterparts. Int Immunol. 2007 Nov;19(11):1271–9.

25.   Fontes M, Orellana D, Palma B, Covas D. Maturation of dendritic cells following exposure to different maturational stimuli. Rev Bras Hematol Hemoter. 2006;28(2):89–96.

26.   Fumio M, Robin P, Sukhwinder S, Aya M, Jurgen S, Shigeko Y. Investigation of Fascin1, a Marker of Mature Dendritic Cells, Reveals a New Role for IL-6 Signaling in CCR7-Mediated Chemotaxis. J Immunol. 2021;207(3):938–49.

27. Schachtner H, Weimershaus M, Stache V, Plewa N, Legler DF, Höpken UE, et al. Loss of Gadkin Affects Dendritic Cell Migration In Vitro. PLoS One. 2015;10(12):e0143883.

28. Michio T, Akihiro H, Satoshi M, Francis H. W. S, Yasutaka N, Ryoyo I, et al. Tracking and quantification of dendritic cell migration and antigen trafficking between the skin and lymph nodes. Sci Rep. 2014 Aug 12;4(6030).

29. L K. Electron microscopic observations of dyskeratosis, apoptosis, colloid bodies and fibrillar degeneration after skin irritation with dithranol. J Cutan Pathol. 1990;17(1):37–44.

30. Nicolas B, Henri A, Louis T, Martine D, Jean D, Veronique Q. Efficient migration of dendritic cells toward lymph node chemokines and induction of T(H)1 responses require maturation stimulus and apoptotic cell interaction. Blood. 2005 Sep 1;106(5):1734–41.

CHAPTER 5

Modelling basal cell carcinoma

C. Gaviria [a,b], E. Rácz [c], L.M. Restrepo [a,d], F. Foijer [b]

[a] Tissue Engineering and cell therapy research Group, School of Medicine, University of Antioquia, Colombia
[b] European Research institute for the Biology of Ageing, University Medical Center Groningen, The Netherlands
[c] Department of Dermatology, University Medical Center Groningen, The Netherlands
[d] Medical Research Institute, School of Medicine, University of Antioquia, Colombia

Manuscript in preparation

ABSTRACT

Basal cell carcinoma (BCC) is one of the most common types of skin cancer, accounting for about 75% of non-melanoma skin cancer. Animal models are commonly used to study tumor growth and test therapeutic agents. Besides ethical issues and the differences between human and animal skin, it has been difficult to obtain mouse models for BCC that faithfully mimic the human condition. Therefore, relevant systems to study human BCC pathology are urgently needed.

In vitro models composed of human skin cells can be adapted to study different human diseases. However, there are a few reports on the culture of BCC, as it has shown to be particularly difficult to grow *in vitro*. Here, we describe a protocol to culture primary BCC and the further generation of 3D models. Using culture plates containing gamma-irradiated 3T3 cells and keratinocytes medium supplemented with rock inhibitor, we were able to obtain cells from all tested tumor biopsies. 3D models were then generated by seeding tumor explants or BCC-derived cells and normal keratinocytes on a fibroblasts-populated fibrin gel.

The BCC-derived cells differed from normal keratinocytes in their morphology and adhesion molecules expression. Moreover, fibrin-based models supported the growth of both tumor explants and cell suspensions and showed to be a promising tool for the 3D culture of primary BCC, recreating relevant features of this type of cancer and providing an alternative system to study human BCC and test therapeutics agents.

INTRODUCTION

Basal cell carcinoma (BCC) is one of the most common human cancers, accounting for 75% of non-melanoma skin cancer and affecting around 1 million people in 2020 [1,2]. It arises from basal cells of the epidermis, tends to grow slowly, and very rarely metastasizes [3,4]. Early treatment of BCCs is essential because as the tumor grows, it becomes more dangerous and can cause significant deformity and scarring, destroying cartilage, and producing considerable morbidity [1,5,6]. Unlike other skin cancers, BCC has no precursor lesions and recurrence is frequent [7].

Currently, the study of cancer pathology and new therapeutic agents is mostly based on animal experiments. Their main limitation, other than ethical issues, is the difficulty of inducing a BCC murine condition that faithfully mimics the human one [5]. Moreover, the differences between the structure of human and animal skin make it difficult to extrapolate results to a human context [8,9].

Xenograft models have been used as cancer study tools as well, but they have not shown reproducibility and usually lack similarity to human BCC [10,11]. Some BCC *ex vivo* models have been successfully described, showing high similarity to native tumors, but they depend on a continuous supply of fresh tumor biopsies, limiting their applicability as a drug testing platform [8].

Proper systems that allow the continuous and accurate study of human BCC pathology are highly desirable. *In vitro* models could serve that purpose, as they are composed of human cells and can be adapted to study different conditions [12], overcoming the necessity of constant biopsies supply.

There are not many reports on the successful cultivation of BCC. Due to its very slow growth, low platting efficiency, contamination with other cell types, and lack of attachment molecules, BCC has been extremely difficult to grow *in vitro*. Bradbeer et al. cultured nodular BCC from explants obtaining 17% growth efficiency [13]. Brysk et al. successfully grew BCC cells from cell suspensions of 8 patients [14] but reached only a few passages, which has also been the limitation of other studies [15,16]. The establishment of a BCC-derived cell line was achieved by using an undifferentiated aneuploid BCC tumor [17], which, however, might not be broadly representative of BCC tumors. There is only one report on the establishment of nodular BCC cultures with 100% efficiency [18]. Nevertheless, the authors could not rule out the possibility that BCC cells had a mesenchymal origin.

Here, we describe a protocol to establish primary BCC cultures with improved proliferation rates and epithelial morphology, yielding cell outgrowth from 100% samples. We further show a method to generate 3D primary BCC models, using a fibroblasts-populated fibrin gel and tumor-derived cells and/or healthy keratinocytes.

MATERIALS AND METHODS

3T3 maintenance and feeder layer preparation

NIH 3T3 cells were maintained in culture in DMEM supplemented with 10% (v/v) fetal bovine serum (FBS) and 1% (v/v) penicillin-streptomycin (all from Gibco). Cells were passaged when 70-80% confluence was reached.

For the establishment of the feeder layer, 3T3 cells were seeded at a density of 12×10^3 cells/cm^2. The next day, cells were gamma-irradiated with a dose of 60 Gy (i3T3) and the medium was refreshed.

Human skin cells isolation and culture

Basal carcinoma cells

After informed consent, biopsies of BCC were obtained from Mohs surgery leftovers performed at the Department of Dermatology at the UMCG, Groningen, the Netherlands. The samples were taken from 24 patients aged from 45 to 95 years. Specifications of all samples are provided in Table 1.

Fresh samples were immediately immersed in DMEM supplemented with 10% (v/v) FBS and 1% (v/v) penicillin-streptomycin. Before processing, samples were washed with 70% ethanol for 30 sec. Tissue dissection and culture were performed in biosafety. One part of the biopsy was frozen while the remainder was used for culture. The biopsies were placed in 100 mm Petri dishes (Greiner Bio-One) and washed thoroughly with phosphate-buffered saline (PBS, Gibco). Each sample was mechanically fragmented and here different processing and culture methods were used:

Tissue pieces were incubated in 0.25% Trypsin (Gibco) under stirring. Then, cells were filtered through a 100 μm cell strainer and Trypsin was inactivated. Cell suspensions were cultured in QN medium (described in Chapter 2) on top of:

1) Non-coated cell culture dishes.
2) Matrigel (Corning).
3) i3T3 cells.
4) i3T3 cells in the presence of 10 uM Rock inhibitor (Y-27632, STEMCELL Technologies).

In another approach, skin fragments were placed on:

5) Non-coated culture dishes.
6) Culture dishes containing i3T3 and in the presence of 10 uM Rock inhibitor.

Explants were air-dried for about 10 min to allow attachment. Thereafter, 2 mL of QN medium were poured gently into dishes without disturbing the explants. The dishes were then incubated at standard conditions (37°C, 5% CO2) and 24 h later additional 2 mL of medium were added. After 2 days, 10 ng/mL Epidermal Growth Factor (EGF, Preprotech) was added to the media.

Keratinocytes and fibroblasts

After informed consent, human skin samples were obtained from blepharoplasties and mammary reductions leftovers, performed at the Department of Plastic Surgery at the UMCG, Groningen, The Netherlands

Samples were washed in PBS, immersed in 70% ethanol for 1 min, and mechanically fragmented. Fragments were placed on 10 mm culture dishes and air-dried for 15 min. Then, 5 mL of QN medium were added. The media was supplemented with 10 uM Rock inhibitor and, on day 2, 10 ng/mL EGF were added. The medium was changed every 2-3 days.

Table 1. Information on the BCC sample set.

Sample	Gender	Age	Localization	UV exposure	Classification
BCC 1	M	73	Nasal ala	High	Nodular
BCC 2	M	88	Ear (helix)	High	Nodular/infiltrative
BCC 3	F	70	Nose (tip)	High	Nodular
BCC 4	F	70	Nose (tip)	High	Nodular
BCC 5	F	50	Nasal ala	Moderate	Nodular
BCC 6	M	74	Nasal ala	High	Nodular
BCC 7	F	48	Nasolabial fold	Moderate	Nodular
BCC 8	M	79	Temple	High	Nodular/infiltrative
BCC 9	F	72	Ear (helix)	High	Nodular/infiltrative
BCC 10	F	64	Forehead	Moderate	Nodular
BCC 11	M	51	Forehead	Moderate	infiltrative
BCC 12	F	45	Forehead	Moderate	infiltrative
BCC 13	F	78	Temple	High	Nodular
BCC 14	M	87	Scalp	High	Nodular/infiltrative
BCC 15	F	69	Scalp	Moderate	Nodular/infiltrative
BCC 16	F	56	Nose/medial canthus	Moderate	Nodular
BCC 17	F	64	Scalp	Moderate	Nodular
BCC 18	M	65	Nasal ala	Moderate	Nodular
BCC 19	M	70	Cheek	Moderate	Nodular
BCC 20	F	80	Nasal ala	Moderate	Nodular
BCC 21	F	84	Nose (sidewall)	Moderate	Nodular
BCC 22	F	95	Temple	Moderate	Nodular/infiltrative
BCC 23	F	86	Nose (sidewall)	High	Nodular
BCC 24	F	87	Nose (sidewall)	Moderate	Nodular

Quantitative RT-PCR

RNA was isolated from BCC-derived cells and healthy skin-derived keratinocytes using the RNeasy kit (Qiagen). Reverse transcription was performed by using 1 µg of total RNA (Superscript II, Invitrogen) and random primers. The resulting cDNA was used as a template for qPCR (ABI PRISM 7700 Sequence Detector) in the presence of SYBR-green (Invitrogen). Tubulin was used to correct the total amount of cDNA. Values in BCC-derived cells were compared to the expression values in normal keratinocytes (normalized to 1). The following primers were used:

BPAG1 Fw ATGAGAACAATTGAGCAGCTGC
BPAG1 Rv GGCAATCTGGGCTTCCAAGATATGT
BPAG2 Fw TCCAGCGGCTCTCCTGGCCCA
BPAG2 Rv TATTCCTGGTCGGCCAGGGGT
b4 integrin chain Fw CGGATGCTGCTTATTGAGAAC
b4 integrin chain Rv GAGGGTGGAGGATGTGCTTAG
b3 laminin 5 chain Fw AACGTGGTGGGTCCCAAAT
b3 laminin 5 chain Rv TGCTCGGATCTGCTCAATCT
EpCAM Fw GCAGCTCAGGAAGAATGTG
EpCAM Rv CAGCCAGCTTTGAGCAAATGAC

Three-dimensional BCC model construction

For the construction of the dermal equivalent, a mix of human plasma, fibroblasts, 0.9% NaCl (Sigma-Aldrich), and tranexamic acid (Sigma-Aldrich) was prepared. To promote fibrin polymerization, 1% $CaCl_2$ (Fisher Chemical) was added and the solution was gently mixed, poured into 12 well ThinCert™ cell culture inserts, 0.4 µm pore diameter (Greiner Bio-One), and incubated (37°C, 5% CO2) for 30 minutes. Subsequently, each gel was covered with DMEM containing 10% FBS, 1% L-glutamine, and 1% penicillin/streptomycin, and incubated overnight at 37 °C.

The next day, the medium was removed, and the gels were equilibrated with QN media for 2h at 37 °C.

Three different approaches were used to construct the epidermal compartment:

1) Explant model: a biopsy fragment of suitable size was placed on top of the dermal compartment. QN medium, supplemented with 10 uM ROCK inhibitor, was added on the basolateral side and, after 2 days, the model was kept in QC, always exposed to the air-liquid interface.

Organotypic 3D models were also generated with varying amounts of healthy keratinocytes and BCC-derived cells:

2) Keratinocytes and BCC mix model: a total of $2x10^5/cm^2$ cells were suspended in 200 µL QN and placed on top of the gels. Different keratinocytes and BCC cells percentages were used. The constructs were incubated for 1.5 h at 37 °C to allow keratinocytes adhesion to the dermal compartment. The models were kept in QN medium supplemented with 10 uM rock inhibitor for 2 days and then QC was used. On day 7, the culture was exposed to the air-liquid interface for 14 days to stimulate keratinocytes differentiation. The medium was changed every other day.

3) Keratinocytes attachment layer model: a fixed number of keratinocytes ($5x10^4$) was resuspended in 200 µL QN and placed on top of the gels. Models were incubated for 1.5 h at 37 °C and kept in QN medium supplemented with 10 uM rock inhibitor overnight. Then, 0-$20x10^4$ BCC-derived cells/cm^2 were seeded on top of the keratinocytes and the tissues were cultured as above-mentioned.

In all cases, rock inhibitor was removed after 7 days.

Histology and immunohistochemistry

On the 21st day, tissues were collected and fixed in 4% paraformaldehyde. After fixation, tissues were dehydrated and embedded in paraffin. Five micrometers sections of the samples were stained with hematoxylin-eosin (H&E). Immunostaining of EpCAM was performed on paraffin sections using an anti-Ber-EP4 antibody.

RESULTS

Establishing a culture system to grow primary BCC

We first tried to determine the culture method that optimized BCC cells attachment and growth. In total, 6 different approaches were used. Data on cell processing and culture methods are shown in Table 2.

To evaluate the effect of different surfaces, we documented morphology and growth capacity during culture. *In vitro* cultures of cells derived from BCC samples are presented in Figure 1.

Cell suspensions failed to grow without the presence of a feeder layer. Cells seeded on non-coated dishes did not show keratinocytes attachment, while only contaminating fibroblasts were present (Figure 1a). When dishes were coated with Matrigel, few samples showed keratinocytes adhesion (Figure 1b) but no growth at all, and they were completely differentiated. The use of i3T3 feeder layers allowed the growth and proliferation of keratinocytes from 67% of samples (Table 2), which took over the culture after some weeks (Figure 1c). Similarly, almost half of the samples processed by explant culture (Table 2) showed the presence of keratinocytes (Figure 1d). In one of the samples, only cells with mesenchymal-like morphology appeared (Figure 1e). However, keratinocytes hardly went any further than passage 1 and fibroblasts contamination was a common problem.

In order to enhance BCC keratinocytes growth and proliferation, the medium was supplemented with 10 uM rock inhibitor (RI), which has been reported to enhance keratinocytes proliferation [19–23]. Due to the inadequate condition of 1 sample and the minuscule size of another, 2 out of 5 seeded cell suspensions did not make it on i3T3 cells in the presence of RI (Table 2).

When tumor explants were placed on a culture dish with an i3T3 feeder layer (Figure 1f-h) and RI, keratinocytes-like cells successfully grew from all samples, and proliferation was significantly improved. After initial harvest, cells were able to proliferate on i3T3, even for later passages. In some cases, they acquired both spindle and epithelioid characteristics (Figure 1h) and after an average of 5 passages, some samples became irregular displaying enlarged-sized cells (compare upper and lower sides cells of Figure 1i) with decreased proliferation rate.

We, therefore, defined QC medium with 10uM RI and the presence of a feeder layer, as the method for expanding BCC-derived cells. Figure 2 shows the schematic of the protocol to grow cells from a BCC sample.

Table 2. Cell culture conditions and success rates on passage 0.

Culture method	No. samples	Cell outgrowth	Success	Comments
Non-coated dish	3	0	0%	FB-like morphology
Matrigel	3	0	0%	Attachment with no growth
Explants	16	7	44%	FB-like morphology in 1 sample
Cell suspensions on i3T3	6	4	67%	-
Cell suspensions on i3T3+RI	5	3	60%	One deteriorated sample*
Explants+i3T3+ RI	7	7	100%	FB-like cells in 1 sample

FB: Fibroblasts, RI: rock inhibitor, *: Underlying infection
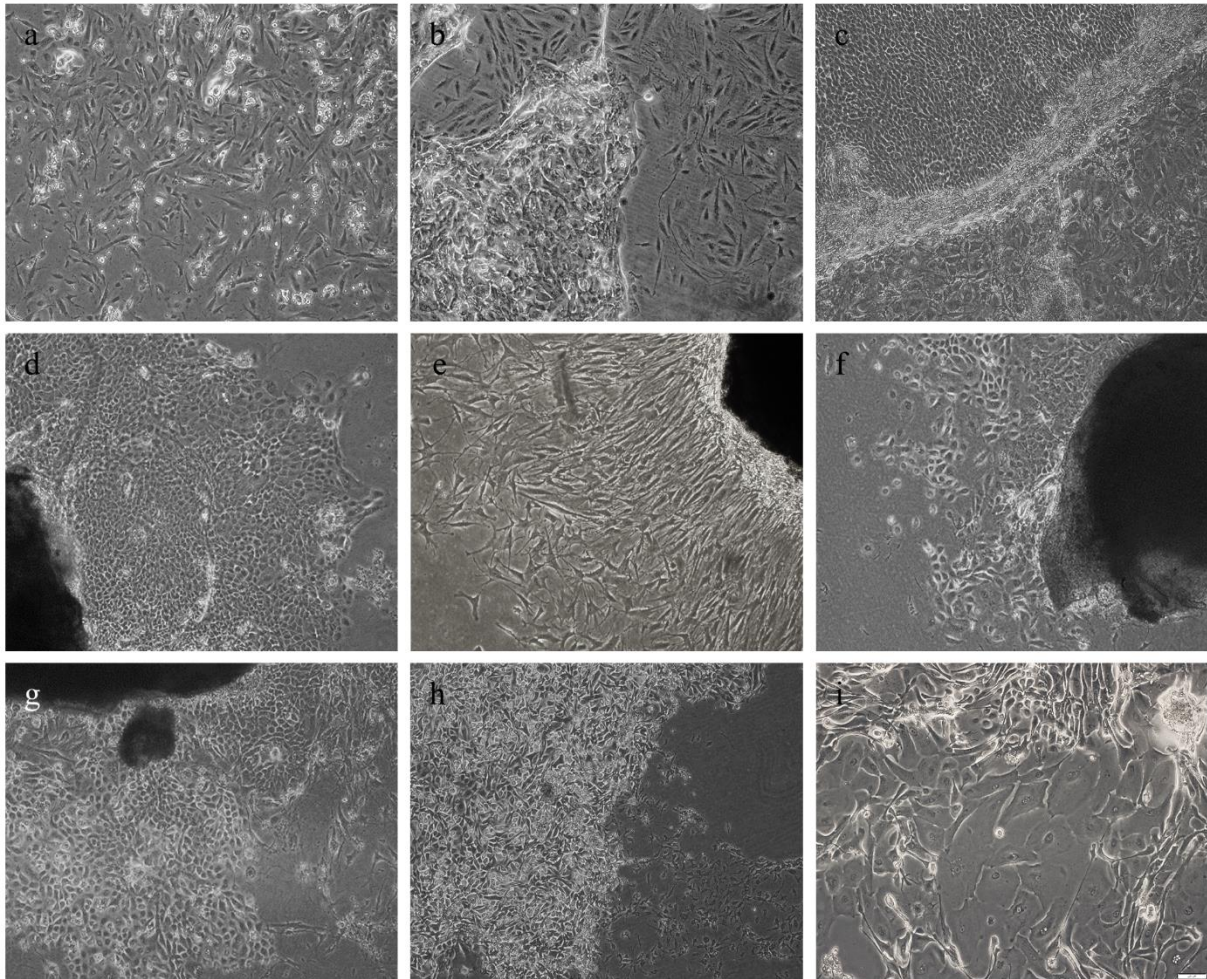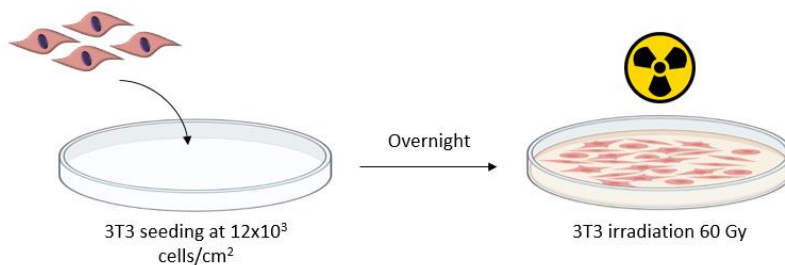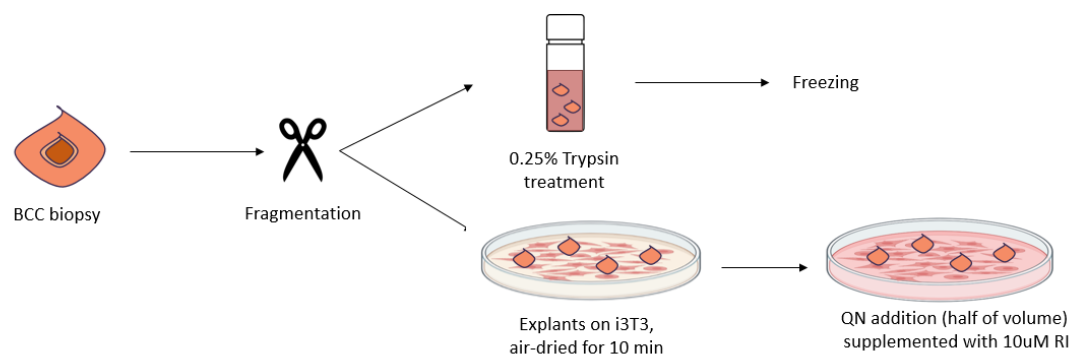
Figure 1. Cultures of primary basal cell carcinoma. Cells derived from Trypsin-treated tissues failed to grow on a) non-coated culture dishes and b) Matrigel-coated dishes but had a 67% success rate on c) gamma-irradiated 3T3 feeder layer. Cells derived from explants d), showing mesenchymal morphology e), and in the presence of rock inhibitor and 3T3 feeder layer at various days of culture, including f) the moment they started to grow, g) when they reached a 40-50% of confluence, and when they started to acquire a spindle-like shape at subsequent passages h). After 5 passages some BCC-derived cells showed enlargement in size and proliferation arrest i).

Day 0. Feeder layer preparation

3T3 seeding at 12×10^3 cells/cm²

Overnight

3T3 irradiation 60 Gy

Day 1. Skin cells isolation and culture

BCC biopsy → Fragmentation

0.25% Trypsin treatment → Freezing

Explants on i3T3, air-dried for 10 min → QN addition (half of volume) supplemented with 10uM RI

Day 2. Medium addition

QC addition supplemented with 10uM RI

BCC cells dettachment

0.05% Trypsin treatment → Remaining 3T3 removed

0.25% Trypsin treatment →

Cell suspension seeding on i3T3

QC + 10uM RI Re-growth from explants

Downstream application
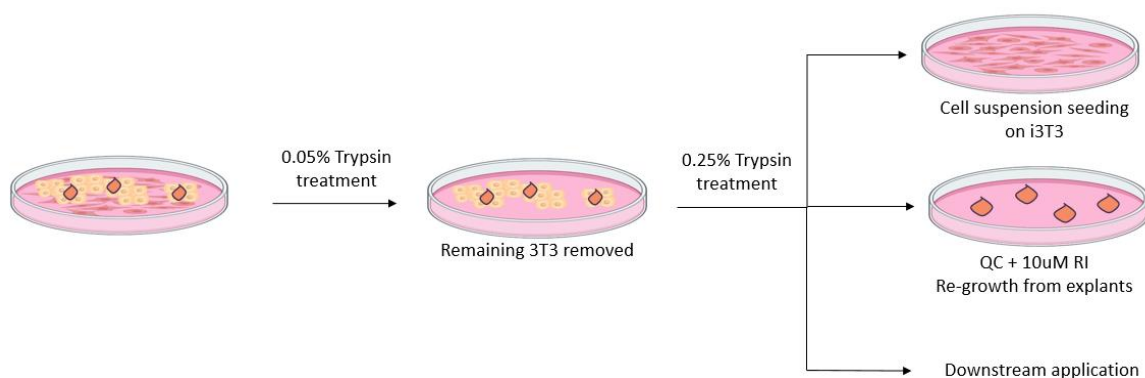
Figure 2. Schematic illustration of the protocol of primary BCC culture

Quantitative PCR

To confirm that the cells obtained by our culture system are indeed BCC cells and not normal keratinocytes or mesenchymal cells, we investigated whether these presented dysregulation of cell-cell and basement membrane (BM) attachment molecules, typical features of BCC [24–30]. For comparison, keratinocytes derived from healthy skin were used to compare mRNA levels.

Figure 3 illustrates the mRNA relative expression of BCC anchoring components. Although non-significant differences were found, transcripts levels of BPAG1, BPAG2, the β4 subunit of the α6β4 integrin, and the β3 chain of laminin 5 were reduced in all tumor-derived cells. There was higher variability for EpCAM, which did not display increased expression, as usually reported for BCC.
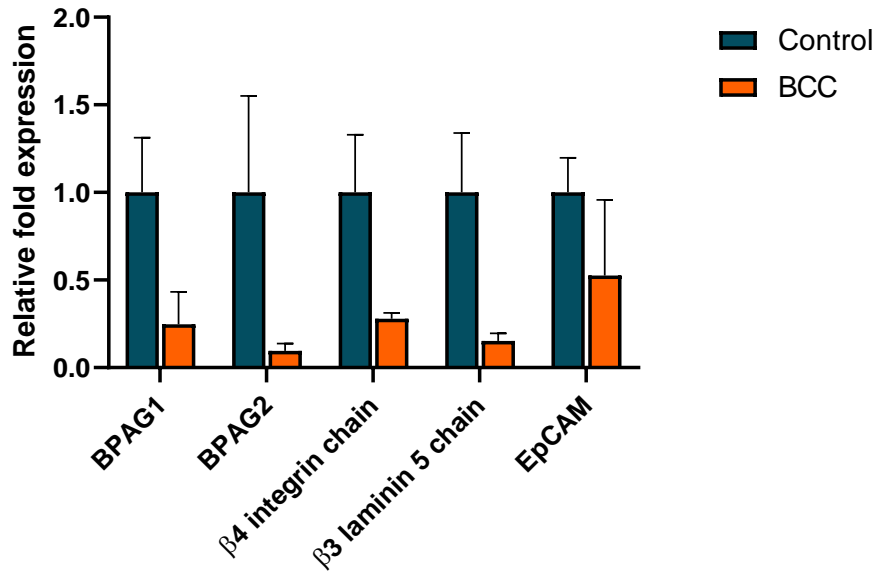
Figure 3. Quantitative PCR showing expression of cell-cell (EpCAM) and BM adhesion molecules (BPAG1, BPAG2, β4 subunit of α6β4 integrin, and β3 chain of laminin 5). Error bars show SEM for 3 BCC tumors (BCC) and 3 healthy skin-derived cells (Control). For statistical analysis, a two-tailed t-test was applied.

Three-dimensional BCC models development

We next investigated whether BCC-derived cells could be used to develop a 3D BCC model.

To faithfully mimic skin tissue, it is necessary to culture cells with malignant potential in the context of a 3D network of healthy cells. To evaluate the effect of the presence of healthy keratinocytes, 3 different epidermal models were constructed by using 1) a BCC explant, 2) a mix of normal keratinocytes and BCC-derived cells, and 3) normal keratinocytes as an attachment layer for BCC-derived cells. RI was used to boost proliferation before the air-liquid interface exposition.

We examined the morphology and BerEP4 expression of the resulting models.

Histology of BCC models

Given the advantages of *ex vivo* explant models when it comes to mimicking skin tissue (they preserve the skin cellular components, structure, and extracellular matrix composition), a BCC explant model was first constructed (Figure 4a). There was lateral migration of biopsy-derived keratinocytes over the dermal compartment (Figure 4b) with disturbed attachment in some places (Figure 4c). Importantly, the large mass of epidermal cells remained viable (Figure 4d) and the characteristic dermal migration of some types of BCC was present (Figure 4e).
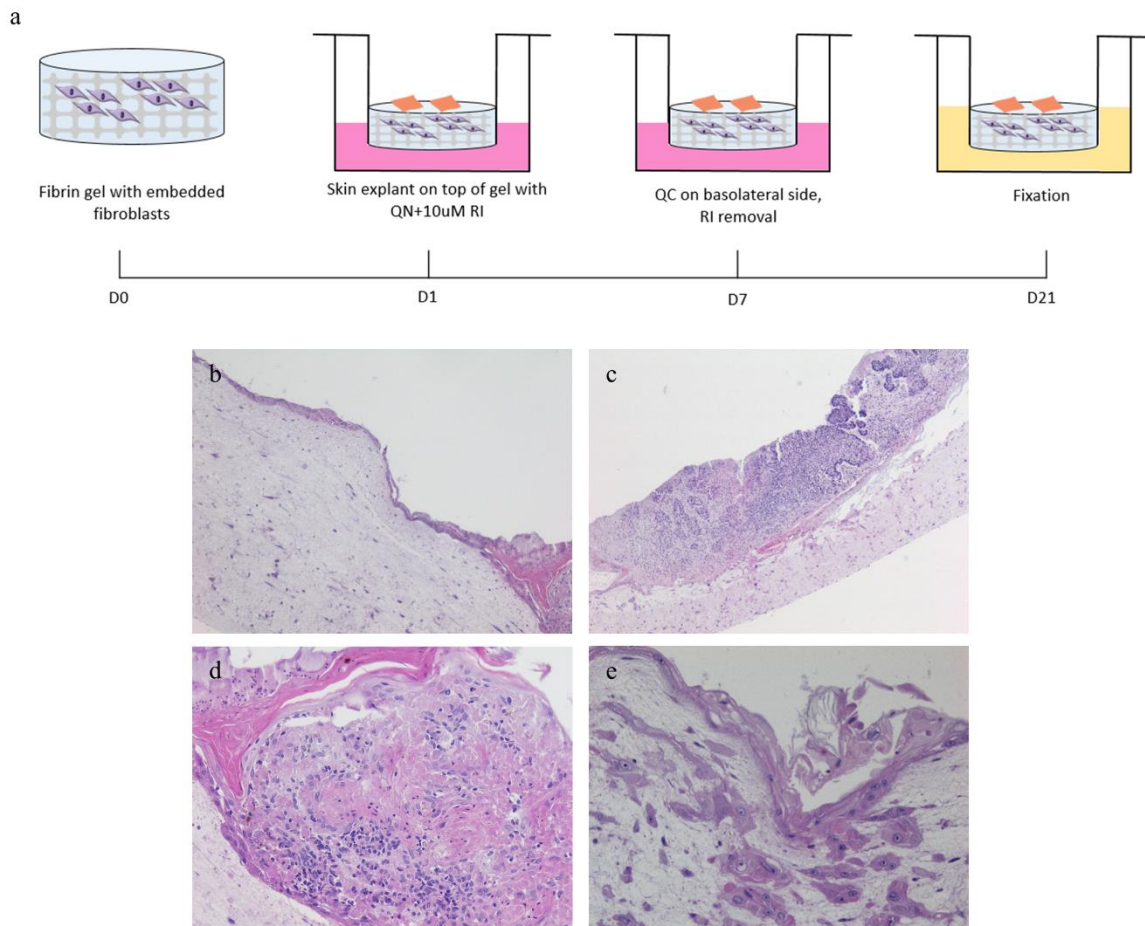
Figure 4. Histological characteristics of BCC explant model generated by seeding a BCC biopsy on a fibroblast-containing fibrin gel. a) Schematic illustration of the protocol for the construction of the model, b) cells migrating from the explant and covering the gel, c) weak attachment between explant and dermal compartment, d) large mass of epidermal cells, e) migration into the dermal compartment.

Knowing that the fibrin-based dermal equivalent can support the culture of BCC explants (Figure 4), we next proceeded to develop a 3D model with cells obtained from skin explants. To this end, cells from 2 nodular BCC samples were used, one for each strategy.

As a first approach, a mix of healthy (KC) and tumor-derived keratinocytes (BCC) were seeded on top of a fibrin gel (Figure 5a). A total of $2 \times 10^5/cm^2$ cells were used. Compared to native skin (Figure 5b), the 100% KCs model showed similar epidermal thickness with a well-differentiated epidermis (Figure 5c). As the percentage of BCC-derived cells increased (Figures 5d-i), the epidermis began to lose its native morphology and acquire an impaired differentiation pattern with dyskeratotic features (black arrows). Basal cells were not easily distinguishable, or they were already flattened (green arrows). Terminal differentiation was compromised as well. The addition of 10% BCC cells (Figure 5d) did not significantly affect epidermal thickness. However, epidermal thinning could be seen as the percentage increased (Figures 5e-g). Interestingly, percentages higher than 50% BCC were accompanied by nuclei in the corneum stratum (red arrows) and poor attachment to the dermal compartment (Figure 5j).
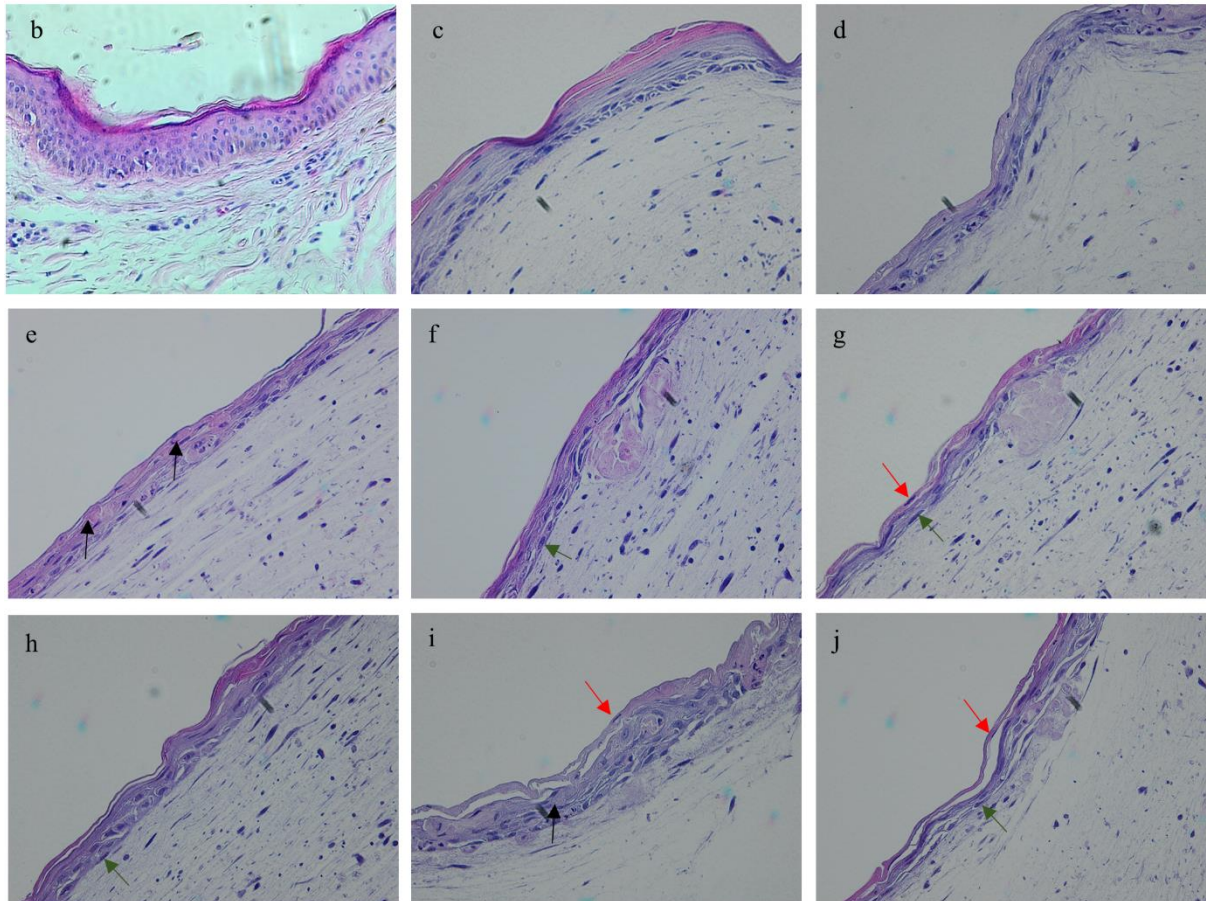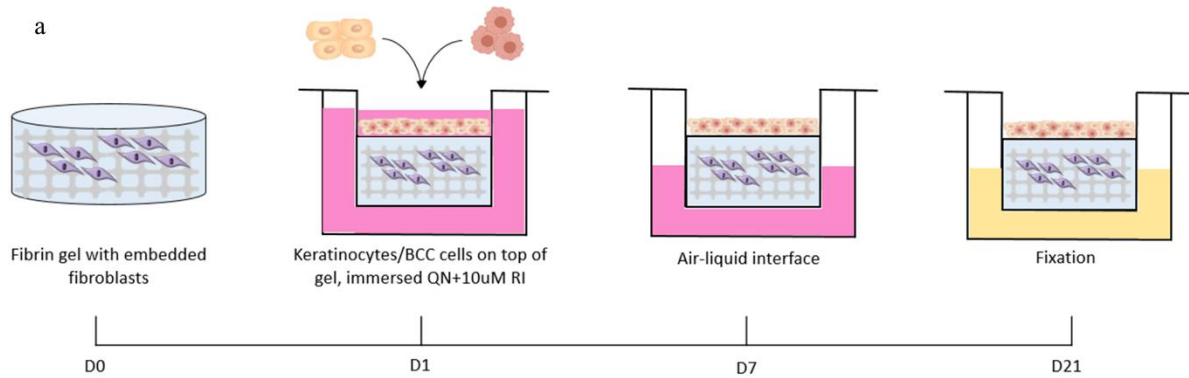
Figure 5. Histological characteristics of and 3D BCC models fabricated with different percentages of healthy (KC) and tumor-derived cells (BCC). a) Schematic illustration of the protocol for the construction of the model, b) native human skin, c) 100% KC and 0% BCC, d) 90% KC and 10% BCC, e) 75% KC and 25% BCC, f) 50% KC and 50% BCC, g) 25% KC and 75% BCC, h) 10% KC and 90% BCC, i) 0% KC and 100% BCC, j) 25% KC and 75% BCC model showing dermal detachment.

Given the alteration of BM adhesion molecules exhibited by BCC, as a second approach we used a fixed number of healthy keratinocytes as an attachment layer for different numbers of BCC cells. An illustration of the protocol and the histological characteristics of the models are presented in Figure 6. The model exclusively composed of KCs (Figure 6b) showed epidermal differentiation and adequate thickness, even though columnar-like basal cells were not easily distinguishable. Models with 2.5×10^4 BCC cells/cm^2 (Figure 6c) displayed a high resemblance to pure KCs equivalents, with differentiation (although not everywhere) and proper epidermal width. Interestingly, epidermal islands became apparent (black arrows) as well as dyskeratotic

figures (red arrows). When the number of BCC cells was doubled (Figure 6d), the size of the epidermis decreased and a tendency for dermal infiltration was appreciated as well (not shown). In models with $10x10^4$ BCC cells (Figure 6e), islands and invasive behavior (black arrow) were noticeable and the epidermal compartment became thinner. Models with greater numbers of BCC cells presented increased impairment of epidermal differentiation and dyskeratosis, as well as a certain degree of parakeratotic cells (Figure 6f). Pure BCC models showed thinner and a more unorganized epidermis, with fewer cell layers (Figure 6g).
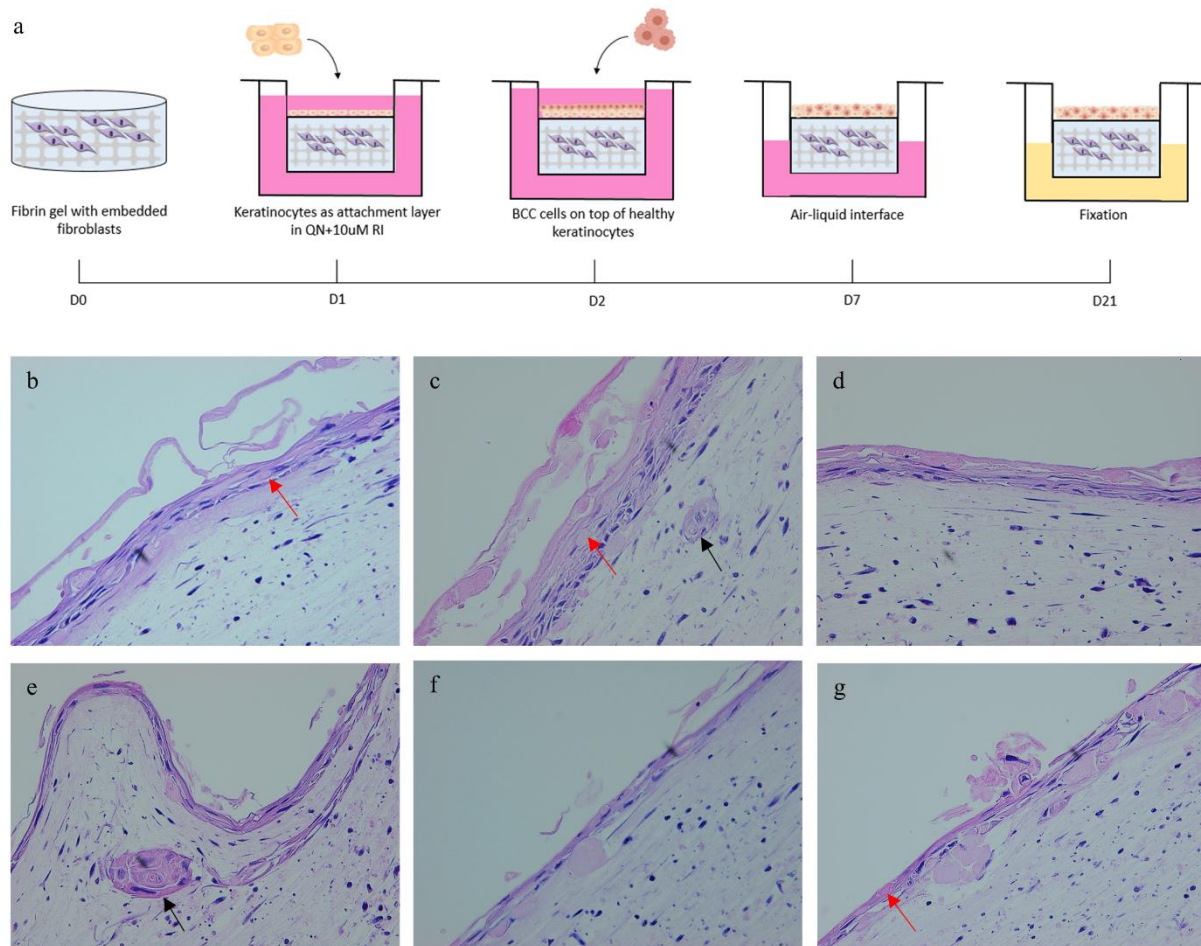

Figure 6. Histological characteristics of 3D BCC models fabricated with healthy keratinocytes (KC) as an attachment layer for tumor-derived cells (BCC). a) Schematic illustration of the protocol for the construction of the model, b) pure KC model. Different numbers of BCC cells were seeded on top of $5x10^4$ KCs/cm^2: c) $2.5x10^4$ BCC cells/cm^2, d) $5x10^4$ BCC cells/cm^2, e) $10x10^4$ BCC cells/cm^2, f) $20x10^4$ BCC cells/cm^2, g) No attachment layer, pure BCC model.

Immunohistochemistry of BCC models

As the epithelial cell adhesion molecule (EpCAM) is strongly increased in BCC, we evaluated its presence in our 3D models by immunohistochemical staining. Figure 7 shows the expression of the EpCAM antibody BerEP4 in the explant model. As expected, cells contained in the inner zone of the explant strongly express BerEP4 (Figure 7a-c), while, at the epidermal-dermal interface, BerEP4 expression was absent or weak (Figure 7b). Interestingly, cells that were able to migrate from the biopsy show low or null expression of the BCC marker, as well as cells that invaded the dermis (Figure 7d).
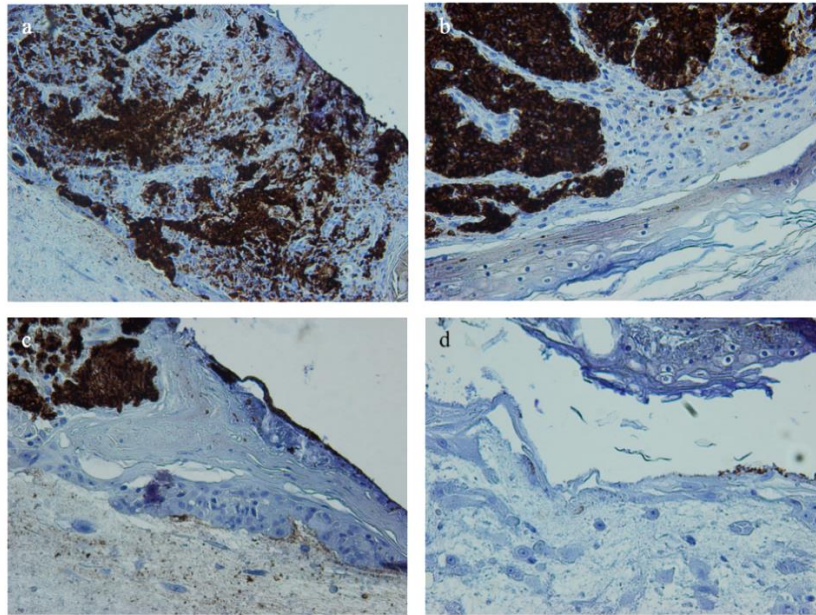
Figure 7. Expression of BerEP4 in the BCC explant model. a) Positive cells within a large epidermal mass, b) magnified image showing BerEP4-expressing cells and weak attachment between the explant and dermal compartment, c) null expression of BerEP4 in the external regions, d) migration and invasion into the dermal compartment.

Figure 8 illustrates BerEP4 expression in models containing a mix of healthy and tumor-derived keratinocytes. The model composed of 100% KC was negative for the BerEP4 staining pattern (Figure 8a). Changes in the expression of this protein were not considerable as the percentage of BCC-derived cells increased (Figures 8b-h). All of them showed absent or weak staining of BerEP4. Of high importance is that BerEP4 appears stronger in areas with structural abnormalities, clefts, or detachments (Figures 8c, e-g, arrows), which are typical features of human BCCs. Interestingly, the 100% BCC model (Figure 8h), showed null-to-weak intensity, with less intratissue detachment. These results are in line with our previous findings showing no upregulation of EpCAM in monocultures (Figure 3) and suggest that EpCAM levels are preserved in both 2D and 3D settings.
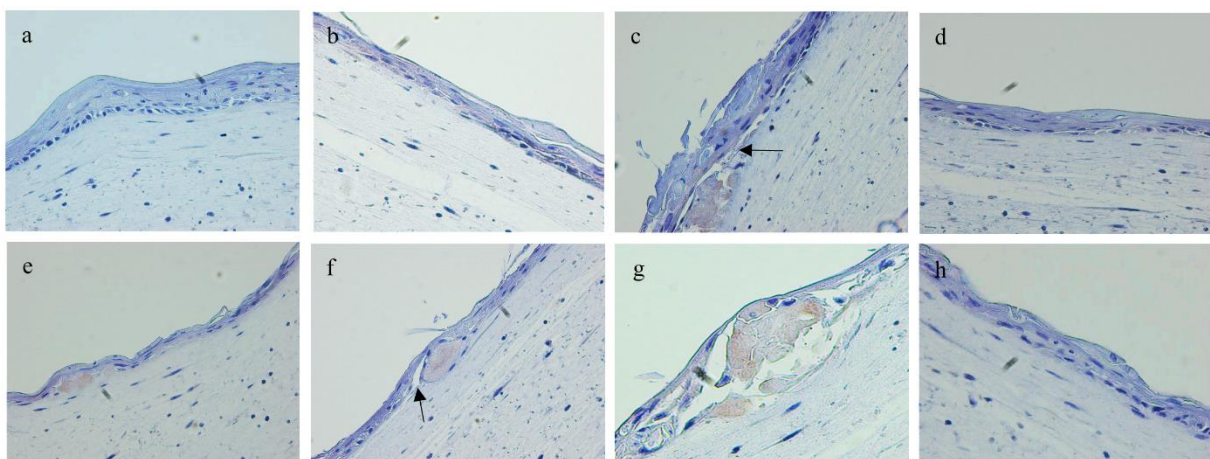

Figure 8. Expression of BerEP4 in 3D BCC models fabricated with different percentages of healthy (KC) and tumor-derived cells (BCC): a) 100% KC showing null expression of BerEP4, b) 90% KC and 10% BCC, c) 75% KC and 25% BCC showing clefts and structural abnormalities, d) 50% KC and 50% BCC, e) 25% KC and 75% BCC, f) 10% KC and 90% BCC, g) close-up of structural abnormality showing weak staining of BerEP4, h) 0% KC and 100% BCC.

Figure 9 presents the BerEP4 expression of models fabricated with healthy keratinocytes as an attachment layer for BCC cells. BerEP4 is present in areas with poor epidermal stratification and dermo-epidermal clefts, with moderate intensity in models containing BCC-derived cells (Figures 9b-f). As the number of tumor cells increases, each model exhibits more BerEP4 positive sections. The model composed of solely BCC cells (Figure 9f) showed the thinnest and unhealthy epidermis with the highest number of positive BerEP4 areas and attachment perturbations. Although at moderate levels, these models show increased BerEP4 intensity, as compared to those fabricated with a mix of healthy and tumor-derived cells (Figure 8).
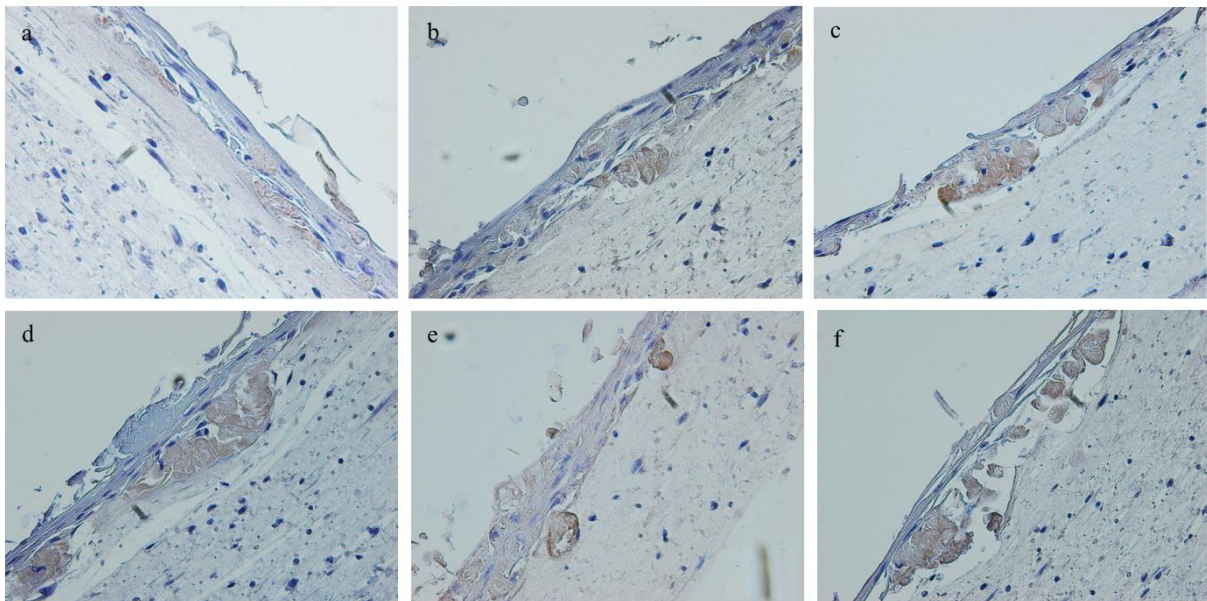

Figure 9. Expression of BerEP4 in 3D BCC models fabricated healthy keratinocytes (KC) as an attachment layer for tumor-derived cells (BCC), a) pure KC model. Different numbers of BCC cells were seeded on top of $5x10^4$ KCs/cm^2: b) $2.5x10^4$ BCC cells/cm^2, c) $5x10^4$ BCC cells/cm^2, d) $10x10^4$ BCC cells/cm^2, e) $20x10^4$ BCC cells/cm^2, f) No attachment layer, pure BCC model ($20x10^4$ BCC cells/cm^2).

Altogether, these results show that, unlike BCC tumor explants, *in vitro* cultured BCC cells present reduced EpCAM levels, which could be increased by using healthy keratinocytes as an attachment layer for BCC cells. Such setting is based on cell-cell instead of BM adhesions, overcoming the limitation of low production of BM attachment molecules in BCC-derived cells.

DISCUSSION

In this study, we describe a protocol to culture primary basal cell carcinoma and show the subsequent generation of three-dimensional BCC models. With the proposed method, successful growth from all BCC samples was achieved. Moreover, fibrin-based dermo-epidermal cultures showed to be a useful tool to develop a 3D BCC model, as they support the growth of both tumor explants and cell suspensions.

We first determined the culture method that better supports primary BCC growth and subculture. A combination of a 3T3 feeder layer along with a media supplemented with Rock inhibitor allowed us to obtain cells from all the tested samples with further expansion, except for 1 case. Human BCC has shown to be difficult to culture and there are not many reports on the successful establishment of a culture method. Explant cultures have led to low efficiencies. For example, Bradbeer et al. achieved outgrowth from only 14% explants of 5 BCC tumors samples [13]. With this technique, we were able to grow cells from 44% samples. Perhaps a more complex media like ours promotes the migration of cells from skin fragments. In agreement with our results, the use of cell suspensions on irradiated 3T3 allowed other authors to successfully grow cells from 47% [15] and 71% [31] samples. In these studies, however, few passages were achieved, probably because of the natural slow growth of BCC-derived cells which facilitates *in vitro* differentiation and the subsequent proliferation arrest.

To overcome this problem, Brysk et al. seeded cell suspensions on type I collagen coated-plated and low calcium medium (KGM), successfully growing 8 BCC samples and reaching 4-5 passages [14]. Additionally, there is one report on the establishment of nodular BCC cultures with 100% efficiency, in which authors used low-calcium and serum-free media, obtaining cells with both spindle and epithelioid morphology [18]. We therefore decided to use culture conditions that favored attachment, growth, and prevent differentiation of cells. Since Asada et al. showed growth from 73% samples when culturing explants on mitomycin-treated 3T3 cells [32] and given the numerous advantages of using a feeder layer for keratinocytes culture [33–35], we tried a combination of explant culture and i3T3 cells. Rock inhibitor was included in the media in an attempt to prevent differentiation. We were able to grow cells from 100% samples, obtaining a keratinocyte-like morphology as well as spindle and epithelioid features, which fits well with previous reports [18,36]. These results therefore highlight the importance of having stromal support along with an undifferentiation-promoting media to culture BCC-derived cells.

Several studies have shown that BCC presents abnormalities in cell-cell and basement membrane anchoring components [24–30,37,38]. Although not significant, our results revealed that all tested BCC samples had decreased levels of mRNA encoding for BPAG1, BPAG2, the b4 subunits of the a6b4 integrin, and the b3 chain of laminin 5. These findings could be confirmed in more high-powered studies. We suggest that this may account for BCCs decreased ability to grow *in vitro*, as the adherence to culture surfaces results compromised and cell attachment is necessary for proliferation of many cell types [39]. Another possibility is that there is no requirement for BCC-derived cells to have the above-mentioned attachment molecules to proliferate, given that anchorage-independent growth is a hallmark of transformed cells. Consequently, BCC *in vitro* growth may improve by using low attachment culture conditions. Indeed, this has been reported by Asada et al., who managed to grow 90% BCC cell suspensions on soft agar [32]. Our results suggest that our BCC cultures exhibit alterations in the synthesis

of attachment molecules that may be worthy of further investigation. It also indicates that BCC-derived cells are likely tumor cells and not contaminating keratinocytes.

EpCAM, the epithelial cell adhesion molecule, is strongly increased in carcinogenesis, especially in BCC, and has been associated with malignant proliferation [40,41]. We found high variability in mRNA levels, with no evidence of upregulation. A possible explanation is that only low EpCAM expressing cells migrate from tissue fragments to the plate surface or that cells lose it as they move. Reports on EpCAM function on migration and proliferation have been inconsistent. Some studies have shown that EpCAM overexpression is associated with enhanced proliferation [40,42] and migration [43], while others have found that its knockdown leads to increased proliferation [44] and migration in epithelial cells [45]. Gaiser et al. suggested that EpCAM downregulation may promote BCC infiltration [46]. Whether EpCAM has any inhibitory effect on the migration of BCC cells remains to be elucidated.

We used explant fragments and BCC-derived cells to develop explant and cell suspensions-derived 3D models, respectively. The explant model displayed lateral migration of biopsy-derived cells with the characteristic dermal invasion of some types of BCC. Of note, the large epidermal BCC mass remained viable. As expected, BerEP4 (anti-EpCAM antibody) was strongly expressed in the central regions of the explant, while migrating cells show weak or non-detectable staining. This is in agreement with our previous results showing variable but still low synthesis of EpCAM in monolayer cultured cells, which also migrated from BCC explants. Areas with a disturbed attachment were observed as well and could be the result of the downregulation of basement membrane anchoring components, as observed in BCC-derived cells. These results indicate that fibrin-based scaffolds are able to support the growth and maintenance of BCC tumor explants, leading to a model that displays great similarity to human BCC, thanks to the preservation of the main cellular components, viability, functionality, and structure found *in vivo*. Therefore, it could represent a promising tool to study BCC biology.

Regarding cell suspension-derived models, we observed loss of both normal epidermal morphology and proper differentiation as the number of BCC-derived cells increased. This is in agreement with the fact that BCC is composed of cells with alterations in stratification and keratin expression [15,32], which, consequently, are unable to produce a normal-like epidermis. Unlike *in vivo* tumors, EpCAM expression was absent or weak but still stronger in models containing BCC cells, contrary to our findings in monolayer cultures. Interestingly, positive staining was observed in places with differentiation impairments and clefts, typical characteristics of BCC tumors [48]. The observed clefts can be the result of the downregulation of basement membrane anchoring components. Some authors have proposed that reduced levels of attachment molecules prevent tumor islands from remaining attached to their BM, which may also play a role in migration and invasion capacity [24,37]. We indeed found alterations in the synthesis of BM adhesion molecules in BCC-derived cells, and interestingly, models fabricated with healthy keratinocytes as an attachment layer for BCC revealed a tendency for dermal infiltration. These results suggest that EpCAM is rather expressed in cells with compromised differentiation and reduced BM adhesion (e.g BCC cells) and that the 3D setting may promote its upregulation. These models, therefore, recapitulate some of the most important characteristics of BCC: impaired differentiation and diminished attachment to BM, features that otherwise will be difficult to appreciate in monolayer cultures. Future investigations could focus

on culture conditions that can preserve EpCAM levels, thereby providing a closer tumor-like morphology.

As far as we know, only two studies have reported the development of a 3D model of BCC, which, unlike ours, were entirely composed of keratinocytes cell lines. Mahmudur [3] seeded NEB1 cells (with targeted suppression of PTCH1) on top of a mix of Matrigel, collagen, and fibroblasts. There was no evidence of tumor development, dermal invasion, or epidermal island formation. The expression of typical BCC markers and the degree of differentiation were not evaluated. Perhaps other characteristics are needed besides suppression of PTCH1 in order to develop a BCC-like morphology. In fact, Bigelow et al. [49] found dermal infiltration dependent on EGFR activity by using HaCat cells overexpressing shh (ptch ligand) on fibroblasts-populated collagen gels. The models exhibited similar BCC morphology, cytokeratin 14 expression, and suprabasal proliferation. The intact expression of attachment molecules possibly facilitated the development of a BCC-like phenotype. Their results show the feasibility of having a 3D *in vitro* model of BCC. Since normal healthy cells were not present, it is not possible to know to what extent it can recreate the initial stages of BCC.

Although we were able to obtain BCC-derived cells that could be further subcultured, passages higher than 5 were not obtained. Our feeder layer requires serum-containing media, which, however, can lead to differentiation of basal keratinocytes, and the amount of rock inhibitor may have not been enough to counter such an effect. We did not study the effect of other rock inhibitor concentrations or low calcium media, thus, it is still possible that higher passages can be achieved with optimized conditions. Regarding 3D model development, relevant BCC features were recapitulated. However, lack of attachment molecules, differentiation stimuli, and the presence of a healthy non-tumoral dermis may have compromised the ability of BCC-derived cells to fully develop into an *in vivo*-like tumor. Future studies could focus on the construction of models with low attachment settings, lower levels of differentiation-promoting conditions, or the use of BCC-derived fibroblasts in the dermal compartment.

Our results underscored the importance of having a feeder layer that provides a means of attachment and releases factors for the growth and proliferation of BCC. More crucial is the inhibition of differentiation, which allowed us to obtain cells from all samples. This opens the door for the creation of specially designed media that totally prevents differentiation and supports the presence of feeder layers, increasing the life spam of current primary BCC cultures. The subsequent creation of 3D models offers, for the first time, a promising system to model primary BCC in a more realistic environment, offering deeper insight into tumor physiology and allowing the study of novel therapeutic agents, interactions between tumor and healthy cells, and disease progression.

In summary, we have established a protocol to culture primary BCC cells showing outgrowth from 100% samples. Our results revealed that a combination of explants, a 3T3 feeder layer, and rock inhibitor, allows the growth, proliferation, and subculture of BCC cells, as judged by their morphology and adhesion molecules expression. Moreover, we found that dermo-epidermal organotypic cultures have the potential to model basal cell carcinoma, recapitulating some of the most relevant characteristics of this type of cancer and could therefore become an important tool to test new therapeutics that target BCC.

ACKNOWLEDGMENTS

REFERENCES

1. Samarasinghe V, Madan V. Nonmelanoma skin cancer. J Cutan Aesthet Surg. 2012 Jan;5(1):3–10.

2. World Health Organization. Non-melanoma skin cancer [Internet]. 2020 [cited 2021 Aug 10]. Available from: https://gco.iarc.fr/today

3. Mahmudur M. Characterisation of a novel in vitro model of Basal cell carcinoma (BCC) through stable PTCH1 suppression in immortalised human keratinocytes. Queen Mary Unoversity of London; 2013.

4. Berking C, Hauschild A, Kölbl O, Mast G, Gutzmer R. Basal Cell Carcinoma - Treatments for the commonest Skin Cancer. Dtsch Arztebl Int. 2014 May 30;111(22):389–95.

5. Gober MD, Bashir HM, Seykora JT. Reconstructing skin cancers using animal models. Cancer Metastasis Rev. 2013;32(1–2):123–8.

6. Canadian Cancer Society. What is non-melanoma skin cancer? [Internet]. [cited 2018 Apr 7]. Available from: http://www.cancer.ca/en/cancer-information/cancer-type/skin-non-melanoma/non-melanoma-skin-cancer/?region=on

7. Saldanha G, Fletcher A, Slater DN. Basal cell carcinoma: A dermatopathological and molecular biological update. Br J Dermatol. 2003;148(2):195–202.

8. Bergers LIJC, Reijnders CMA, van den Broek LJ, Spiekstra SW, de Gruijl TD, Weijers EM, et al. Immune-competent human skin disease models. Drug Discov Today. 2016;21(9):1479–88.

9. Hill DS, Robinson NDP, Caley MP, Chen M, Toole EAO, Jane L. A novel fully-humanised 3D skin equivalent to model early melanoma invasion. Mol Cancer Ther. 2016;14(11):2665–73.

10. Hochberg M. Experimental Models for BCC. J Dermatology Clin Res. 2013;1(1).

11. Carlson JA, Combates NJ, Stenn KS, Prouty SM. Anaplastic neoplasms arising from basal cellcarcinoma xenotransplants into SCID-beige mice. J Cutan Pathol. 2002;29(5):268–78.

12. Garlick J a. Engineering skin to study human disease--tissue models for cancer biology and wound repair. Adv Biochem Eng Biotechnol. 2007;103(January):207–39.

13. Bradbeer M, Bourne AJ, Ayberk H, Tang SK, Marks R. Growth and antigenic characteristics of basal cell carcinoma in culture. Arch Dermatol Res. 1988 Jan;280(4):228–34.

14. Brysk MM, Santschi CH, Bell T, Wagner RF, Tyring SK, Rajaraman S. Culture of basal cell carcinoma. J Invest Dermatol. 1992;98(1):45–9.

15. Hernandez AD, Hibbs MS, Postlethwaite AE. Establishment of basal cell carcinoma in

culture: Evidence for a basal cell carcinoma-derived factor(s) which stimulates fibroblasts to proliferate and release collagenase. J Invest Dermatol. 1985;85(5):470–5.

16.   Kubilus J, Baden HP, McGilvray N. Filamentous Protein of Basal Cell Epithelioma: Characteristics In Vivo and In Vitro. J Natl Cancer Inst. 1980 Nov;65(5):869–75.

17.   Chiang LC, Chiang W, Yu HS, Sheu HM, Chen HY. Establishment and characterization of a continuous human basal cell carcinoma cell line from facial skin (I) cytological behavior of early passages. Kaohsiung J Med Sci. 1994 Apr;10(4):170–6.

18.   Grando SA, Schofield OM, Skubitz AP, Kist DA, Zelickson BD, Zachary CB. Nodular basal cell carcinoma in vivo vs in vitro. Establishment of pure cell cultures, cytomorphologic characteristics, ultrastructure, immunophenotype, biosynthetic activities, and generation of antisera. Arch Dermatol. 1996;132(10):1185–93.

19.   Chapman S, Liu X, Meyers C, Schlegel R, McBride A. Human keratinocytes are efficiently immortalized by a Rho kinase inhibitor. J Clin Invest. 2010;120(7):2619–26.

20.   McMullan R, Lax S, Robertson VH, Radford DJ, Broad S, Watt FM, et al. Keratinocyte Differentiation Is Regulated by the Rho and ROCK Signaling Pathway. Curr Biol. 2003;13(24):2185–9.

21.   Anderson ED, Sastalla I, Earland NJ, Mahnaz M, Moore IN, Otaizo-Carrasquero F, et al. Prolonging culture of primary human keratinocytes isolated from suction blisters with the Rho kinase inhibitor Y-27632. PLoS One. 2018;13(9):1–16.

22.   Liu X, Ory V, Chapman S, Yuan H, Albanese C, Kallakury B, et al. ROCK inhibitor and feeder cells induce the conditional reprogramming of epithelial cells. Am J Pathol. 2012;180(2):599–607.

23.   Chapman S, McDermott DH, Shen K, Jang MK, McBride AA. The effect of Rho kinase inhibition on long-term keratinocyte proliferation is rapid and conditional. Stem Cell Res Ther. 2014;5(2).

24.   Korman NJ, Hrabovsky SL. Basal cell carcinomas display extensive abnormalities in the hemidesmosome anchoring fibril complex. Exp Dermatol. 1993;2(3):139–44.

25.   Pentel M, Helm KF, Maloney MM. Cell Surface Molecules in Basal Cell Carcinomas. Dermatologic Surg. 1995;21(10):858–61.

26.   Verhaegh M, Beljaards R, Veraart J, Hoekzema R, Neumann M. Adhesion molecule expression in basal cell carcinoma. Eur J Dermatol. 1998 Jun;8(4):252–5.

27.   Sollberg S, Peltonen J, Uitto J. Differential expression of laminin isoforms and β4 integrin epitopes in the basement membrane zone of normal human skin and basal cell carcinomas. J Invest Dermatol. 1992;98(6):864–70.

28.   Savoia P, Trusolino L, Pepino E, Cremona O, Marchisio PC. Expression and topography of integrins and basement membrane proteins in epidermal carcinomas: Basal but not squamous cell carcinomas display loss of α6β4 and BM-600/nicein. J Invest Dermatol. 1993;101(3):352–8.

29. Fairley JA, Heintz PW, Neuburg M, Diaz LA, Giudice GJ. Expression pattern of the bullous pemphigoid-180 antigen in normal and neoplastic epithelia. Br J Dermatol. 1995;133(3):385–91.

30. Lazarova Z, Domloge-Hultsch N, Yancey KB. Epiligrin is decreased in papulonodular basal cell carcinoma tumor nest basement membranes and the extracellular matrix of transformed human epithelial cells. Exp Dermatol. 1995;4(3):121–9.

31. Kubilus J, Baden HP, McGilvray N. Filamentous protein of basal cell epithelioma: Characteristics in vivo and in vitro. J Natl Cancer Inst. 1980;65(5):869–75.

32. Asada M, Schaart F-M, Detmar M, Mischke D, de Almeida HL, Gollnick H, et al. Growth Characteristics and Differentiation of Basal Cell Carcinoma In Vitro–Immunohistochemical, Gel Electrophoretic, and Ultrastructural Analysis. J Invest Dermatol. 1992;99(4):474–81.

33. Rheinwald JG, Green H. Serial cultivation of strains of human epidermal keratinocytes: the formation of keratinizing colonies from single cells. Cell. 1975 Nov;6(3):331–43.

34. Green H. The birth of therapy with cultured cells. BioEssays. 2008;30(9):897–903.

35. Gray TE, Thomassen DG, Mass MJ, Barrett JC. Quantitation of cell proliferation, colony formation, and carcinogen induced cytotoxicity of rat tracheal epithelial cells grown in culture on 3T3 feeder layers. In Vitro. 1983;19(7):559–70.

36. Grando SA, Olivia M, Kist DA, Zelickson BD, Amy P, Zachary CB. Nodular Basal Cell Carcinoma in vivo vs in vitro. Arch Dermatol. 1996;132:1185–93.

37. Chopra A, Maitra B, Korman NJ. Decreased mRNA expression of several basement membrane components in basal cell carcinoma. J Invest Dermatol. 1998;110(1):52–6.

38. Nishiyama T, Amano S, Tsunenaga M, Kadoya K, Takeda A, Adachi E, et al. The importance of laminin 5 in the dermal-epidermal basement membrane. J Dermatol Sci. 2000;24(SUPPL. 1).

39. Hacking SA, Khademhosseini A. Cells and Surfaces in vitro. In: Biomaterials Science: An Introduction to Materials: Third Edition. Elsevier Inc.; 2013. p. 408–27.

40. Münz M, Kieu C, Mack B, Schmitt B, Zeidler R, Gires O. The carcinoma-associated antigen EpCAM upregulates c-myc and induces cell proliferation. Oncogene. 2004 Jul 29;23(34):5748–58.

41. Chaves-Pérez A, MacK B, Maetzel D, Kremling H, Eggert C, Harréus U, et al. EpCAM regulates cell cycle progression via control of cyclin D1 expression. Oncogene. 2013 Jan 31;32(5):641–50.

42. De Boer CJ, Van Krieken JHJM, Janssen-van Rhijn C, Litvinov SV. Expression of Ep-CAM in normal, regenerating, metaplastic, and neoplastic liver. J Pathol. 1999;188(2):201–6.

43. Osta WA, Chen Y, Mikhitarian K, Mitas M, Salem M, Hannun YA, et al. EpCAM is overexpressed in breast cancer and is a potential target for breast cancer gene therapy.

Cancer Res. 2004 Aug 15;64(16):5818–24.

44.   Wu CJ, Mannan P, Lu M, Udey MC. Epithelial cell adhesion molecule (EpCAM) regulates claudin dynamics and tight junctions. J Biol Chem. 2013 Apr 26;288(17):12253–68.

45.   Mueller JL, McGeough MD, Peña CA, Sivagnanam M. Functional consequences of EpCam mutation in mice and men. Am J Physiol - Gastrointest Liver Physiol. 2014 Feb 15;306(4).

46.   Gaiser MR, Hirsch D, Gaiser T. Loss of epithelial cell adhesion molecule (EpCAM) in infiltrative basal cell carcinoma. Int J Clin Exp Pathol. 2018;11(1):406–12.

47.   Mackiewicz-Wysocka M, Bowszyc-Dmochowska M, Strzelecka-Weklar D, Dańczak-Pazdrowska A, Adamski Z. Basal cell carcinoma - Diagnosis. Vol. 17, Wspolczesna Onkologia. 2013. p. 337–42.

48.   McArdle JP, Roff BT, Muller HK. Characterization of retraction spaces in basal cell carcinoma using an antibody to type IV collagen. Histopathology. 1984;8(3):447–55.

49.   Bigelow RLH, Jen EY, Delehedde M, Chari NS, McDonnell TJ. Sonic hedgehog induces epidermal growth factor dependent matrix infiltration in HaCat keratinocytes. J Invest Dermatol. 2005;124(2):457–65.

50.   Sellheyer K. Basal cell carcinoma: Cell of origin, cancer stem cell hypothesis and stem cell markers. Vol. 164, British Journal of Dermatology. Br J Dermatol; 2011. p. 696–711.

51.   Gache Y, Brellier F, Rouanet S, Al-Qaraghuli S, Goncalves-Maia M, Burty-Valin E, et al. Basal cell carcinoma in Gorlin's patients: A matter of fibroblasts-led protumoral microenvironment? PLoS One. 2015;10(12):1–21.

CHAPTER 6

ADDEMDUM

Single-cell DNA sequencing reveals distinct molecular types of basal cell carcinoma with unique transcriptome features

C. Gaviria [a,b,&], B. Bakker [a,&], J. Terra [b], L. Zhou [a,*], E. Rácz [c,*], S. Paljić, J. Garcia-Martinez, V. Oliveira, P. L. Bakker [a], D.C.J. Spierings [a], M. F. Jonkman [c], F. Foijer [a]

[a]European Research Institute for the Biology of Ageing, University Medical Centre Groningen, The Netherlands
[b]Tissue Engineering and cell therapy research Group, School of Medicine, University of Antioquia, Colombia
[c]Department of Dermatology, University of Groningen, University Medical Centre Groningen, The Netherlands

[&,*]These authors contributed equally

ABSTRACT

Aneuploidy, a hallmark of cancer, is the result of chromosomal instability (CIN) during mitosis. While some aneuploid cancers display stable karyotypes, other tumors display cell-to-cell karyotype variability indicative of CIN. CIN cancers are typically associated with poor clinical outcome, as they are endowed with the potential to adjust their genomes to changing conditions including therapy. To further explore this, we assessed the degree of aneuploidy and CIN in basal cell carcinoma (BCC) and investigated whether the karyotypic makeup of tumors was associated with distinct transcriptional responses.

Samples from 11 BCC patients were processed for single-cell whole-genome sequencing (scWGS) to measure aneuploidy and karyotype heterogeneity. In parallel, samples were processed for transcriptome analysis. To confirm scWGS analysis, we determined chromosome mis-segregation rates in primary BCC cultures by live-cell time-lapse imaging,

scWGS revealed different grades of aneuploidy between BCCs, ranging from euploidy to tumors with up to 7 aneusomic chromosomes. A subset of BCCs displayed intratumor karyotype heterogeneity, indicating that CIN can play a role in BCC. Importantly, in vitro cultures corroborated the presence of a CIN phenotype in a subset of tumors. Samples were clustered into three groups based on the level of aneuploidy and intratumor karyotype heterogeneity. Karyotype-driven group classification was also reflected by the tumour transcriptomes and revealed distinct gene expression signatures related to aneuploidy and CIN.

While BCCs are typically classified based on histopathological features, we find that BCCs can be stratified based on karyotypic landscape. Importantly, this classification is linked to distinct molecular features and could thus be the starting point of a molecular classification system for BCC including a readout for CIN. Importantly, the approach that we have developed is broadly applicable and could therefore also improve the diagnosis and treatment of other cancer types.

Genomic heterogeneity driven by chromosomal instability (CIN) is thought to drive therapy resistance in cancer. We studied karyotype heterogeneity and its effect on the transcriptome in the skin cancer basal cell carcinoma (BCC). We identified transcriptional signatures distinguishing aneuploid from CIN BCCs that may be useful for the stratification of tumors and prediction of treatment response.

INTRODUCTION

Cancer cells frequently display chromosomal instability (CIN), the process that drives abnormal chromosome distribution during mitosis. CIN results in cells with an abnormal DNA content, *i.e.* aneuploidy. In untransformed cells, aneuploidy leads to a stress response resulting in decreased proliferation, senescence, or cell death [1]. In contrast, cancer cells take advantage of CIN to drive tumorigenesis through the generation of new karyotypes, providing cancer cells with great potential to acquire additional tumorigenic traits involved in *e.g.* immune evasion and resistance to chemotherapy [2–5].

Although the terms 'aneuploidy' and 'CIN' are often used interchangeably, they are in fact different phenomena as cells can be stably aneuploid without a CIN phenotype [6]. While stably aneuploid cells generally grow slower [7,8], CIN cells often display increased cell death, presumably as a result of the emergence of unfavorable karyotypes [6,9,10]. It is therefore conceivable that aneuploidy and CIN provoke different responses at the RNA level in primary tumors. Understanding the contribution of stable aneuploidy to cancer development versus that of CIN will therefore help to improve treatment strategies.

The recent advent of single-cell whole-genome sequencing (scWGS) technology facilitates addressing this question, as it allows to infer CIN from intratumor karyotype heterogeneity in primary tumor samples and thus discriminate stable aneuploid cancers from those exhibiting a CIN phenotype [11–14]. While several studies have investigated aneuploidy and CIN in cancer and their effects on driver mutations [4,15], little is known on whether aneuploidy and CIN trigger distinct transcriptional responses in cancer.

In this study, we investigated this issue using primary basal cell carcinoma (BCC) samples. BCCs are epidermal tumors for which data on genome-wide cytogenetics is scarce [16,17]. Most BCCs can be cured by complete surgical resection. However, in a subset of patients, surgical excision is restricted by tumor location, or have BCCs progressed towards an advanced stage and/or metastasized [18,19]. These patients are treated with chemo- or radiotherapy, bringing along the inherent risk of developing therapy resistance.

To better understand the contribution of CIN and aneuploidy to BCC, we subjected a cohort of BCCs to single-cell whole-genome sequencing (scWGS) to infer CIN and performed RNA-sequencing to measure matching transcriptomes. We also estimated the frequency of mitotic errors in a subset of cultured BCCs to confirm CIN inferences and to further characterize primary BCC cultures. This revealed transcriptional signatures that discriminate aneuploid BCCs from euploid BCCs, and stably aneuploid BCCs from aneuploid BCCs exhibiting CIN, suggesting that CIN provokes a distinct transcriptional response. As CIN tumors are believed to be more aggressive and have a tendency to become drug-resistant [5,20], a CIN-induced transcriptome could become a powerful readout for diagnosis to stratify tumors for treatment in the future.

MATERIALS AND METHODS

Basal cell carcinoma sample isolation and processing

BCC samples were obtained from surplus material from Mohs surgery performed at the Department of Dermatology at the UMCG, Groningen, the Netherlands.

Half of the sample was stored immediately in RNAlater (Thermo Fisher Scientific) and stored at 4°C overnight followed by transfer to -80°C until RNA isolation. The remaining half was processed for single-cell WGS. For this purpose, samples were pre-wetted using PBS (Gibco) and cut into 1 mm³ cubes, followed by treatment with Dispase-II (Merck Millipore) for 1 hour at 4°C on a roller mixer. Samples were then treated with 0.05% trypsin-EDTA and incubated at 37°C for 15 minutes. Dispase and trypsin were inactivated by FBS. Homogenization was performed by repeated resuspension for 30 to 60 seconds until cellular clumps disassociated. Ice-cold PBS/FBS was added to the samples, which then were passed through a 100 µm cell strainer and collected, followed by an additional passage through a 40 µm strainer. Samples were centrifuged at 500×g for 8 minutes at 4°C and washed twice with PBS/FBS before resuspension in PBS. Cell viability and counts were assessed using trypan blue and a TC-20 automated cell counter (Biorad). Samples were finally resuspended at 107 cells per mL in FBS with 10% DMSO and stored at -80°C until single-nuclei sort.

Primary cells culture

Basal carcinoma cells

The system culture established in Chapter 5 was followed. Briefly, fresh samples were washed with 70% ethanol for 30 sec before processing. Tissues were mechanically fragmented and skin fragments were placed on 60 mm culture dishes containing i3T3 cells as a feeder layer. Explants were air-dried for about 10 min and thereafter, QN medium (described in Chapter 2) supplemented with 10 uM rock inhibitor (Y-27632, STEMCELL Technologies) was poured gently into dishes without disturbing the explants. After 2 days, 10 ng/mL Epidermal Growth Factor (EGF, Preprotech) was added to the media.

For subculture, cells were differentially detached: i3T3 were first detached with 0.05% trypsin-EDTA (Sigma-Aldrich) and then BCC cells were harvested following 0.25% trypsin-EDTA treatment. Cell suspensions were frozen or seeded on i3T3 for further expansion.

Keratinocytes

After informed consent, human skin samples were obtained from blepharoplasties and mammary reductions leftovers, performed at the Department of Plastic Surgery at the UMCG, Groningen, The Netherlands.

The protocol described in Chapter 5 was followed. Briefly, samples were immersed in 70% ethanol for 1 min, and mechanically fragmented. Fragments were placed on 10 mm culture dishes and air-dried. Thereafter, skin pieces were cultured in QN medium and, after 2 days, 10 ng/mL EGF were added. All media was supplemented with 10 uM rock inhibitor.

Primary cells labeling and time-lapse imaging

To visualize the DNA, the PIGZ-H2B-mCherry plasmid and 2 packaging vectors (PAX and VSV) were first transfected into 293T cells. After 48h, the media containing retroviral particles was harvested and filtered with a 0.45 μm filter (Sigma), and the culture media was changed with fresh DMEM containing 10% FBS, 1% L-glutamine, and 1% penicillin/streptomycin. This procedure was repeated two times more and the media was stored at -80°C until use.

Keratinocytes and BCC-derived cells were transduced by refeeding them with the media containing retroviral particles plus 4 μg/ml Polybrene (EMD Millipore) and 10 μM ROCK inhibitor. After the 3rd transduction, retroviral media was removed, and then fresh media was added into infected cells.

For time-lapse, between 75000 and 150000 cells were seeded on imaging dishes (Greiner) containing either Matrigel or i3T3. After 24h, cells were imaged for 48h on a DeltaVision Elite imaging station (Applied Precision, GE Healthcare). Images were taken every 4-6 min using the 40x objective.

Single-cell whole-genome sequencing and AneuFinder analysis

Samples for scWGS samples stored in FBS and 10% DMSO were thawed, washed with PBS, and incubated in staining buffer (100 mM Tris-HCl [pH7.4], 154 mM NaCl, 1 mM CaCl2, 0.5 mM MgCl2, 0.2% BSA, 0.1% NP40, 10 μg/mL Hoechst 33358, and 10 μg/mL propidium iodide [PI] in ultrapure water) for a minimum of 20 minutes at 4°C in the dark. Single G1 nuclei were sorted using a FACSJazz (BD Biosciences) into 96-well plates containing 5 μL freezing buffer (1X ProFreeze and 7.5% DMSO in PBS). Plates were stored at -80°C until processed for single-cell library preparation using a Bravo automated liquid handling platform (Agilent Technologies, Santa Clara, CA, USA) [21]. Clusters for sequencing were generated using an Illumina cBot. Libraries were sequenced (single-end 50 bp) on a HiSeq 2500 (Illumina, San Diego, USA) at ERIBA, and demultiplexed using standard Illumina software (bcl2fastq v.1.8.4). Sequencing reads were mapped to the human reference genome (hg19/GRCh37) using Bowtie2 (v.2.2.4), and duplicate reads were marked using BamUtil (v.1.0.3). Aligned sequencing libraries were curated and analyzed for copy number alterations using AneuFinder (v.1.8.0) at an average bin size of 2 Mb. GC-correction and variable bin width strategies were applied as described before [13].

RNA-sequencing library preparation and analysis

For transcriptome analysis, RNA was isolated from BCC samples followed by quality control on a Bioanalyzer (Agilent). RNA sequencing libraries were prepared with poly(a) selection using the NEXTflex kit (Bioo Scientific). Individual libraries were barcoded and pooled followed by sequencing. Demultiplexed sequencing reads were aligned to the human reference (GRCh37) using a splicing-aware algorithm (STAR [25]). Differential gene expression was determined using DESeq2 [26]. Genes were considered differentially expressed (DE) at a significance of FDR < 0.05 (p-values adjusted using Benjamini-Hochberg [BH]). GO-term and KEGG pathway enrichment analyses were performed on significant DE genes using WebGestaltR [27]. Heatmaps for gene expression profiles were generated using the heatmap2 and pheatmap packages within R, plotting normalized log2 gene expression values.

Sequencing data availability

Unaligned sequencing data have been submitted to the European Nucleotide Archive (ENA) and are available only upon request due to EU patient privacy legislation (accession number PRJEB28285).

Supplementary data can be found online:

https://www.biorxiv.org/content/10.1101/492199v1.supplementary-material

RESULTS

Single-cell whole-genome sequencing reveals karyotype heterogeneity in BCC

Tumor samples were collected from 11 patients diagnosed with BCC alongside with healthy control tissue where possible (median age: 74.5 years, Table 1). The histopathological assessment revealed that the cohort included the most common subtypes: nodular/infiltrative, infiltrative, micronodular, or nodular (Figure 1a). To circumvent the limitations of traditional karyotyping methods [22], we subjected samples to scWGS (24 cells per sample) to quantify aneuploidy and intratumor copy number heterogeneity (Figure 1b) [11,23]. 72.7 ± 15.6% (mean ± SD) of the libraries passed quality control, additional scWGS quality metrics can be found in Table S1.

With the exception of BCC5, all BCCs displayed structural and/or numerical abnormalities in multiple or most cells (Figure 1c), indicating reasonable tumor cell purity. Non-aneuploid cells in aneuploid BCCs are likely non-cancer cells that surround the cancer nodules. Besides whole chromosome abnormalities, a subset of BCCs also harbored structural aberrations typically involving the gain or loss of whole chromosome arms, *e.g.* involving loss of Chr. 9p (Figure 1c). Interestingly, in addition to aneuploidy, two BCCs (BCC3 and BCC9) exhibited significant karyotype heterogeneity, a strong indication for ongoing CIN [21,23].

To stratify the BCCs based on aneuploidy and karyotype heterogeneity for subsequent transcriptional analysis, we calculated the aneuploidy and heterogeneity scores using AneuFinder [23] for the tumor karyotypes as a whole, as well as for individual chromosomes (Figure 1d). For these calculations, euploid libraries were excluded, circumventing an impact of non-cancer cell libraries on heterogeneity scores. Together, these analyses revealed that the BCCs could roughly be grouped into three distinct karyotypic subtypes: BCCs 1, 4, 5, 6, 7, and 8 showed little to no aneuploidy, with 0 to 2 aneusomic chromosomes (group 1; near-euploid). BCCs 2, 10, and 11 displayed a much larger number of aneusomic chromosomes, but no intratumor heterogeneity (group 2; stably aneuploid). Finally, BCC3 and BCC9 displayed both multiple aneusomic chromosomes as well as intratumor heterogeneity and were therefore classified as CIN (group 3; CIN). Together, these data reveal that basal cell carcinoma exhibit widely varying karyotypes with a subset displaying intratumor heterogeneity.

Table 1. information on the BCC sample set.

Sample ID	Gender	Age	Topography	UV exposure	Classification	scWGS	RNA-seq	Matched healthy skin	In vitro culture
BCC1	M	77	Nasal ala	Low	Nodular				
BCC2	F	54	Temple	Moderate	Nod./infilt.				
BCC3	M	78	Cheek	High	Micronodular				
BCC4	M	85	Upper lip	High	Infiltrative				
BCC5	M	58	Chin	High	Nod./infilt.				
BCC6	M	74	Ear	High	Nodular				
BCC7	F	41	Next to eye	High	Nod./infilt.				
BCC8	M	55	Upper lip	Moderate	Micronodular				
BCC9	F	75	Forehead	Moderate	Nodular				
BCC10	F	75	Forehead	Moderate	Nodular				
BCC11	M	89	Ear	High	Nod./infilt.				

BCC12	M	70	Cheek	Moderate	Nodular	
BCC13	F	80	Nasal ala	Moderate	Nodular	
BCC14	F	56	Nose/medial canthus	Moderate	Nodular	

Green blocks indicate whether a sample was processed for single-cell whole genome sequencing (scWGS), RNA sequencing or in vitro culture
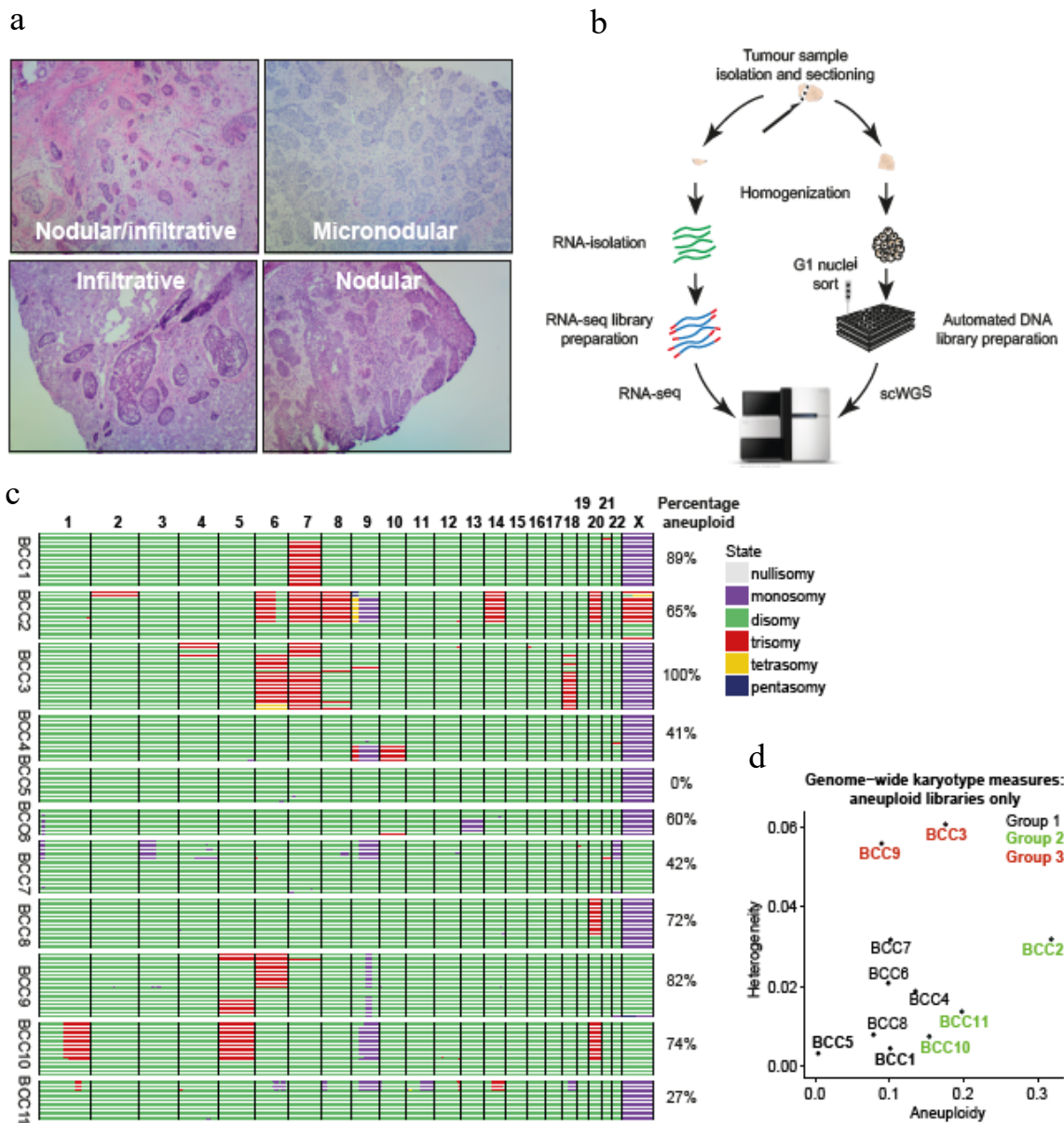

Figure 1. Single-cell whole-genome sequencing reveals varying degrees of karyotype heterogeneity in BCC. a. Representative images of the BCC classification, based on H&E staining. b. Schematic overview of the sample processing pipeline, from homogenization to library preparation for scWGS and transcriptome analysis (RNA-seq). c. Genome-wide copy number heatmaps of 11 BCC samples, with individual cells in rows and genome position in columns. Chromosome boundaries are indicated in black lines, with colors corresponding to the most likely assigned copy number state per 2 Mb bin as determined by AneuFinder. The percentage of aneuploidy indicates the fraction of libraries that display aneuploidy for at least 1 chromosome arm. d. Genome-wide aneuploidy and heterogeneity scores for the aneuploid libraries. Samples processed further for RNA-sequencing are highlighted in bold.

CIN phenotype in BCC cultures

Even though scWGS experiments reveal considerable levels of karyotype heterogeneity in a subset of BCC samples, we cannot rule out that these consisted of several different stably aneuploidy cells. To further confirm a possible CIN phenotype, we labeled keratinocytes and BCC-derived cells with an H2B-mCherry fusion protein. We determined the chromosome mis-segregation rate in 3 BCC samples-derived cells using time-lapse imaging. To make a comparison, keratinocytes from healthy biopsies were analyzed in parallel.

BCC cells and, to a lesser extent, keratinocytes exhibited CIN. We found significant differences between BCC13 and its healthy counterpart, showing 60% of mitosis with signs of unbalanced chromosome distribution (Figure 2, left panel). These results confirm the existence of a CIN phenotype in a subset of cultured BCCs, and further suggest that BCC cultures can preserve some of their *in vivo* mitotic characteristics.
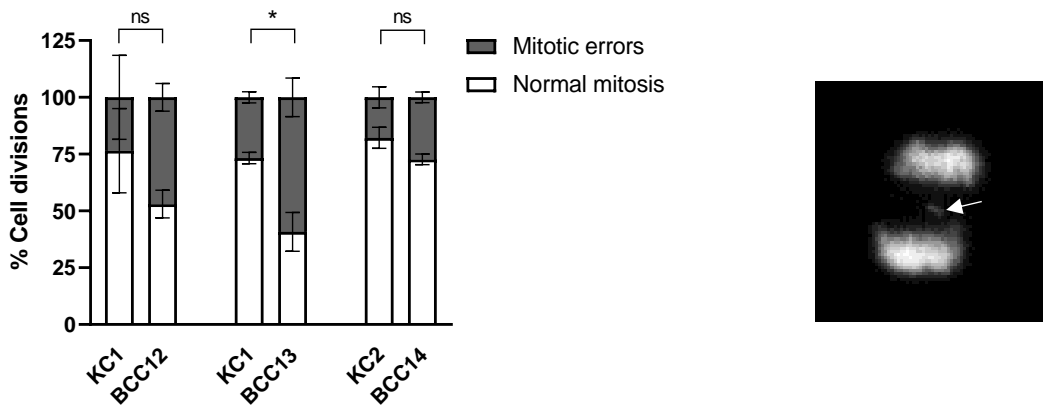
Figure 2. Frequency of mitotic errors as analyzed by live-cell time-lapse imaging of the labeled BCC-derived cells. The average number of cell divisions was 53 for KC1, 89 for KC2, 46 for BCC12, 40 for BCC13, and 80 for BCC14. Right panel: still frame of a mitotic cell from BCC12 labeled with H2B-mCherry, showing a mitotic error (lagging chromosome, white arrow). For statistical analysis, a two-tailed student's t-test was applied. ns:non-significant, *: p<0.05. Data represent at least 3 biological replicates.

Transcriptome analysis reveals general deregulation of SHH, cell cycle, and cilia genes in BCC

To determine the impact of aneuploidy and/or CIN on the tumor transcriptomes, we next subjected a subset of BCCs from each cluster alongside with healthy control skin samples to RNA sequencing (Figure 1d, Figure 3a). Interestingly, principal component analysis (PCA) revealed a clear separation between karyotypic subgroups (compare Figure 1d to Figure 3a) indicating that CIN and aneuploidy have a strong impact on the tumor transcriptomes. We determined which genes were significantly dysregulated in BCC in general as compared to control skin. 5,197 genes were differentially expressed (DE) between healthy skin and BCC (Wald test, FDR<0.05; Figure 3b – left panel) and enriched for functions in skin/epidermis development, cell cycle regulation, and cilium biology (Figure 3b – right panel). This fits well with current literature, which frequently reports keratinization alterations (epidermal

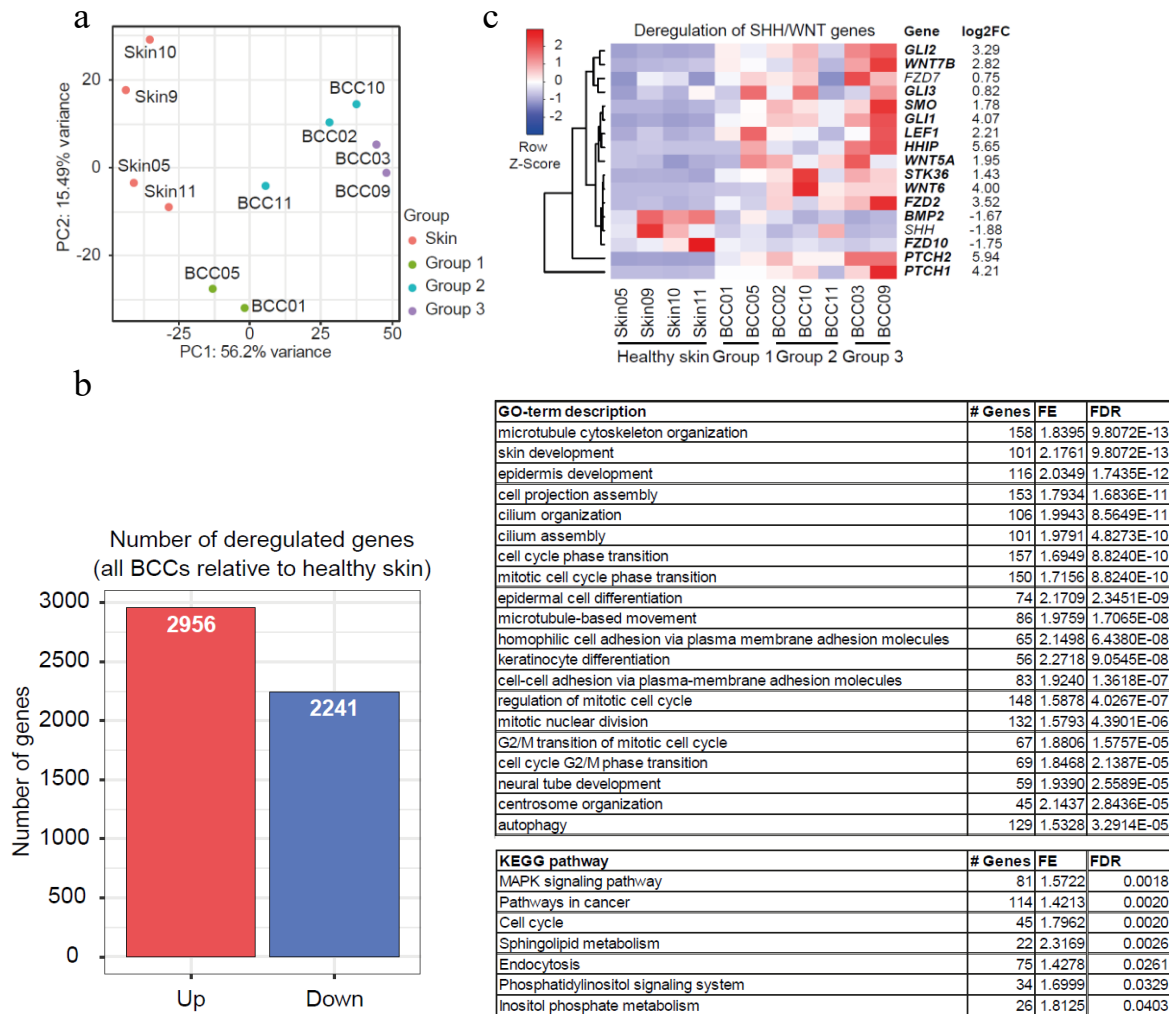development) and dysregulation of the Hedgehog signalling pathway in BCC (Figure 3c)[16,18,19,24–26].

Figure 3. Aneuploidy and CIN-specific transcriptome signatures in basal cell carcinoma. a. Principal component analysis (PCA) of the RNA-seq libraries, showing the percentage of contribution of PC1 and PC2 to variance, and color-coded by group identifier. b. The number of significant DE genes up- and downregulated between all BCCs and healthy skin (left panel) and GO & KEGG-pathway enrichment analysis (right panels). Where indicated, columns show GO-term or KEGG pathway description, the number of observed genes, fold enrichment (FE) over expected observations, and BH-adjusted p-value (FDR). c. Expression heatmap of commonly deregulated genes in basal cell carcinoma, related to SHH and WNT signaling. Normalized expression values are expressed as z-scores (by gene). Gene names highlighted in bold are significantly dysregulated (FDR < 0.05).

Altogether, we conclude that BCCs can be subdivided into three distinct karyotypic classes that are associated with distinct transcriptome features, with the CIN phenotype having the strongest impact on the tumor transcriptome.

DISCUSSION

In this study, we examined aneuploidy and intratumor karyotype heterogeneity in a panel of BCCs, a feature that, to our knowledge, has not been studied before for this cancer. We found that BCCs can be grouped into three karyotypic types: near-euploid, stably aneuploid, and CIN. Of note, the aneuploidy scores were similar between stably aneuploid and CIN tumors, suggesting that differences between stably aneuploid and CIN tumors are the sole consequence of the CIN phenotype.

To conform the existence of a CIN phenotype, we employed the *in vitro* BCC culture system previously described (Chapter 5) and subjected a subset of samples to time-lapse imaging. Our results revealed mitotic aberrations in 1 out of 3 samples, confirming that, in both tumors and *in vitro* cultures, some but not all BCCs display ongoing CIN. These results corroborate the observations derived from scWGS indicating the existence of CIN in BCC and further suggest that cells growing from tumor samples represent true BCC, as they present distinct mitotic features. Further experiments are needed to directly correlate the karyotypic features of BCC tumors and their *in vitro* counterpart.

We next investigated whether BCC is associated with distinct transcriptional responses by performing RNA sequencing in BCCs and control skin samples. Indeed, this revealed common dysregulations across all BCCs: enrichment in skin development functions, cell cycle regulation, and cilium biology, as well as alterations in the Hedgehog pathway. This is in agreement with previous findings showing mutations in genes involved in the Hedgehog pathway [27][28] and perturbations in epidermal differentiation [29]. Of note, our results show that CIN and aneuploidy strongly affect tumor transcriptomes.

Our findings are not only relevant for the fundamental understanding of aneuploidy and CIN in cancer, but also bear clinical relevance. For instance, several Sonic Hedgehog inhibitors are at various stages of clinical trials [18,19] for the treatment of inoperable BCCs (for instance locally advanced or metastatic BCC) [18]. As CIN BCCs would be particularly at risk of developing resistance against such drugs, our molecular classification for BCCs (using single-cell genomics, transcriptome analysis, or possibly evidence of DNA damage) could aid in predicting therapy resistance when treating patients suffering from advanced or metastatic BCC.

ACKNOWLEDGEMENTS

Author contributions

J.T. and E.R. provided patient material and performed histopathological diagnosis. B.B., L.Z., S.P. J.G.M. and V.O. processed patient material. C.G cultured samples and performed live-cell imaging. B.B. performed single-nuclei sorts and analysed sequencing data. P.L.B. performed RNA-seq library preparation. D.C.J.S. supervised scWGS and RNA-sequencing. B.B. and F.F. wrote the manuscript. M.F.J. and F.F. conceptualized the study and provided funding.

REFERENCES

1.   Williams BR, Amon A. Aneuploidy: cancer's fatal flaw? Cancer Res. 2009 Jul;69(13):5289–91.

2.   Sansregret L, Vanhaesebroeck B, Swanton C. Determinants and clinical implications of chromosomal instability in cancer. Nat Rev Clin Oncol. 2018;15:139–50.

3.   Bakhoum SF, Landau DA. Chromosomal Instability as a Driver of Tumor Heterogeneity and Evolution. Cold Spring Harb Perspect Med. 2017;7:a029611.

4.   Davoli T, Xu AW, Mengwasser KE, Sack LM, Yoon JC, Park PJ, et al. Cumulative Haploinsufficiency and Triplosensitivity Drive Aneuploidy Patterns and Shape the Cancer Genome. Cell. 2013;155(4):948–62.

5.   McGranahan N, Rosenthal R, Hiley CT, Rowan AJ, Watkins TBK, Wilson GA, et al. Allele-Specific HLA Loss and Immune Escape in Lung Cancer Evolution. Cell. 2017;171:1–13.

6.   Schukken KM, Foijer F. CIN and Aneuploidy: Different Concepts, Different Consequences. BioEssays. 2017;

7.   Tang Y-C, Williams BR, Siegel JJ, Amon A. Identification of aneuploidy-selective antiproliferation compounds. Cell. 2011 Feb;144(4):499–512.

8.   Pavelka N, Rancati G, Zhu J, Bradford WD, Saraf A, Florens L, et al. Aneuploidy confers quantitative proteome changes and phenotypic variation in budding yeast. Nature. 2010;468(7321):321–5.

9.   Libouban MAA, de Roos JADM, Uitdehaag JC, Willemsen-Seegers N, Mainardi S, Dylus J, et al. Stable aneuploid tumors cells are more sensitive to TTK inhibition than chromosomally unstable cell lines. Oncotarget. 2017;8(24):38309–25.

10.   Simon J, Bakker B, Foijer F. CINcere modelling: What have mouse models for chromosome instability taught us? Results Cancer Res. 2015;200:39–60.

11.   van den Bos H, Spierings DCJ, Taudt AS, Bakker B, Porubský D, Falconer E, et al. Single-cell whole genome sequencing reveals no evidence for common aneuploidy in normal and Alzheimer's disease neurons. Genome Biol. 2016;17(1).

12.   Bakker B, Taudt A, Belderbos M, Porubsky D, Spierings D, De T, et al. Single cell sequencing reveals karyotype heterogeneity in murine and human tumors. Genome Biol. 2016;17:1–15.

13.   Navin N, Kendall J, Troge J, Andrews P, Rodgers L, McIndoo J, et al. Tumor evolution inferred by single-cell sequencing. Nature. 2011;472(7341):90–4.

14.   Gao R, Davis A, McDonald TO, Sei E, Shi X, Wang Y, et al. Punctuated copy number evolution and clonal stasis in triple-negative breast cancer. Nat Genet. 2016;48(10):1119–30.

15.   Sack LM, Davoli T, Li MZ, Li Y, Xu Q, Naxerova K, et al. Profound Tissue Specificity

in Proliferation Control Underlies Cancer Drivers and Aneuploidy Patterns. Cell. 2018;173(2):499-514.e23.

16. Jayaraman SS, Rayhan DJ, Hazany S, Kolodney MS. Mutational Landscape of Basal Cell Carcinomas by Whole-Exome Sequencing. J Invest Dermatol. 2014;134:213–20.

17. Mertens F, Heim S, Mandahl N, Johansson B, Mertens O, Persson B, et al. Cytogenetic Analysis of 33 Basal Cell Carcinomas. Cancer Res. 1991;51:954–7.

18. Migden MR, Lynn A, Chang S, Dirix L, Stratigos AJ, Lear JT. Emerging trends in the treatment of advanced basal cell carcinoma. Cancer Treat Rev. 2018;64:1–10.

19. Kudchadkar R, Lewis K, Gonzalez R. Advances in the Treatment of Basal Cell Carcinoma : Hedgehog Inhibitors. Semin Oncol. 2012;39(2):139–44.

20. McClelland SE. Role of chromosomal instability in cancer progression. Endocrine-related cancer. 2017.

21. Foijer F, Albacker LA, Bakker B, Spierings DC, Yue Y, Xie SZ, et al. Deletion of the MAD2L1 spindle assembly checkpoint gene is tolerated in mouse models of acute T-cell lymphoma and hepatocellular carcinoma. Elife. 2017;6.

22. Bakker B, van den Bos H, Lansdorp PMPM, Foijer F. How to count chromosomes in a cell: An overview of current and novel technologies. BioEssays. 2015;37(5).

23. Bakker B, Taudt A, Belderbos ME, Porubsky D, Spierings DCJ, de Jong T V, et al. Single-cell sequencing reveals karyotype heterogeneity in murine and human malignancies. Genome Biol. 2016;17(1):115.

24. Misago N, Satoh T, Narisawa Y. Cornification (Keratinization) in Basal Cell Carcinoma : A Histopathological and Immunohistochemical Study of 16 Cases. J Dermatol. 2004;31(12):637–50.

25. Goetz SC, Ocbina PJR, Anderson K V. The Primary Cilium as a Hedgehog Signal Transduction Machine. Methods Cell Biol. 2009;94:199–222.

26. Skoda AM, Simovic D, Karin V, Kardum V, Vranic S, Serman L. The role of the Hedgehog signaling pathway in cancer : A comprehensive review. Bosn J Basic Med Sci. 2018;18(1):8–20.

27. Mahmudur M. Characterisation of a novel in vitro model of Basal cell carcinoma (BCC) through stable PTCH1 suppression in immortalised human keratinocytes. Queen Mary Unoversity of London; 2013.

28. Samarasinghe V, Madan V. Nonmelanoma skin cancer. J Cutan Aesthet Surg. 2012;5(1):3–10.

29. Asada M, Schaart F-M, Detmar M, Mischke D, de Almeida HL, Gollnick H, et al. Growth Characteristics and Differentiation of Basal Cell Carcinoma In Vitro– Immunohistochemical, Gel Electrophoretic, and Ultrastructural Analysis. J Invest Dermatol. 1992;99(4):474–81.

CHAPTER 7

General discussion

Animal models are extremely important to study skin biology, cutaneous toxicity, and its associated diseases. Nonetheless, their main limitations include not only the differences found between human and animal skin [1,2] but also ethical issues, which has compelled the development of alternative methods in line with the 3 rules guidelines: reduction, refinement, and replacement of animals in experiments [1].

Different approaches have been used in the construction of *in vitro* alternatives including dermo-epidermal models, which however are not yet validated for toxicological purposes, largely lack a proper immune component, and have tremendous potential to improve current *in vitro* skin cancer models. The dermal compartment is usually represented by a collagen matrix with embedded fibroblasts or a fibroblasts-derived matrix. Fibrin has emerged as an alternative biopolymer with several advantages: 1) its precursors can be easily obtained from blood, allowing the generation of autologous scaffolds, 2) presents customizable properties such as fiber thickness or matrix pore size, useful for tissue engineering applications, 3) isolation and processing is highly cost-effective [3], and 4) provides many attachment sites for cells, promoting migration and cell growth [4].

In this thesis, we generated full-thickness fibrin-based skin models for applications in toxicology, immunology, and cancer.

Culturing primary keratinocytes: effects on fibrin-based full-thickness models

An essential step for producing skin equivalents is cell isolation and culture. Two widely used methods to obtain keratinocytes are explant culture and 3T3 feeder layers. Therefore, we first obtained keratinocytes by both systems and investigated their suitability to produce fibrin-based full-thickness models. We found that the use of a feeder layer provides higher final cell density and led to tissues with a healthier and thicker epidermis, as compared to the explant culture method. This is consistent with the fact that feeder layers contribute to the suppression of keratinocyte differentiation and extend keratinocytes' life span [5,6], which leads to highly proliferative cells with the capacity to firstly cover the dermal surface and later differentiate generating a stratified epidermis.

Another crucial aspect of keratinocytes culture is medium composition. A number of studies have highlighted the importance of using low calcium concentration as it reduces the proliferation rate and promotes sequential differentiation of keratinocytes [7–10]. Our finding that early passage cells produce models with higher TEER values supports this notion since these cultures would contain a greater number of undifferentiated and highly proliferative cells that can lead to increased cell density and the subsequent formation of stronger tight junctions.

Altogether, our findings showed that feeder layer-derived keratinocytes generate fibrin-based skin equivalents with improved histological features as compared to explant culture. Of note, a tighter epidermal barrier is achieved when early passage keratinocytes are used.

Our results highlight the necessity of using undifferentiated and highly proliferative keratinocytes for the generation of skin models, which will create healthy and ordered basal and suprabasal layers with an improved epidermal barrier. This is especially important in

pharmaco-toxicological applications, for which the morphology and barrier function of the tissues should be verified before the application of any chemical testing protocol [11,12].

Validation of fibrin-based skin models for irritation and corrosion tests

In the last years, tremendous efforts have been done in the development of human skin equivalents to evaluate toxicological responses. Most of them, however, are only composed of keratinocytes [13–15], ignoring the effect of other skin constituents like the dermis, that have the ability to respond to toxic stimuli and express inflammatory mediators like cytokines [16].

Knowing that feeder layer-derived keratinocytes produce dermo-epidermal tissues with proper morphology and barrier function, we proceeded to evaluate their performance for chemical hazard identification following OECD test guidelines [11,12]. Our model displayed a prediction capacity of 86% and 94% for irritation and corrosion, respectively, fulfilling the precision values criteria established by the OECD. For comparison, we also tested the validated model EpiDerm[TM] and found 75% accuracy for irritation and 43% for corrosion. Since EpiDerm[TM] is validated for the OECD protocols, the lower performance is attributed to quality decrease during long shipping times, as shown by the high number of annulated tests.

Another approach to assess irritation potential is based on the measurement of cytokines production and release. However, literature reports on this matter have been somehow inconsistent. Previous studies have shown that IL-1α measurements can lead to a distinction of irritant potency in both epidermal and full-thickness models [17,18]. In contrast, a study performed on SkinEthic[TM] concluded that quantification of IL-1α release does not increase performance when the model is challenged with irritant chemicals [19]. As for IL-6 and IL-8, increases of both [20] or just IL-8 [21] have been reported following exposure. Indeed, we found that EpiDerm[TM] levels of IL-8 increased after irritant treatment, improving its prediction capacity. On the other hand, we found that cytokines release in the dermo-epidermal fibrin-based model was differently altered by the tested substances, indicating first that our model is able to release a number of cytokines and second, that the induction of cytokines after irritant exposure could be chemical- and model-specific.

Taken together, these findings show that fibrin-based 3D skin equivalents can discriminate irritation and corrosion, making it a promising tool for toxicological applications. Having a local model represents an advantage for the commercialization of products in developing countries like Colombia and would prevent quality loss during international models shipping. Whether there is an association between cytokine release and irritation potential, needs to be determined in further experiments.

Besides irritation and corrosion, allergic responses are another undesired effect following chemical exposure. As a result of the existing difficulties for discriminating between irritants and allergens (e.g., they both have cytotoxic effects and generate cytokine-mediated responses [22]), pertinent *in vitro* protocols for the evaluation of sensitizers are still missing.

Towards the generation of an immune skin model

Currently, the identification and evaluation of skin sensitizers are mainly based on animal experimentation. However, as previously discussed, ethical factors and the questionable results obtained in animal experiments have accelerated the development of *in vitro* tests for determining the sensitization potential of chemicals [23–25].

To date, most available *in vitro* models are mainly composed of keratinocytes and/or fibroblasts, but largely lack the immune component. Important progress has been achieved by the addition of other cell types, but not many immune 3D constructs have been described involving the use of dendritic cells [26], Langerhans cells [24–28], or cell lines [24,25]. To our knowledge, no protocol makes use of a co-culture of keratinocytes and CD14+ cells.

We took the first step towards this aim and incorporated, for the first time, freshly isolated CD14+ cells into 3D fibrin-based substitutes. As we previously showed that our model secretes a cocktail of factors and cytokines, we hypnotized that this complex cytokine network could lead to the generation of dendritic cells from peripheral blood precursors. Indeed, we found that our culture system promotes CD14+ cells differentiation into dendritic cells, as judged by the presence of langerin- and CD1a-positive cells within the tissues. Importantly, our data showed that they effectively migrate throughout the fibrin network after chemical exposure, highlighting the possibility of performing migration and sensitization studies.

This methodology broadened the potential applications of fibrin-based dermo-epidermal models by incorporating dendritic cells with migratory capacities. Considering the population heterogeneity of CD14+ cells [29,30] and the complex microenvironment of skin models [26,31], our approach opens the door to the generation of improved immunocompetent models composed of different populations of immune cells. This represents an advantage over current sensitization assays since distinct dendritic cells subsets could differently respond to sensitizers and irritants.

In addition to the incorporation of immune cells, skin equivalents can also be adapted to model human skin diseases like cancer, providing a system to better understand early neoplastic progression, the biological properties of tumor cells, cell proliferation, gene activation, and invasive phenotype [2,32].

Modelling basal cell carcinoma

Most efforts for *in vitro* diseased models have been mainly focused on the development of melanoma and squamous cell carcinoma substitutes [33]. Current *in vitro* models for basal cell carcinoma (BCC) consist mainly of 2D cultures that can only replicate a few characteristics of the *in vivo* counterpart. To gain insight into this pathology, it is necessary to culture cells with malignant potential in the context of a 3D network of healthy cells. We, therefore, describe the development of 3D models of primary BCC.

The addition of BCC-derived cells to the 3D structure involves the initial 2D culture and propagation of tumor cells. As BCC cultures have been extremely difficult to establish, we firstly described a protocol to culture primary BCC. Combining different keratinocytes

culture methods, we found that BCC expansion is efficiently promoted by conditions that favor attachment and undifferentiation. Thus, a combination of explants, 3T3 feeder layers, and a complex media supplemented with rock inhibitor led to the successful growth and of cells from BCC samples.

Having established a successful protocol to propagate BCC-derived cells, we next constructed 3D fibrin-based models. Given the advantages of *ex vivo* explants in terms of structural and cellular composition, a BCC explant model was first generated. It remained viable and exhibited strong expression of the BCC marker EpCAM, as well as lateral migration of biopsy-derived keratinocytes over the dermal compartment, and the typical BCC dermal invasion. This model showed a high resemblance to human BCC and confirmed the feasibility of maintaining the BCC phenotype under our culture conditions.

Considering the necessity of explants models for a continuous supply of tumor biopsies, we also developed models from suspensions of healthy keratinocytes and tumor-derived cells. We found that, as the percentage of BCC-derived cells increased, these models displayed loss of epidermal normal morphology and differentiation and exhibited disturbed attachment to the dermal component, typical features of BCC [34,35,44,45,36–43]. This agreed with our transcriptome analysis of primary BCC tumors showing dysregulation of cell adhesion components. Unlike the explant model, expression of EpCAM was null-to-weak, underscoring the necessity of understanding its role on BCC cells migration and culture. These models, therefore, recreated some of the most relevant characteristics of BCC, which, otherwise will be difficult to appreciate in 2D cultures.

In summary, we generated a new protocol for the culture and propagation of BCC-derived cells. The subsequent incorporation in 3D models show that fibrin-based gels support the culture and growth of both BCC tumor explants and cell suspensions. Hence, dermo-epidermal organotypic cultures represent a promising system to model primary basal cell carcinoma, as they recapitulate relevant BCC tumor features. They could therefore become an important tool to test new therapeutic agents that target BCC. Importantly, it would represent the first 3D primary BCC model. Further research is still needed to overcome attachment alterations and reproduce other BCC characteristics like suprabasal proliferation and stronger EpCAM expression.

The development of several types of cancer, including BCC, can be triggered by different genetic alterations. Chromosomal instability (CIN) and aneuploidy are frequently displayed in cancer and provide cancer cells with great potential to generate highly malignant and therapeutic resistant tumors [46–48]. Together with 3D modelling, understanding the contribution of CIN and aneuploidy to tumor development can be of help to improve treatment strategies.

Understanding cancer at the molecular level

Thus far, cytogenetic studies of BCC are scarce. Therefore, we made use of our BCC culture method to better characterize BCC pathology. We performed molecular profiling of primary BCC tumor samples and found 3 karyotypic classes: near-euploid, stably aneuploid, and chromosomal instable (CIN), linked to specific transcriptomal features. With our BCC culture system, we were able to evaluate the mitotic characteristics of BCC-derived cells to

confirm the CIN phenotype predicted by single-cell whole-genome sequencing. These findings provided not only a different classification system that could improve the diagnosis and treatment of BCC, but also, a validation of our culture system for the obtainment of primary BCC cells.

These results emphasized the importance of the genetic make-up in tumor formation and prognosis. As 3D substitutes provide a highly suitable structure for the proper functioning of signaling pathways [49], a deeper understanding of cancer cytogenetics together with 3D modelling could offer the opportunity to test therapies targeting specific pathways in models that faithfully mimic the *in vivo* environment.

CONCLUDING REMARKS

Current efforts are focused on the development of highly complex skin models for several applications. This thesis describes the generation and adaptation of fibrin-based dermo-epidermal models for toxicology, immunology, and cancer research.

The proper cultivation of epidermal cells is presented as a fundamental factor for achieving a successful skin model, as it provides the basis for the generation of a well-stratified epidermis on a fibrin-based support, which in turn, allowed the validation of the skin equivalents for toxicity screening purposes. The subsequent addition of other components further increased the complexity of the model, which demonstrated to support the growth of other types of cells by 1) allowing the generation and maintenance of dendritic cells with migratory abilities, and 2) by recapitulating many relevant characteristics of human BCC. As such, fibrin-based skin scaffolds proved to be highly suitable systems to mimic different skin environments and a promising tool for immune and cancer studies.

In vitro models that faithfully represent different skin conditions offer a deeper and more accurate understanding of the biological mechanisms behind the human skin. Particularly, fibrin-based dermo-epidermal models offer new opportunities to study healthy and diseased skin and provides a platform to test potential toxic compounds and novel therapeutic agents.

FUTURE PERSPECTIVES

Although relevant *in vitro* skin models have been engineered, the addition of one or more components can increase the representation of native skin. Concerning skin models containing a dermal compartment, future research should aim to elucidate the mechanism behind cytokine production and release, which seem to differ between pure epidermal and full-thickness models [21] and have provided somehow contradictory results [17–20]. If a link between such biomarkers and irritant potency is indeed found, this would allow the sub-classification of irritants and, likely, contribute to the identification of sensitizers.

The incorporation of other cell types into 3D skin equivalents has led to important progress towards the generation of immunocompetent and cancer models. The challenge in this matter is to effectively integrate different cellular components in a setting that allows their growth, maintenance, and proper communication. This implies the formulation of highly specialized media that support the growth of several cell types with different nutrient requirements. In this regard, for CD14+ cells-containing models, it is necessary to 1) identify the subset of

dendritic cells within the tissue, and 2) avoid their maturation and/or differentiation into undesired phenotypes. For basal cell carcinoma, it is mandatory to prevent differentiation and, at the same time, promote stratification of normal keratinocytes. In addition, it would be interesting to establish low attachment culture conditions that may help with the growth and development of BCC-like tumors in a 3D setting.

Cytogenetic studies, on the other hand, could strongly add to all sorts of *in vitro* substitutes. The identification of pathology-related genotypes or pathways could be of help in modelling the initial (and eventually the late) stages of diseases or testing novel therapeutic strategies that target the specific pathway.

In the distant future, interests could focus on vascularized skin models. They permit a more physiological transport of nutrients and molecules and have shown promising results as perfusable systems[50] and for testing potential drug treatments [51,52], enabling the study of efficacy and possible side effects of therapeutic agents. These kinds of systems are not only useful for pharmaco-toxicological applications but also for immune and skin diseased studies. They represent a milestone for cancer research, as they could recreate the metastatic events that take place after tumor formation. As for immunology, the incorporation of vascular endothelium would allow mimicking the migration of immune cells to the skin tissue after proper stimuli, as recently reported by Kwak et al. [53].

In conclusion, *in vitro* models are a powerful and promising tool to increase our knowledge of many biological properties of human skin. Still, the methods and technology have to evolve in order to better reflect the *in vivo* situation. As no model reproduces all the features of the skin, the system of choice should represent the specific condition to be studied, which is easily achievable thanks to the customizable properties of 3D skin models.

REFERENCES

1. Bergers LIJC, Reijnders CMA, van den Broek LJ, Spiekstra SW, de Gruijl TD, Weijers EM, et al. Immune-competent human skin disease models. Drug Discov Today. 2016;21(9):1479–88.

2. Hill DS, Robinson NDP, Caley MP, Chen M, Toole EAO, Jane L. A novel fully-humanised 3D skin equivalent to model early melanoma invasion. Mol Cancer Ther. 2016;14(11):2665–73.

3. Gsib O, Egles C, Bencherif SA. Fibrin: An Underrated Biopolymer for Skin Tissue Engineering. J Mol Biol Biotechnol. 2017;2(1:3).

4. Schneider-barthold C, Baganz S, Wilhelmi M, Scheper T. Hydrogels based on collagen and fibrin – frontiers and applications. Bionanomaterials. 2016;17(1–2):3–12.

5. Green H. The birth of therapy with cultured cells. BioEssays. 2008;30(9):897–903.

6. Gray TE, Thomassen DG, Mass MJ, Barrett JC. Quantitation of cell proliferation, colony formation, and carcinogen induced cytotoxicity of rat tracheal epithelial cells grown in culture on 3T3 feeder layers. In Vitro. 1983;19(7):559–70.

7. Pillai S, Bikle DD, Mancianti M-L, Cline P, Hincenbergs M. Calcium regulation of growth and differentiation of normal human keratinocytes: Modulation of differentiation competence by stages of growth and extracellular calcium. J Cell Physiol. 1990;143(2):294–302.

8. Bikle DD, Xie Z, Tu C-L. Calcium regulation of keratinocyte differentiation. Expert Rev Endocrinol Metab. 2012;7(4):461–72.

9. Borowiec A-S, Delcourt P, Dewailly E, Bidaux G. Optimal Differentiation of In Vitro Keratinocytes Requires Multifactorial External Control. Mantovani R, editor. PLoS One. 2013 Oct;8(10):e77507.

10. Elsholz F, Harteneck C, Muller W, Friedland K. Calcium - a central regulator of keratinocyte differentiation in health and disease. Eur J Dermatology. 2014;24(6):650–61.

11. OECD. 431 OECD Guideline for the testing of chemicals. In Vitro skin corrosion: reconstructed human epidermis (RHE) test method. [Internet]. 2016. Available from: https://read.oecd-ilibrary.org/environment/test-no-431-in-vitro-skin-corrosion-reconstructed-human-epidermis-rhe-test-method_9789264264618-en#page1

12. OECD. 439 OECD Guideline for the testing of chemicals. In Vitro Skin Irritation: Reconstructed Human Epidermis Test Method. [Internet]. OECD; 2015 [cited 2016 Nov 12]. Available from: https://read.oecd-ilibrary.org/environment/test-no-439-in-vitro-skin-irritation-reconstructed-human-epidermis-test-method_9789264242845-en#page1

13. EpiDerm^TM - Overview - MatTek Corporation [Internet]. Available from: https://www.mattek.com/products/epiderm/

14. EpiSkin. EpiSkin epidermal model [Internet]. [cited 2021 Aug 1]. Available from:

https://www.episkin.com/Episkin

15. EpiSkin. SkinEthic RHE Reconstructed Human Epidermis [Internet]. [cited 2021 Aug 1]. Available from: https://www.episkin.com/SkinEthic-RHE

16. MacNeil S. Progress and opportunities for tissue-engineered skin. Nature. 2007 Feb 22;445(7130):874–80.

17. Walters RM, Johnson J&, Hilberer A, Medimmune NB. In vitro assessment of skin irritation potential of surfactant-based formulations by using a 3-D skin reconstructed tissue model and cytokine response. Altern to Lab Anim. 2016;44:523–32.

18. Kidd DA, Johnson M, Clements J. Development of an in vitro corrosion/irritation prediction assay using the EpiDerm^{TM} skin model. Toxicol Vitr. 2007;21(7):1292–7.

19. Pellevoisin C, Videau C, Briotet D, Grégoire C, Tornier C, Alonso A, et al. SkinEthic^{TM} RHE for in vitro evaluation of skin irritation of medical device extracts. Toxicol Vitr. 2018;50:418–25.

20. Mallampati R, Patlolla RR, Agarwal S, Babu RJ, Hayden P, Klausner M, et al. Evaluation of EpiDerm full thickness-300 (EFT-300) as an in vitro model for skin irritation: Studies on aliphatic hydrocarbons. Toxicol Vitr. 2010;24(2):669–76.

21. Bernhofer L., Seiberg M, Martin K. The Influence of the Response of Skin Equivalent Systems to Topically Applied Consumer Products by Epithelial--Mesenchymal Interactions. Toxicol Vitr. 1999;13(2):219–29.

22. SW S, MJ T, S S-S, PJ van B, DM B, TJ S, et al. Induction of cytokine (interleukin-1alpha and tumor necrosis factor-alpha) and chemokine (CCL20, CCL27, and CXCL8) alarm signals after allergen and irritant exposure. Exp Dermatol. 2005 Feb;14(2):109–16.

23. Gibbs S, Corsini E, Spiekstra SW, Galbiati V, Fuchs HW, DeGeorge G, et al. An epidermal equivalent assay for identification and ranking potency of contact sensitizers. Toxicol Appl Pharmacol. 2013;272(2):529–41.

24. Kosten IJ, Spiekstra SW, Gruijl TD De, Gibbs S. MUTZ-3 derived Langerhans cells in human skin equivalents show differential migration and phenotypic plasticity after allergen or irritant exposure. Toxicol Appl Pharmacol. 2015;287(1):35–42.

25. Bock S, Said A, Müller G, Schäfer-korting M, Zoschke C, Weindl G. Characterization of reconstructed human skin containing Langerhans cells to monitor molecular events in skin sensitization. Toxicol Vitr. 2018;46:77–85.

26. Bechetoille N, Dezutter-Dambuyant C, Damour O, André V, Orly I, Perrier E. Effects of solar ultraviolet radiation on engineered human skin equivalent containing both langerhans cells and dermal dendritic cells. Tissue Eng. 2007;13(11):2667–79.

27. Facy V, Flouret V, Régnier M, Schmidt R. Reactivity of Langerhans cells in human reconstructed epidermis to known allergens and UV radiation. Toxicol Vitr. 2005;19(6):787–95.

28. Régnier M, Staquet MJ, Schmitt D, Schmidt R. Integration of Langerhans cells into a pigmented reconstructed human epidermis. J Invest Dermatol. 1997 Oct;109(4):510–2.

29. Kapellos T, Bonaguro L, Gemünd I, Reusch N, Saglam A, Hinkley E, et al. Human Monocyte Subsets and Phenotypes in Major Chronic Inflammatory Diseases. Front Immunol. 2019;10(2035).

30. Wołkow P, Gębska A, Korbut R. In vitro maturation of monocyte-derived dendritic cells results in two populations of cells with different surface marker expression, independently of applied concentration of interleukin-4. Int Immunopharmacol. 2018 Apr 1;57:165–71.

31. Régnier M, Patwardhan A, Scheynius A, Schmidt R. Reconstructed human epidermis composed of keratinocytes, melanocytes and Langerhans cells. Med Biol Eng Comput [Internet]. 1998 Nov [cited 2016 Jul 16];36(6):821–4. Available from: http://link.springer.com/10.1007/BF02518889

32. Odashiro AN, Pereira PR, Marshall JC, Godeiro K, Burnier MN. Skin cancer models. Drug Discov Today Dis Model. 2005;2(1):71–5.

33. Semlin L, Schäfer-Korting M, Borelli C, Korting HC. In vitro models for human skin disease. Drug Discov Today. 2011;16(3–4):132–9.

34. Mackiewicz-Wysocka M, Bowszyc-Dmochowska M, Strzelecka-Weklar D, Dańczak-Pazdrowska A, Adamski Z. Basal cell carcinoma - Diagnosis. Vol. 17, Wspolczesna Onkologia. 2013. p. 337–42.

35. Hernandez AD, Hibbs MS, Postlethwaite AE. Establishment of basal cell carcinoma in culture: Evidence for a basal cell carcinoma-derived factor(s) which stimulates fibroblasts to proliferate and release collagenase. J Invest Dermatol. 1985;85(5):470–5.

36. Asada M, Schaart F-M, Detmar M, Mischke D, de Almeida HL, Gollnick H, et al. Growth Characteristics and Differentiation of Basal Cell Carcinoma In Vitro– Immunohistochemical, Gel Electrophoretic, and Ultrastructural Analysis. J Invest Dermatol. 1992;99(4):474–81.

37. Korman NJ, Hrabovsky SL. Basal cell carcinomas display extensive abnormalities in the hemidesmosome anchoring fibril complex. Exp Dermatol. 1993;2(3):139–44.

38. Pentel M, Helm KF, Maloney MM. Cell Surface Molecules in Basal Cell Carcinomas. Dermatologic Surg. 1995;21(10):858–61.

39. Verhaegh M, Beljaards R, Veraart J, Hoekzema R, Neumann M. Adhesion molecule expression in basal cell carcinoma. Eur J Dermatol. 1998 Jun;8(4):252–5.

40. Sollberg S, Peltonen J, Uitto J. Differential expression of laminin isoforms and β4 integrin epitopes in the basement membrane zone of normal human skin and basal cell carcinomas. J Invest Dermatol. 1992;98(6):864–70.

41. Savoia P, Trusolino L, Pepino E, Cremona O, Marchisio PC. Expression and topography of integrins and basement membrane proteins in epidermal carcinomas: Basal but not squamous cell carcinomas display loss of α6β4 and BM-600/nicein. J Invest Dermatol.

1993;101(3):352–8.

42. Fairley JA, Heintz PW, Neuburg M, Diaz LA, Giudice GJ. Expression pattern of the bullous pemphigoid-180 antigen in normal and neoplastic epithelia. Br J Dermatol. 1995;133(3):385–91.

43. Lazarova Z, Domloge-Hultsch N, Yancey KB. Epiligrin is decreased in papulonodular basal cell carcinoma tumor nest basement membranes and the extracellular matrix of transformed human epithelial cells. Exp Dermatol. 1995;4(3):121–9.

44. Chopra A, Maitra B, Korman NJ. Decreased mRNA expression of several basement membrane components in basal cell carcinoma. J Invest Dermatol. 1998;110(1):52–6.

45. Nishiyama T, Amano S, Tsunenaga M, Kadoya K, Takeda A, Adachi E, et al. The importance of laminin 5 in the dermal-epidermal basement membrane. J Dermatol Sci. 2000;24(SUPPL. 1).

46. Walther A, Houlston R, Tomlinson I. Association between chromosomal instability and prognosis in colorectal cancer: a meta-analysis. Gut. 2008;57(7):941–50.

47. McGranahan N, Burrell R, Endesfelder D, Novelli M, Swanton C. Cancer chromosomal instability: therapeutic and diagnostic challenges. EMBO Rep. 2012;13(6):528–38.

48. Donnelly N, Storchová Z. Dynamic karyotype, dynamic proteome: buffering the effects of aneuploidy. Biochim Biophys Acta - Mol Cell Res. 2014 Feb 1;1843(2):473–81.

49. Garlick J a. Engineering skin to study human disease--tissue models for cancer biology and wound repair. Adv Biochem Eng Biotechnol. 2007;103(January):207–39.

50. Baltazar T, Merola J, Catarino C, Xie CB, Kirkiles-Smith NC, Lee V, et al. Three Dimensional Bioprinting of a Vascularized and Perfusable Skin Graft Using Human Keratinocytes, Fibroblasts, Pericytes, and Endothelial Cells. Tissue Eng - Part A. 2020 Mar 1;26(5–6):227–38.

51. Liu X, Michael S, Bharti K, Ferrer M, Song MJ. A Biofabricated Vascularized Skin Model of Atopic Dermatitis for Preclinical Studies. Biofabrication. 2020 Apr 8;12(3):035002.

52. Matei A-E, Chen W, Kiesewetter L, Györfi A-H, Li Y-N, Trinh-Minh T, et al. Vascularised human skin equivalents as a novel in vitro model of skin fibrosis and platform for testing of antifibrotic drugs. Ann Rheum Dis [Internet]. 2019 [cited 2021 Aug 11];78:1686–92. Available from: http://ard.bmj.com/

53. Kwak BS, Jin S-P, Kim SJ, Kim EJ, Chung JH, Sung JH. Microfluidic skin chip with vasculature for recapitulating the immune response of the skin tissue. Biotechnol Bioeng. 2020 Jun 1;117(6):1853–63.

APPENDICES

LIST OF PUBBLICATIONS

Published

C. Gaviria, N.Y. Becerra, J.D. Vergara, L.A. Correa, S. Estrada, L.M. Restrepo. *Dermo-epidermal organotypic cultures for in vitro evaluation of skin irritation and corrosion.* Toxicology in Vitro, 2020, vol. 63, p. 104657.

In submission process

Catalina Gaviria, Luz Marina Restrepo. *Modelling skin cancer: what can in vitro models offer?* Submitted to Journal of Dermatology Research, 2021

Catalina Gaviria, Natalia Becerra, Luis A. Correa, Sergio Estrada, Luz Marina Restrepo. *Explant culture and feeder layer as a source keratinocytes for the construction of human skin equivalents: a pilot study.* Submitted to Health Science Reports, 2021.

Catalina Gaviria-Agudelo, Laura J. Jilderda, Judith E. Simon, Alex M. Heberle, Petra L. Bakker, Christy Hong, Maurits Roorda, Marcel A.T.M. van Vugt, Kathrin TheDieck, Floris Foijer. *Overexpression of the PRMT5-MEP50 complex counteracts protein aggregation and proteotoxicity in cells displaying CIN.* To be submitted to Developmental Cell Journal.

C. Gaviria, B. Bakker, **,** J. Terra, L. Zhou, E. Rácz, S. Paljić, J. Garcia-Martinez, V. Oliveira, P. L. Bakker, D.C.J. Spierings, M. F. Jonkman, F. Foijer. *Single-cell DNA sequencing reveals distinct molecular types of basal cell carcinoma with unique transcriptome fea*tures. Currently preprinted at: https://www.biorxiv.org/content/10.1101/492199v1, 2018. To be submitted after my contribution as a co-author.

EVENTS PARTICIPATION

Catalina Gaviria, Luis Alfonso Correa, Emoke Rácz, Sergio Estrada, Natalia Becerra, Luz Marina Restrepo, Floris Foijer. "Fibrin-based dermo-epidermal organotypic models of skin and skin cancer". 20th Kolff Conference. Groningen, Netherlands. 2019.
*No certificate was given for this event. For any inquiries please contact Kolff PhD Council: i.dudurych@umcg.nl

Cellular Imaging Light course, Department of Biomedical Sciences of Cells and Systems, University Medical Center Groningen, University of Groningen. Groningen, The Netherlands. 2019.

Microbiological Safety course, Department of Medical Biology & Infection Prevention, University Medical Center Groningen, University of Groningen. Groningen, The Netherlands. 2019.

Gaviria C, Restrepo LM, Correa LA, Patiño MI, Estrada S, Becerra N. "Dermo-epidermal organotypic cultures for the assessment of irritation and corrosion". XLV European Society for Artificial Organs (ESAO) Congress. Madrid, Spain. 2018.

Catalina Gaviria, Julián Vergara, Luz Marina Restrepo, Luis Alfonso Correa, Sergio Estrada, Natalia Becerra. "Comparison of explant culture and enzymatic digestion methods for human skin equivalents development". 7th International conference on Tissue Engineering & Regenerative Medicine. Barcelona, Spain. 2017.

GRADO DE ORIGINALIDAD

En los últimos años ha venido creciendo el interés por desarrollar alternativas contra la experimentación animal, dadas las cuestiones éticas asociadas y las claras diferencias entre la piel animal y humana. De hecho, Colombia se suma a la Unión Europea y, bajo la ley 2047, ha prohibido el uso de animales en pruebas cosméticas.

En este sentido, el campo de la ingeniería de tejidos ha hecho enormes esfuerzos en el estudio y generación de modelos de piel *in vitro*, incluyendo cultivos bi (2D) y tridimensionales (3D). Los modelos 2D, sin embargo, no ofrecen la complejidad de la estructura 3D y, por lo tanto, no imitan muy bien el fenotipo y el comportamiento de la piel nativa. Los modelos 3D, por otro lado, reflejan más fielmente la situación *in vivo* y representan una poderosa alternativa a la experimentación con animales. Los sustitutos 3D comercialmente disponibles son típicamente epidérmicos, los cuales resultan favorecidos con la adición de un componente dérmico que proporciona una condición más fisiológica y permite el estudio de diferentes procesos biológicos que involucran interacciones dermo-epidérmicas.

Teniendo en cuenta lo anterior, el grado de originalidad de este trabajo se sustenta en diversos aspectos:

1. Se desarrollan modelos dermo-epidérmicos que utilizan como base scaffolds de fibrina. La fibrina se presenta como un biopolímero altamente accesible, maleable y compatible con el crecimiento y migración de diferentes tipos de células. Pocos autores han hecho uso de la fibrina para modelos cutáneos. Hasta donde sabemos, se ha utilizado en la generación de un modelo hipodérmico o como modelo dérmico en injertos de piel. Esta tesis proporciona un equivalente cutáneo con mayor complejidad que los modelos epidérmicos, cuya creación se ve simplificada gracias al uso de la fibrina como componente dérmico y que resultan ser validados en pruebas de toxicidad.

2. La mayoría de los modelos 3D actuales carecen de un componente inmune, lo que limita uso en pruebas de sensibilidad y estudios inmunológicos. En este trabajo se describe por primera vez la creación de un equivalente creado con células CD14+ como precursores de células dendríticas. Interesantemente, se demuestra que el miroambiente de nuestro modelo promueve la diferenciación de CD14+ y permite la migración de las células dendríticas generadas, dando lugar a un sistema altamente prometedor en la generación de estructuras con diferentes tipos de células inmunes.

3. Dada la enorme dificultad que supone el cultivo de células de carcinoma basal (BCC), hay solo unos cuantos reportes sobre el tema, con una eficiencia no muy alta. En esta tesis hemos generado un nuevo protocolo para el cultivo de células de BCC en el que se obtuvo crecimiento de todas las biopsias y que permitió la posterior utilización tanto en microscopia como en la generación de sistemas 3D. En el primer caso, se reporta por primera vez una cuantificación del número de mitosis anormales en células de BCC. En el segundo caso, se muestra el potencial de equivalentes dermo-epidérmicos para modelar BCC, los cuales recrean varias características de este tipo de cáncer y, por lo tanto, pueden ser una herramienta valiosa para probar agentes terapéuticos. Esto contribuye enormemente al campo de los modelos de cáncer, ya que a la fecha no existen equivalentes *in vitro* de BCC en los que se pueda estudiar esta condición.

ACKNOWLEDGEMENTS

Fueron la manera perfecta de descargar el estrés de la semana. No olvidaré nuestro viaje a la montaña más alta de los Países Bajos y estaré siempre agradecida por haberlos encontrado en esta parte del mundo. Elizabeth y Angie, gracias por su valiosa compañía y por esos días y noches de chicas y, por supuesto, por esa fiesta de fin de año que nunca olvidaremos.

Agradezco especialmente a María Isabel y a Oli, quienes han estado desde el principio. Isa, gracias por tu compañía y por ser mi apoyo en Groningen. Todos los cafés, las cervezas, los postres, y las noches de cine y de comida hicieron esta etapa más llevadera. A Oli, gracias por estar pendiente aun estando tan lejos. Nuestro pequeño grupo de PhD sirvió de apoyo en temas académicos y personales y me sacó infinitas risas.

A mis amigos especiales. Laura, gracias por tu amistad. Tus consejos, ayuda y apoyo incondicional han enriquecido mi vida. Ana, tu presencia es invaluable. No solo impresionas con tus habilidades en todos los campos, sino por ser una persona autentica, bonita y transparente. A Mauricio, quien siempre me motiva y escucha con la mejor actitud. Gracias por los chistes ñoños y por nuestro espectacular viaje europeo. A Julián, por convertirse en el mejor compañero dentro y fuera del laboratorio, por sus sabios y prácticos consejos y por sacarme tantas risas con sus parodias. A Daniel, gracias por la compañía incondicional y participar en todo lo que pasa a 10000 km de distancia.

A mi familia, mis papás y mis hermanas. Gracias por siempre estar ahí, ayudarme aun cuando no era necesario y por interesarse en mi trabajo preguntando como estaban las células. Especialmente a mis papás que constantemente me recuerdan que tengo un lugar seguro donde regresar siempre.